Spin-orbit coupling effects in two-electron coupled quantum dots

Dissertation

zur Erlangung des Doktorgrades
der Naturwissenschaften (Dr. rer. nat.)
der Naturwissenschaftlichen Fakultät II-Physik
der Universität Regensburg

vorgelegt von

Fabio Baruffa
aus Napoli, Italien

Mai 2010

The PhD thesis was submitted on May 2010

The colloquium took place on 16th of July 2010

Board of examiners:

Prof. Dr. S. Ganichev	Chairman
Prof. Dr. J. Fabian	1st Referee
Prof. Dr. M. Grifoni	2nd Referee
Prof. Dr. G. Bali	Examiner

Contents

Acknowledgments

These few lines I would like to dedicate to all those people who, in one way or another, have contributed to my scientific and life experience in Regensburg.
First of all I would sincerely thank Prof. Jaroslav Fabian, for his continuous support. Without his help and patience I would not be able to go forward and understand the beauty of the research in physics.
The next thank goes to Dr. Peter Stano. He has taught me how to attack a problem and find the right combination between the numerics and the analytical work.
I wish to thanks all members of the Spintronics group. I have learnt many things from each of you: Sergej Konschuh, Martin Raith, Benedikt Scharf, Martin Gmitra and Alex Matos-Abiague.
Always present to give me advices and to make me feel less distant to mine own city are my parents Antonia and Bruno, my brother Dario and my girlfriend Melania...most of this work is dedicated to them.

Introduction

In the last thirty years, we have seen the evolution and the development of the semiconductor devices and large scale applications to realize computational instruments. The Moore's law [1], announced around 1970, asserts that our technology allows to double the number of transistors in electronic circuits, as well as the computer power, approximately every two years. This empirical law was properly valid till the 1980. Nowadays it starts to hit the limits. In the next fifteen years we expect that the structural limits of growing the capacity and the computational speed of the traditional computer technology will be reached. Therefore, in the last years, the scientific community has been enormously interested in the study of new devices and laws to apply in this new computer era.

A calculation process is basically a physical process running on a machine which obeys certain specific rules and laws. The classical theory of the computation was made on a abstract universal model machine (the Turing Machine) which operates using the principles set in 1936 by Alan Turing [2] and afterwards developed in the 40s by John von Neumann. The basic principle is that the Turing machine is an idealization of a mechanical computational device based on the classical physics rules. Although the technology progress allowed to produce very powerful device to speed-up the computational time, the basic principles have remained essentially unchanged.

The recent progresses in the devices development aim to reduce the dimensions of the electronic component up to the nanometer scale. At these dimensions the matter obeys the quantum mechanics rules. The *quantum computation* comes as a combination of the classical information theory and the quantum physics.

At the beginning of the 80s, the first idea to realize a computational model as an isolated quantum system was considered. R. Feymann established that there cannot exist any classical Turing machine able to simulate certain physical phenomena without an exponential slowdown of its performance [3]. On the other hand he was able to avoid this disconcerting problem imagining a universal quantum simulator, which works in more efficient way [4]. After his result, many scientists started to think how to use the quantum mechanics laws for the computation. Indeed in the 1994 P. Shor proposed a quantum algorithm to factorize a number by its prime [5]. Classically, the complexity of the problem is exponential in time, but using the quantum laws

he showed the polynomial complexity of the problem. The factorization problem is defined as follows: for a given number N, the product of two prime numbers P and Q, the algorithm has to be able to find P and Q. The Tab. 0.1 shows the comparison of the computational time between the classical and the quantum computers for the Shor problem. We see that for the factorization of a 400 digits number it is enough

	Quantum Computer with 70 Qubits	Net. of 100 Workstations of Classical Computers
Factorization of a number with 130 digits	1 month	1 month
Factorization of a number of 400 digits	3 years	10^{10} years (Age of the Universe)

Table 0.1.: Comparison between a classical and a quantum computer: the complexity and the computational time are reported [6].

to have a small quantum computer with respect to an extensive network of computer workstation. This is due to one of the most important property of the quantum computation: the intrinsic *parallellism*.

This amazing result appealed to many physicists to work on the quantum computation. Many proposals have been put forward to realize a quantum-bit, also called *qubit*. The most important are

- polarization of the light;
- electron spins in semiconductor quantum dots;
- nuclear spins of atoms in a molecole addressed through NMR;
- ions confined in an optical trap;
- superconducting Josephson junction.

Whatever physical implementation is used for the quantum computation processes, some criteria have to be fulfilled. This issue was addressed by DiVicenzo [7] setting up a list of five criteria, the so-called *DiVincenzo criteria*. They fix the rules how the realization of a qubit is possible. All the criteria will be discussed specifically for quantum dot systems, which are the subject of this thesis.

The electron spins in quantum dots are natural and viable qubits for quantum computing [8] as evidenced by the impressive recent experimental progress [9],[10] in spin detection and spin relaxation [11],[12] as well as in coherent spin manipulation

[13],[14]. In coupled dots, the two-qubit quantum gates are realized by manipulating the exchange coupling between the electrons, which originates in the Coulomb interaction and the Pauli principle [8],[15]. How is the exchange coupling modified by the presence of the spin-orbit coupling? In general, the usual (isotropic) exchange changes its magnitude while a new, functionally different form of exchange, called *anisotropic*, appears, breaking the spin-rotational symmetry. Such changes are a nuisance from the perspective of the error correction [16], although the anisotropic exchange could also induce quantum gating [17],[18].

The anisotropic exchange of coupled localized electrons has a convoluted history [19],[20],[21],[22],[23],[24],[25]. The question boils down to determining the leading order in which the spin-orbit coupling affects both the isotropic and anisotropic exchange. At zero magnetic field, the second order was suggested [26], with later revisions showing the effects are absent in the second order [27],[19]. The analytical complexities make a numerical analysis particularly useful.

In this thesis we study the electronic properties of laterally coupled quantum dots [28]. We focus on two electrons, since we investigate the possibility of spin manipulation, via exchange coupling, for quantum computation applications. The spin-orbit interaction in such system is always present, even if it can be reduced or increased, depending on the aim and the applications one wants to have. Understanding the influence on the spin-orbit interaction is crucial, since it leads to new interactions (such as the already mentioned anisotropic exchange) and spin-relaxation. We show that indeed the anisotropic exchange is present but, in contrast to previous views, only at finite magnetic fields. Even then, it remains weak, boosting prospect for error-free quantum computation with spin qubits. We propose, in addition, a new and highly accurate (numerically tested) two-qubit Hamiltonian [29], to model the system dynamics under realistic physical conditions.

The thesis is organized as follows: In the first chapter we give an overview of the main properties of the quantum computation. In the second chapter we analyze the most recent experiments and applications for the quantum dot systems. In the third chapter we give the main results of the single electron quantum dot physics and in particular how the tunneling energy is influenced by the spin-orbit interaction. In the fourth chapter the details of the role of the spin-orbit interaction on the two-electron quantum dots spectrum are given, with the comparison between our derived spin Hamiltonian and numerics. In the fifth chapter we discuss the numerical method we have used to diagonalize the full two electron Hamiltonian and also analyze the Coulomb interaction and the precision of our numerical results.

1. Overview of Quantum Computation

In this chapter we study the most important properties and peculiarities of the quantum computation. The main differences between the classical and the quantum unit of information are highlighted. We give also an example on how the intrinsic parallelism of the quantum mechanics formalism can improve the current computations. The DiVincenzo criteria of the physical realization of a quantum computer are discussed, focusing mainly on quantum dot systems.

1.1. Classical unit of information: the *bit*

The basic element of a classical computer is a bit. It is a digital number composite by a two level physical system, either "0" or "1" [30]. The two levels should be separated by an energy barrier such that a small external perturbation does not modify the structure of the initial state. All implementations, such as electrical, magnetical or mechanical, are similar to a simple two states switch. It can be in either ON or OFF state and it is suitably interpreted. For example for the standard RAM memory of a computer the charge of a capacitor encodes these informations, while for a magnetic system, a magnetization domain is used for the same goal. The system is initialized in a proper state by applying an external force. If we measure the state of the system by applying an external perturbation, we should find exactly the same state which was prepared in the step before. In principle, if the bit is constructed correctly, the *read-out* operation reproduces the information stored during the writing time.

To represent the classical bit states or the so-called *Cbits*, a symbolic notation is needed. We shall use the symbol $|\ \rangle$, into which we place the value, 0 or 1, represented by that state. Thus the two distinguishable states of a Cbits are $|0\rangle$ or $|1\rangle$ [31]. For example a 5 Cbits state, which corresponds to the 11001 digits, the notation

$$|1\rangle|1\rangle|0\rangle|0\rangle|1\rangle, \tag{1.1}$$

is used. For a couple of Cbits we have only 4 possible states

$$|0\rangle|0\rangle,\ |0\rangle|1\rangle,\ |1\rangle|0\rangle,\ |1\rangle|1\rangle. \tag{1.2}$$

One can iterate simply that formalism for a given N Cbits.

It is also useful to express the vectors in terms of components, representing the two orthogonal states of a single Cbit as column vectors

$$|0\rangle \to \begin{pmatrix} 1 \\ 0 \end{pmatrix}, \qquad |1\rangle \to \begin{pmatrix} 0 \\ 1 \end{pmatrix}. \tag{1.3}$$

This helpful choice points out the existence of differences with the quantum bits. In the two Cbits case, the vectorial space has 4 dimensions and the basis set is

$$|00\rangle, |01\rangle, |10\rangle, |11\rangle. \tag{1.4}$$

An easy generalization can be done to represent the multiple Cbits using the properties of the tensor product. One particular example for 3 Cbits state is

$$\begin{pmatrix} x_0 \\ x_1 \end{pmatrix} \otimes \begin{pmatrix} y_0 \\ y_1 \end{pmatrix} \otimes \begin{pmatrix} z_0 \\ z_1 \end{pmatrix} \to \begin{pmatrix} x_0y_0z_0 \\ x_0y_0z_1 \\ x_0y_1z_0 \\ x_0y_1z_1 \\ x_1y_0z_0 \\ x_1y_0z_1 \\ x_1y_1z_0 \\ x_1y_1z_1 \end{pmatrix}. \tag{1.5}$$

The structure defined by the tensor product for N Cbits needs a 2^n-dimensional space where each column vector represents one of the 2^n possible states that can be built from N Cbits.

The amount of information kept in N Cbits or in a c-register is $S = \log_2 W = c$, where $W = 2^c$ represents the number of the possible configurations of a register. The classical algorithms use the Boolean logic and only few logic gates, where the most important is the NAND gate, also called *universal gate* [32].

1.2. Quantum unit of information: the *qubit*

The main property of the two dimensional vector representing the state of a Cbit is that in the whole vectorial space of the two orthogonal vectors $|0\rangle$ and $|1\rangle$ there are only two possible states, no other combinations are allowed. The quantum mechanics provides us physical systems that do not endure this limitation. To distinguish the classical bit from the quantum bit, it has been called *qubit*. The states $|0\rangle$ and $|1\rangle$ do not compose all kind of qubit states. Indeed a quantum two level system can be also in a superposition of both: $|\psi\rangle = \alpha|0\rangle + \beta|1\rangle$, where α and β are complex

numbers such that $|\alpha|^2 + |\beta|^2 = 1$. Hence the two states form an orthogonal basis in the Hilbert space of the qubit, $\mathcal{H}_2 = span\{|0\rangle, |1\rangle\}$, More general, the state of the qubit can be represented as (up to a common phase factor)

$$|\psi\rangle = \cos(\theta/2)e^{-i\varphi/2}|0\rangle + \sin(\theta/2)e^{i\varphi/2}|1\rangle. \tag{1.6}$$

If we represent the two possible states as the South and the North pole of a two dimensional sphere, all kinds of combinations can be viewed as a point on the surface of that sphere. It is called Bloch sphere (Fig. 1.1).

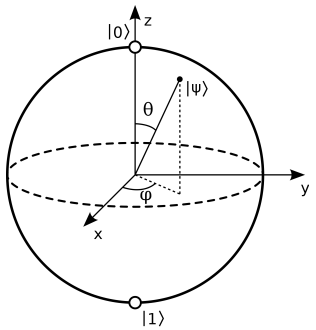

Figure 1.1.: Bloch sphere for a single qubit. The north pole corresponds to the ground state of the qubit $|0\rangle$, the south pole corresponds to the exited state $|1\rangle$. Each point on the sphere represents one of the possible superpositions of the two basis states, where θ is the polar angle and φ is the azimuthal angle in the x-y plane.

The polar angle θ corresponds to the probability coefficient of the state, while the azimuthal angle φ is the phase of the qubit. Furthermore in each point of that sphere one can associate a unit vector, with the center at the origin of the coordinate system

$$\hat{\psi} = \sin\theta\cos\varphi\hat{x} + \sin\theta\sin\varphi\hat{y} + \cos\theta\hat{z} \tag{1.7}$$

where $\hat{x}$, $\hat{y}$ and $\hat{z}$ are the unit vectors of the three coordinate axes.

Similarly as in the general case of a single qubit in an arbitrary linear superposition of two possible classical state, one can also construct a superposition of 4 states as

$$|\Psi\rangle = \alpha_{00}|00\rangle + \alpha_{01}|01\rangle + \alpha_{10}|10\rangle + \alpha_{11}|11\rangle \rightarrow \begin{pmatrix} \alpha_{00} \\ \alpha_{01} \\ \alpha_{10} \\ \alpha_{11} \end{pmatrix}, \tag{1.8}$$

with the complex amplitudes and normalization

$$|\alpha_{00}|^2 + |\alpha_{01}|^2 + |\alpha_{10}|^2 + |\alpha_{11}|^2 = 1. \tag{1.9}$$

The generalization to N quibits is obviously a superposition of 2^N classical states, with the corresponding normalization.

Once we have two qubits, one in the state $|\psi\rangle = \alpha_0|0\rangle + \alpha_1|1\rangle$ and the other in the state $|\phi\rangle = \beta_0|0\rangle + \beta_1|1\rangle$, the coupled state is

$$\begin{aligned} |\Psi\rangle &= |\psi\rangle \otimes |\phi\rangle = (\alpha_0|0\rangle + \alpha_1|1\rangle) \otimes (\beta_0|0\rangle + \beta_1|1\rangle) = \\ &= \alpha_0\beta_0|00\rangle + \alpha_0\beta_1|01\rangle + \alpha_1\beta_0|10\rangle + \alpha_1\beta_1|11\rangle \rightarrow \begin{pmatrix} \alpha_0\beta_0 \\ \alpha_0\beta_1 \\ \alpha_1\beta_0 \\ \alpha_1\beta_1 \end{pmatrix} \end{aligned} \tag{1.10}$$

It is important to note that the general two-qubits state Eq. (1.8) is a particular case of the state Eq (1.10) if and only if $\alpha_{00}\alpha_{11} = \alpha_{01}\alpha_{10}$. Since the four amplitudes in Eq. (1.8) are related only by the normalization condition, this relation does not necessarily hold and the general two-qubits state, Eq. (1.10), is not a product of two single qubit states. The same conclusion is valid for a general N-qubit state: the main difference with the Cbits, which can be only in one of the 2^N possible states, an N qubit state can be in a superposition of these 2^N product states which do not correspond to a product of a single qubit state. More precisely, the state can be in a not separable state.

For example, if the system is in the state

$$|\Psi\rangle = \frac{1}{\sqrt{2}}(|0\rangle_1 \otimes |1\rangle_2 - |1\rangle_1 \otimes |0\rangle_2), \tag{1.11}$$

where the subscript stays for either first or second qubit, we see that each qubit is correlated to each other such that the measure of a qubit can influence the other, because of the not separability of the states. The two qubits are called *EPR coupled* or entangled [33].

The consequence of this particular state is crucial in the quantum computation. Indeed, if we are able to measure the state of the first qubit and we get $|0\rangle_1$, it implies that the second qubit is in the state $|1\rangle_1$. This means that if we have two polarized electrons, by the direction of their spins, a measurement of the first spin influences the second electron, although the spin detectors can be very far apart. The entanglement is very important for the transmission of secure keys between two parties [32].

The writing and the reading operations of a qubit state are completely asymmetric. Exciting the system by an external force in resonance with the transition frequency of the two states and manipulating the amplitude and the duration, it is possible to initialize the state in any desidered superposition. Hence it is possible to write on a qubit any possible state. The interesting phenomena occurs when the energy is measured: we find always one of the two possible energy values stored in the

$|0\rangle$ and $|1\rangle$ state with a probability $P_0(|\psi\rangle) = \cos^2(\theta/2)$ or $P_1(|\psi\rangle) = \sin^2(\theta/2)$ respectively. The superposition collapses either in the North or in the South state of the Bloch sphere. It is not even possible to measure an intermediate value of the energy corresponding to that superposition. On a quantum computer one realizes a reversible operation, which transforms the initial state into a final state by doing a reversible operation. The only irreversible operation is the measurement, but it is the only way how one can extract the physical information form a qubit.

We conclude the discussion of the Bits by a following resume table of the most important Bits properties [31].

CBITS vs. QBITS	**Cbits**	**Qubits**
States of n Bits	$\|x\rangle$	$\sum \alpha_x \|x\rangle,\ \sum \|\alpha_x\|^2 = 1$
Subsets of n Bits	Correspond always to states	do not correspond generally to states
Reversible operation on states	Permutations	Unitary transformations
Can state be learned from Bits?	Yes	No
To learn a state from Bits	Examine them	Measure them
Information acquired	x	x with probability $\|\alpha_x\|^2$
State after acquiring	Same: still $\|x\rangle$	Different: now $\|x\rangle$

1.3. Logical quantum gate

Up to now, we have described the main properties of the computational states. The important assignment now is to see how the evolution of the state can realize an operation. In a classical computer, the operations are performed by using logical gates which accomplish a certain task. The most important classical single bit gate is the NOT gate, which implements the negation operation on the states. The true table is $|1\rangle \to |0\rangle$ and $|0\rangle \to |1\rangle$. To define a similar operation on a qubit, we do not restrict ourself to fix the action only on the states $|0\rangle$ and $|1\rangle$, but we have to specify also the action on the superposition state. The NOT gate has to transform $\alpha|0\rangle + \beta|1\rangle$ in the state $\alpha|1\rangle + \beta|0\rangle$. The operation that implements this transformation is a linear operator, in particular a unitary operator.

In quantum mechanics the evolution of the system is described by an unitary operator U composed by the ordinary evolution operator of the physical system. Once we have the system Hamiltonian $H(t)$, we write

$$|\psi(t)\rangle = U|\psi(0)\rangle = Te^{-i\int_0^t d\tau H(\tau)}|\psi(0)\rangle, \tag{1.12}$$

where T stays for the temporal order operator. There are several classes of operations, depending on how many qubits we use. We have the single qubit operations, the two qubits operations and so on. The *quantum gates* are defined as all possible unitary transformations acting on a single or a double qubit. In the work of Barenco et *al.* [34], it is shown that any quantum algorithm can be decomposed in a series of only two kinds of operations: the single qubit and the two qubit operations. Geometrically the quantum gates are continuous rotations in a complex vectorial space. It has been shown that a group of universal gates is composite of an arbitrary single qubit rotation and a two qubit SWAP operation.

1.3.1. Single qubit gate

A well-known representative of a single qubit gate is the Hadamard operation, defined by the following unitary matrix

$$U_H = \frac{1}{\sqrt{2}}\begin{pmatrix} 1 & 1 \\ 1 & -1 \end{pmatrix}, \tag{1.13}$$

in the basis of $\{|0\rangle, |1\rangle\}$ states. Denoting with $|a\rangle$, $(a = 0, 1)$ the qubit state, the application of this gate brings to the state

$$H|a\rangle = \frac{(-1)^a|a\rangle + |1-a\rangle}{\sqrt{2}}. \tag{1.14}$$

The adding of a possible phase in the wavefunction can be done using the transformation

$$(\phi) = \begin{pmatrix} 1 & 0 \\ 0 & e^{i\phi} \end{pmatrix} \qquad |a\rangle \overset{\phi}{\longmapsto} e^{ia\phi}|a\rangle. \tag{1.15}$$

It is possible to build a set of four operations which generate a more general pure state of a single qubit by

$$\begin{aligned}(\phi + \frac{\pi}{2})H(2\theta)H|0\rangle &= e^{i\theta}\begin{pmatrix} \cos\theta & -i\sin\theta \\ e^{i\phi}\sin\theta & ie^{i\phi}\cos\theta \end{pmatrix}\begin{pmatrix} 1 \\ 0 \end{pmatrix} = \\ &= \cos\theta|0\rangle + e^{i\phi}\sin\theta|1\rangle. \end{aligned} \tag{1.16}$$

Accordingly the Hadamard operation and the phase gates are the only single qubit operation needed to characterize a single qubit.

1.3.2. Single qubit dynamics

When we discussed the Hadamard transformation as a representive of a single qubit gate we did not care how such a gate can actually be realized. Now we want to focus on the temporal evolution of a single qubit built by using a spin 1/2 system. Applying an external magnetic field to the electron, the spin state can be modified. The Hamiltonian describing this coupling can be written as

$$H(t) = \frac{\hbar}{2}\begin{pmatrix} \omega_0 & \omega_1 e^{-i(\omega t+\phi)} \\ \omega_1 e^{i(\omega t+\phi)} & -\omega_0 \end{pmatrix}, \tag{1.17}$$

where $\omega_0/2\pi$ is the frequency of the system transition, $\omega_1/2\pi$ and $\hbar\omega_1$ are the frequency and the amplitude of the external oscillating field, respectively.

Each hermitian matrix 2×2 can be written in function of the density matrix and the Pauli matrices. In particular, the density operator of a single particle can be parameterized as

$$\rho = \frac{1}{2}(\mathbf{1} + \mathbf{s}\cdot\boldsymbol{\sigma}) = \frac{1}{2}\begin{pmatrix} 1+s_z & s_x - is_y \\ s_x + is_y & 1-s_z \end{pmatrix}, \tag{1.18}$$

where the vector $\vec{s} = (s_x, s_y, s_z)$ is the Bloch vector. In the same way the 2×2 Hamiltonian is written as

$$H = \frac{\hbar}{2}(\Omega_0\mathbf{1} + \boldsymbol{\Omega}\cdot\boldsymbol{\sigma}), \tag{1.19}$$

where Ω is the Rabi vector. Placing the equations Eq. (1.18) and Eq. (1.19) in the equation of motion for the density operator

$$i\hbar\frac{d}{dt}\rho = [H, \rho], \tag{1.20}$$

and using the identity

$$(\mathbf{a}\cdot\boldsymbol{\sigma})(\mathbf{b}\cdot\boldsymbol{\sigma}) = (\mathbf{a}\cdot\mathbf{b}) + i(\mathbf{a}\times\mathbf{b})\cdot\boldsymbol{\sigma} \tag{1.21}$$

we find the following equation of motion for the Bloch vector

$$\frac{d}{dt}\mathbf{s} = \boldsymbol{\Omega}\times\mathbf{s}. \tag{1.22}$$

This equation has a simple geometrical solution: the $\mathbf{s}$ vector rotates around the $\vec{\Omega}$ vector with angular frequency $|\boldsymbol{\Omega}|$.

From the Eq. (1.22) it is easy to note the typical situation occurred in the quantum computation. Using the RWA (Rotating Wave Approximation [35]) the oscillating field can be replaced by a rotating field. This leads to

$$\Omega_x = \omega_1\cos(\omega t+\phi), \qquad \Omega_y = \omega_1\sin(\omega t+\phi), \qquad \Omega_z = \omega_0. \tag{1.23}$$

To solve the equation Eq. (1.22), it is convenient to consider the evolution of the vector $\mathbf{s}$ as a rotation around the z axis with frequency ω. More precisely we write

$$\mathbf{s}(t) = R_z(\omega t)\mathbf{s}'(t) \qquad \mathbf{\Omega}(t) = R_z(\omega t)\mathbf{\Omega}'(t) \tag{1.24}$$

where $R_z(\omega t)$ is the rotational matrix around the z axis

$$R_z(\omega t) = \begin{pmatrix} \cos(\omega t) & -\sin(\omega t) & 0 \\ \sin(\omega t) & \cos(\omega t) & 0 \\ 0 & 0 & 1 \end{pmatrix} = \exp(\omega t M_z), \tag{1.25}$$

with

$$M_z = \begin{pmatrix} 0 & -1 & 0 \\ 1 & 0 & 0 \\ 0 & 0 & 0 \end{pmatrix}. \tag{1.26}$$

Replacing the equation Eq. (1.24) in Eq. (1.22) and considering

$$\frac{d}{dt}R_z(\omega t) = R_z(\omega t)(\omega M_z), \qquad M_z\mathbf{s}' = \hat{z} \times \mathbf{s}', \tag{1.27}$$

where $\hat{z}$ is the unit vector along the z direction, we obtain

$$\frac{d}{dt}\mathbf{s}' = \mathbf{\Omega}' \times \mathbf{s}', \tag{1.28}$$

where the vector $\mathbf{\Omega}'$ is independent on the time,

$$\Omega'_x = \omega_1 \cos(\phi), \qquad \Omega'_y = \omega_1 \sin(\phi), \qquad \Omega'_z = \omega_0 - \omega_1. \tag{1.29}$$

This can simply verified calculating $R_z^{-1}\Omega(t)$.

By controlling the intensity of the coupling $\hbar\omega_1$, the frequency ω and the phase ϕ of the external field it is possible to initialize any vector $\mathbf{\Omega}$. This implies that if we know the initial state of the qubit, with a single rotation we can place the Bloch vector $\mathbf{s}$ in any direction in the space.

1.3.3. Two qubit gate

We now discuss the quantum gate which operates on a two qubit state. The general two qubit operation is the controlled NOT or exclusive disjunction, the XOR operation. The gate operates by changing the output of the second bit if the first one is 1, otherwise it stays the same. The truth table is given as follows:

$\|a,b\rangle$	$\|a,a\oplus b\rangle$
$\|00\rangle$	$\|00\rangle$
$\|01\rangle$	$\|01\rangle$
$\|10\rangle$	$\|11\rangle$
$\|11\rangle$	$\|10\rangle$

where the control qubit is $|a\rangle$ and the target qubit is $|b\rangle$. An important conceptual difference between the XOR gate in boolean and quantum computers is that in the quantum gate, the number of inputs and outputs are always identical. The quantum bits are both still present after the gate operation.

We can represent the XOR gate in the two qubit basis

$$B = \{|00\rangle, |01\rangle, |10\rangle, |11\rangle\}, \tag{1.30}$$

as the following matrix

$$U_{XOR} = \begin{pmatrix} 1 & 0 & 0 & 0 \\ 0 & 1 & 0 & 0 \\ 0 & 0 & 0 & 1 \\ 0 & 0 & 1 & 0 \end{pmatrix}. \tag{1.31}$$

The XOR gate is very important since it can create an entangled state. Let us set the control qubit $|a\rangle$ to a superposition of states $|a\rangle = 1/\sqrt{2}(|0\rangle - |1\rangle)$ and the target qubit to $|b\rangle = |1\rangle$. The total state is the tensor product of two states $1/\sqrt{2}(|0\rangle - |1\rangle) \otimes |1\rangle$ which is not an entangled state. Performing the XOR gate, the result of the operation is $1/\sqrt{2}(|01\rangle - |10\rangle)$, an entangled state.

The XOR gate is only one of many possibilities to have the two qubit operations. Another important possible gate is the so-called SWAP gate, which exchanges the value of the two qubit state. The matrix representation is

$$U_{SWAP} = \begin{pmatrix} 1 & 0 & 0 & 0 \\ 0 & 0 & 1 & 0 \\ 0 & 1 & 0 & 0 \\ 0 & 0 & 0 & 1 \end{pmatrix}. \tag{1.32}$$

This gate, however, does not have the entangling property of the XOR gate and does not suffice for the quantum computation. But it turns out that its square root does [36]. Since the SWAP is the time evolution operator generated by the appropriate Hamiltonian, for the spins in quantum dots the square root can be implemented by turning on the exchange energy between two electrons for half of the time needed for

the swapping. The Hamiltonian which provides this operation has the Heisenberg form

$$H_s(t) = J(t)\boldsymbol{\sigma}_1 \cdot \boldsymbol{\sigma}_2, \tag{1.33}$$

where $J(t)$ is the time dependent exchange coupling and $\boldsymbol{\sigma}_{1,(2)}$ are the Pauli matrices. If the exchange coupling is tuned such that $\int dt J(t) = J_0\tau_s = \pi/2$, the time evolution corresponds to the square-root swap. With this operation, one can obtain the XOR gate by

$$U_{XOR} = \exp\left[i(\pi/2)\sigma_{z,1}\right] \exp\left[-i(\pi/2)\sigma_{z,2}\right] U_{SWAP}^{1/2} \exp\left[i(\pi)\sigma_{z,1}\right] U_{SWAP}^{1/2}, \tag{1.34}$$

which is a combination of square-root of SWAP, $U_{SWAP}^{1/2}$, and single-qubit rotation $\exp\left[i(\pi)\sigma_{z,1}\right]$. This is proven to be the universal gate, useful to assembly any quantum algorithm [7]. Understanding how the exchange coupling influences the spin state is very important, since it can be tuned experimentally and used for spin manipulation [13].

1.4. Quantum parallelism

The vector used in the quantum computation with 2^N states is, for example,

$$\|x\rangle = |0\rangle_n \otimes |0\rangle_{n-1} \otimes |0\rangle_{n-2} \otimes |0\rangle_{n-3} \otimes ...|0\rangle_4 \otimes |1\rangle_3 \otimes |1\rangle_2 \otimes |1\rangle_1. \tag{1.35}$$

Each qubit of that state can be in one of its possible eigenstates. To simplify the notation, we indicate the vector in Eq. (1.35) with the compact symbol $\|x\rangle$, where x is an integer number from 0 to $2^n - 1$, which is a binary representation corresponding to the vector Eq. (1.35). For example in this case, the state $\|x\rangle$ corresponds to the state $\|7\rangle$.

The idea of the *quantum parallelism* can be seen from the following argument. Let us consider an entangled state of two qubits and apply on it a quantum operation $\mathcal{U}$. Since the linearity of the operator, we get

$$\mathcal{U}\left(\frac{1}{\sqrt{3}}|0\rangle_1 \otimes |0\rangle_2 + \sqrt{\frac{2}{3}}|1\rangle_1 \otimes |1\rangle_2\right) = \frac{1}{\sqrt{3}}\mathcal{U}|0\rangle_1 \otimes |0\rangle_2 + \sqrt{\frac{2}{3}}\mathcal{U}|1\rangle_1 \otimes |1\rangle_2. \tag{1.36}$$

As the result of the computation, we obtain the same superposition of the initial state in the final state. Furthermore the operation takes place for all state simultanesly. This important feature is called *quantum parallelism*. This gives the possibility to perform complex operations in parallel, whereas there is significant effort for a classical computer.

Let us suppose to do a certain unitary transformation $\mathcal{U}_f$ depending on a function f. We indicate with $\|f(x)\rangle$ the state that was $\|x\rangle$ in the previous case, where $f(x)$ can assume the following integer values: $f(x) = 0, 1, 2, ..., 2^n - 1$. Since $\mathcal{U}_f$ is a unitary transformation, it is invertible. Therefore the function f is bijective and its action is to permutate the integers $\{x\}$. At this stage, we take a double number of qubits $2n$ and define $\mathcal{U}_f$ on the space of the $2n$-qubits as the following:

$$\|x\rangle \otimes \|0\rangle \xrightarrow{\mathcal{U}_f} \|x\rangle \otimes \|f(x)\rangle. \tag{1.37}$$

We call the set of the first n qubits *input register* and the rest *output register*. To show better the concept of the quantum parallelism, we take as the input register state

$$\begin{aligned} \|s\rangle &= \frac{1}{2^{n/2}} \sum_{x=0}^{2^n-1} \|x\rangle = \frac{1}{2^{n/2}}(\|0\rangle + \|1\rangle + \|2\rangle + ... + \|n-1\rangle + \|n\rangle) = \\ &= \frac{1}{2^{n/2}}\big[|0\rangle_n \otimes |0\rangle_{n-1} \otimes ... \otimes |0\rangle_1 + |0\rangle_n \otimes |0\rangle_{n-1} \otimes ... \otimes |1\rangle_1 \\ &+ ... + |1\rangle_n \otimes |1\rangle_{n-1} \otimes ... \otimes |1\rangle_1\big], \end{aligned}$$

which can be rewritten as

$$\|s\rangle = \frac{1}{\sqrt{2}}(|0\rangle_1 + |1\rangle_1) \otimes ... \otimes \frac{1}{\sqrt{2}}(|0\rangle_n + |1\rangle_n). \tag{1.38}$$

This state can be obtained from the initial state $|0\rangle_1|0\rangle_2 \otimes ... \otimes |0\rangle_n$, submitting each qubits to a single qubit gate of the Hadamard type, which rotates the spin. The action of $\mathcal{U}_f$ gives

$$\|s\rangle \otimes \|0\rangle = \frac{1}{2^{n/2}} \sum_{x=0}^{2^n-1} \|x\rangle \otimes \|0\rangle \xrightarrow{\mathcal{U}_f} \frac{1}{2^{n/2}} \sum_{x=0}^{2^n-1} \|x\rangle \otimes \|f(x)\rangle. \tag{1.39}$$

Note that in one single operation we calculate $f(x)$ in all 2^n possible input values. If, for example, we have 100 qubits in the input register, $f(x)$ is calculated on $2^{100} \approx 10^{30}$ different values of input at the same time. This amazing parallelism can not be achieved in the classical computer.

Let us focus now on the extraction of the information from the state in Eq. (1.39). To show how the measurement operation works, let us suppose to measure the single states of all qubits in the input and output registers. With the same propability 2^{-n} we can find each state in the input register. If we assume to find a value $\|x_0\rangle$ as the result of the measurement in the input register, the result of the measurement in the output register will be $\|f(x_0)\rangle$. Therefore we compute $f(x_0)$ for a random

chosen value. All other informations are lost, since the total wavefunction (Eq. 1.39) collapses in the single component $\|x_0\rangle \otimes \|f(x_0)\rangle$.

We could think that there is no advantage with respect to the classical computation for the calculation of the value of $f(x)$ in a point chosen randomly. The aim of the quantum algorithms is to have an easy access to the data in the final state and to be sure that the data can not be generated in simple way by a classical algorithm, as one can see in the Shor algorithm.

An important difficulty is to keep the coherence of the entangled state of many qubits. Unfortunately it is impossible to isolate each qubit from the external environment during the computation. The coupling with the environment allows for decoherence or the collapse of the quantum state. One solution is to apply as error-correction algorithm, but it can work only for a short decoherence time.

1.5. DiVincenzo criteria for Quantum Computation

One of the main reasons why the study of mesoscopic physics is becoming more popular is the possibility to use the physical properties of the systems to build a quantum computer. Different propositions for possible devices are based on the rules of quantum mechanics, but all of them depend of special requirements reviewed by DiVincenzo [7]. These criteria are briefly discussed below.

1. It is needed to have a scalable quantum two-level system. Each qubit should be separately identifiable and externally addressable. Its physical parameters should be accurately known, including the internal Hamiltonian of the qubit, the presence of couplings to the other states and other qubits, and the couplings to the external fields that might be used to manipulate the state of the qubit. Furthermore it should be possible to have a collection of qubits.

2. It should be possible to initialize the state of the qubits to a simple state, such as $|00....\rangle$. To do so, the system has to be decoupled to the other qubits and perform an experiment to address the quantum register in its lower state.

3. The decoherence time has to be much longer than the gate operation. Decoherence time characterizes the dynamics of a qubit in contact with its environment and it is identified as the principal mechanism for the emergence of classical behavior. If the decoherence time is $10^4 - 10^5$ times the clock time of the quantum gate operation, one can use the quantum error correction algorithm to avoid the problem.

4. It is needed to have a set of quantum gates. This is the heart of quantum computing. This involves to have one-body Hamiltonian for each qubit such to control precisely the dynamics by the external potential. Then a two-body Hamiltonian is required involving nearby qubits. It should be possible to turn on and off the external control to couple and decouple the qubits. In a typical operation, the one- or two-body Hamiltonian will be turned on smoothly from zero to some value and then turned off again, all within a clock cycle. The pulse has to be controlled about one part in 10^4.

5. The capability to measure the qubit state is necessary. The read-out operation is the result of the quantum measurement. It is useful for the measurement to have high quantum efficiency (at least 50%). If it is lower, multiple copies of the system are running simultaneously to reduce the possible errors.

1.6. Quantum dots as qubit

Loss and DiVincenzo proposed a qubit system formed from the spin states $|\uparrow\rangle$ and $|\downarrow\rangle$ of an electron confined in a quantum dot [8]. This proposal is quite general, since it can be applicable in any confined structure. The quantum dot structure is realized from a two-dimensional electron gas (2-DEG) in which the electrons are confined in small islands by the voltage applied on the metallic gates, as shown schematically in Fig. 1.2. The number of electrons can be determined by Coulomb

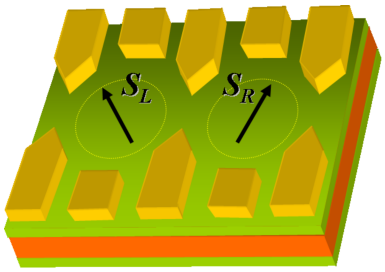

Figure 1.2.: Two electron spins in coupled quantum dots as proposed by Loss and DiVincenzo [8]. The top gates define the lateral confinement and are used also to tune the interaction between them.

blockade measurements and the spin states can be controlled by external magnetic fields. Furthermore, since this is based on a solid state device, it is also possible to form quantum dots arrays by an extension of the picture. This physical system is very fascinating, since it fulfills all the five DiVincenzo criteria, as we will see below.

Criterion 1. This is naturally satisfied by a genuine spin-1/2 system, which by its nature has a doubly-degenerate ground state to serve as qubit. The size of the dot should be small enough to avoid the possibility to occupy the next higher levels. Finally the extension of this simple picture can be done to obtain a quantum dot array.

Criterion 2. To initialize the state is relatively straightforward, but involves an additional magnetic field. In a magnetic field $\mathbf{B} = (0, 0, B_z)$ the degenerate ground state splits into two levels by the Zeeman interaction. The energy difference is $E_Z = g\mu_B\hbar B_z$, with Landé factor $g = -0.44$ for GaAs and μ_B the Bohr magneton. This is the two level system used as qubit. The initial state can be addressed by allowing the electron spin to reach its thermodynamic ground state at low temperature T, with $|E_Z| \gg k_B T$ (with Boltzmann constant k_B).

Criterion 3. A lot of attention has been devoted in fundamental mesoscopic device to characterize the source of decoherence of electrons in small structures. The spin coherence time can be completely different from the charge coherence times but, in some circumstances, it can be orders of magnitude larger. This is the main motivation of Loss-DiVincenzo spin qubits proposal. This is the most difficult task to achieve. Furthermore the decoherence time τ_ϕ is not the only parameter which determines the goodness of a quantum computer. The amount of coherent computation which can be performed depends on the ratio τ_ϕ/τ_s, where τ_s denotes the switching time of the computer.

Criterion 4. The qubit states can be manipulated with an ac magnetic field applied in the dot plane. The Hamiltonian used for the gate operations is

$$H(J, \mathbf{B}_1, \mathbf{B}_2) = J(t)\boldsymbol{\sigma}_1 \cdot \boldsymbol{\sigma}_2 + \mu\mathbf{B}_1(t) \cdot \boldsymbol{\sigma}_1 + \mu\mathbf{B}_2(t) \cdot \boldsymbol{\sigma}_2, \tag{1.40}$$

where J is the exchange energy. Each spin is coupled to the local magnetic field $\mathbf{B}_i$ by the Zeeman interaction proportional to the magnetic moment $\mu = (g/2)\mu_B$. The coupling between the electrons depends on the potential barrier between them. It can be controlled by voltages applied on the top-gates.

Criterion 5. A lot of progresses have been done to improve the read-out techniques. Two read-out schemes exist, one for a single quantum dot with $|\uparrow\rangle$, $|\downarrow\rangle$ as qubit states, and one with the singlet $|S\rangle$ and the triplet $|T_0\rangle$ state of a two-electron quantum. Both schemes have in common that the spin state is first converted into a charge state, which is then detected by the current through an adjacent quantum point contact (QPC). More details are given in the next chapter.

2. Quantum Dots (QD)

In this chapter we review how the quantum dot is realized between the interface of two semiconductors and show relevant experimental results. We first discuss the two dimensional electron gase and the fabrication of the quantum dot system based on the GaAs heterostructures. We comment on the choice of the parabolic shape potential for modeling the two dimensional confinement. In the last part different scheme of read-out measurements are given, togheter with the details of the gate operation.

2.1. Two dimensional electron gas (2-DEG)

The recent developments of the fabrication and growing techniques for the nanostructures, allow to create electronic devices where the electrons are confined in a region of the order of nanometers, the quantum dots [37] [38] [9]. The quantum dot is a small island on a semiconductor structure, which can be filled with electrons and controlled by an external voltage. The fabrication of lateral gated quantum dots starts with a semiconductor heterostructure, where two different materials are placed adjacent to each other (see Fig. 2.1a). These layers, in our case GaAs and AlGaAs, are grown on top of each other using molecular beam epitaxy (MBE), resulting in a very clean sample. By doping the n-AlGaAs layer with Si, free electrons are introduced. Due to different band gaps, the electrons start to be trapped in a potential well, with a quasi triangular shape. Approximating the electron states as $\Psi(x, y, z) = \phi(x, y)\chi(z)$, where $\chi(z)$ is the ground state of a Hamiltonian with the confinement potential of the heterostructure, one can replace all operators depending on the z variable by the quantum averaging. The electrons belonging to the quantum well are free of moving in the plane (indicates as xy plane), while the motion along the perpendicular direction z is inhibited (2D approximation). The two-dimensional electron gas is created. The motion along z is quantized and the energy can assume only discrete values E_j ($j = 0, 1, 2, ...$). In the effective mass approximation (we will discuss it in the next chapter), the energy E of an electron in the conduction band is

$$E = E_j + \frac{\hbar^2(k_x^2 + k_y^2)}{2m^*}. \tag{2.1}$$

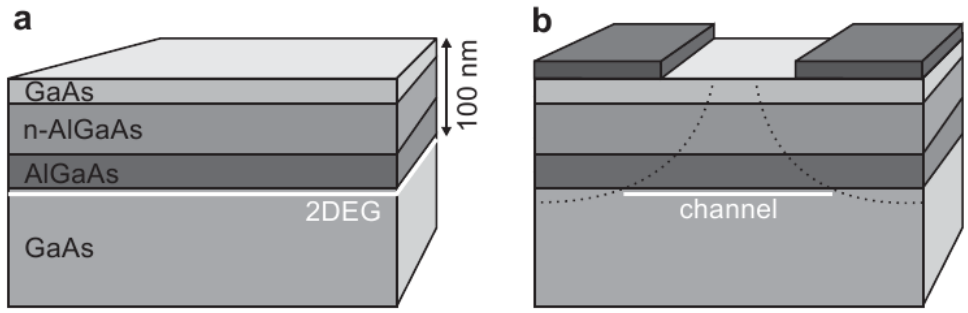

Figure 2.1.: Semiconductur heterostructure used to have a 2-DEG. a) In the white region, approximately 100 nm below the surface, between GaAs and AlGaAs a 2-DEG is formed. b) The metallic electrodes on the surface of the structure deplete locally the region to confine the electron in one and in zero dimensions as well. (source http://qt.tn.tudelft.nl/ lieven/ TU-Delft).

If the temperature is low enough and the energy separation between the lowest two states, E_1 and E_0, is larger than the Fermi energy, $E_{F0} = E_F - E_0$, the electrons are bound to move in the $j = 0$ subband. Finally on the top of the structure the gate pattern is defined (see Fig. 2.1b), to reduce again the confinement region.

2.2. Quantum dot fabrication

Lateral GaAs quantum dots are created from GaAs and AlGaAs heterostructure using electron-beam lithography. This allows to have complicated gate structures on the top of the semiconductor surface (Fig. 2.2). By applying negative voltages to the gates, the 2-DEG is locally depleted, creating one or more small islands from the large 2-DEG reservoirs. These islands are the quantum dots. Since the system is strongly confined, the level structure of each quantum dot is discrete. The level separation is smaller than the separation of the energies along the perpendicular direction. For example, given a simplified treatment, we can consider the well that confines the electron in the plane as

$$V(z) = \begin{cases} 0 & |z| < L/2 \\ V_0 & |z| > L/2 \end{cases}, \tag{2.2}$$

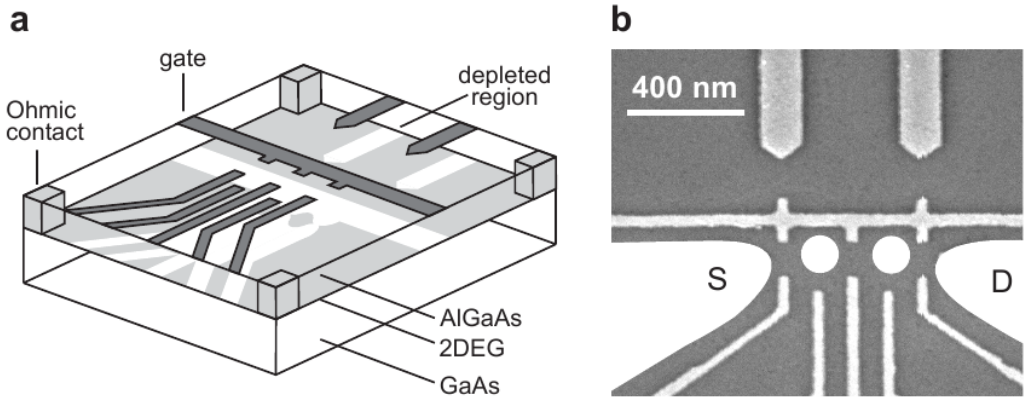

Figure 2.2.: a) Schematic view of a double quantum dot realized by metal surface gates. The grey region corresponds to the depleted region. The electron tunnels one by one controlled by the voltage on the gates. The Ohmic contact is connected to the measurement equipment. b) Scanning electron microscope image of a realistic device. The two circles indicate two quantum dots connected to source (S) and drain (D) reservoirs. The upper gates are used to create quantum point contacts. Ref. [39].

where L is the width of the well. The Hamiltonian is separated in the plane and the perpendicular direction

$$H = \left(-\frac{\hbar^2}{2m_e^*}\frac{\partial^2}{\partial z^2} + V(z)\right) + \left[-\frac{\hbar^2}{2m_e^*}\left(\frac{\partial^2}{\partial x^2} + \frac{\partial^2}{\partial y^2}\right) + V(x,y)\right], \tag{2.3}$$

where m_e^* is the effective mass of the electron. Choosing the solution in the form

$$\Psi(x,y,z) = \phi(x,y)\chi(z), \tag{2.4}$$

for the z component we have

$$\left(-\frac{\hbar^2}{2m_e^*}\frac{\partial^2}{\partial z^2} + V_0\right)\chi(z) = \epsilon\chi(z). \tag{2.5}$$

It is possible to have bound states (discrete levels) only if $\epsilon < V_0$. With the appropriate boundary conditions for the wavefunctions χ, we find periodic functions for the well. In the limit of infinitely deep well $V_0 \to \infty$, the energy is

$$\epsilon_n = \frac{\hbar^2\pi^2 n^2}{2m_e^* L^2}. \tag{2.6}$$

Using the realistic GaAs parameters and a width of $L \approx 1$nm, the level separation between the ground state and the first exited state is

$$\Delta = \frac{\hbar^2 \pi^2}{2 m_e^* L^2} \approx 5 \text{ eV}. \tag{2.7}$$

This value is much larger than the level separation in the (x, y) plane, which is of the order of several meV. In the typical experiment, the temperature is below 1K, which corresponds to $E \approx 0.08$ meV. In this way we ensure that the only occupied state along z is the ground state, since the thermal energy does not allow transitions to higher states. Hence the wavefunction along z is $\chi(z)$, for each $\phi(x, y)$.

2.3. Confinement potential

In quantum dots the lateral confinement $V(x, y)$ allows to reduce the electron motion initially free to move in a 2-DEG. Usually the shape is like a disk with lateral dimensions larger than the thickness of the 2-DEG plane. The lateral confinement of the quantum dot is quite similar to the Coulomb potential, which bounds the electron in an atom. For this reason they are called also artificial atoms. Since the shape of the inplane confinement strongly depends on the fabrication of the dot and on the gate voltages, the lateral confinement potential is approximated by simple models. Only a comparison to the experiments answers which model is a good description.

In the case of a very small quantum dot, when the lateral dimension is of the same order as the characteristic length of the variation of the confinement potential, a good approximation is a Gaussian well,

$$V(\vec{r}) = -V_0 \exp(-r^2/L^2), \tag{2.8}$$

or also Pösschl-Teller potential,

$$V(\vec{r}) = -V_0 \cosh^{-2}(-r^2/L^2). \tag{2.9}$$

In most of realistic cases a satisfactory model for the quantum dots is the parabolic shape potential

$$V(\vec{r}) = V_0 + kr^2. \tag{2.10}$$

Observing the position of the absorption resonance picks for a far-infrared radiation and its independence on the number of the electrons in quantum dots (as consequence of the Kohn theorem) [40], the conclusion is that the potential Eq. (2.10) can be used as a good model.

Kumar et *al.* [41] determinated the effective single-particle confinement for a square-shaped quantum dot. They used a self-consistent Hartree approach, where the

electrostatic confinement was incorporated by a self-consistent solution of the combined Hartree and Poisson equations. They found that in the limit of small particle numbers, the effective confinement can have a symmetry very close to circular, even if the confinement was formed by a square-shaped gates. On the basis of their work, the simple isotropic harmonic oscillator was adopted as the standard quantum dot model potential for electronic structure calculations, in both exact diagonalization and mean-field approaches.

2.4. Coulomb blockade

The transport properties in quantum dots are studied by connecting it with a nearby gate which controls the voltage across the system. The number of electrons can be modified and measured showing peaks in the conductance. The electron charge e in the confined island is quantized and the transport is regulated by the Coulomb blockade. Let us suppose to have a dot with N electrons. The energy to add an additional electron is $\mu(N+1)$, where μ is the chemical potential inside the dot. This is defined as the difference between the energy of the dot with $N+1$ and N electrons

$$\mu(N+1) = U(N+1) - U(N). \tag{2.11}$$

If one electron leaves the dot, the energy released is equal to $\mu(N)$. One can estimate the energy U by using a simple electrostatic model for non interacting electrons. It is given by

$$U(N) = C^{-1}(-eN + C_g V_g)^2, \tag{2.12}$$

where C_g is the dot capacitance, V_g is the gate voltage and C is the total dot capacitance. Tuning the gate voltage, the discrete values of the chemical potential shifts and can be in resonance with the chemical potential of the reservoir. Therefore one electron can tunnel off from the dot or tunnel in from the reservoir.

Let us suppose the dot is connected to a reservoir with chemical potential μ_S. If $\mu(N) > \mu_S$, the system can lower its energy allowing one electron to leave the dot. On the other hand, in the condition where $\mu(N+1) < \mu_S$ one electron can tunnel in the dot. The electrons will be hopping to and from the dot until the chemical potential of the dot and the reservoir gets adjusted. Furthermore the situation can change by applying an external voltage. If the dot is connected to the source and drain with chemical potential μ_S and μ_D, respectively, a transport window $\mu_S - \mu_D = -eV_{SD}$ opens up. If the dot chemical potential lies within the transport window, $\mu_S > \mu(N) > \mu_D$, the number of electrons inside the dot changes cyclically through $N \to N-1 \to N$. Once an electron leaves the dot into the drain, another electron

is coming in from the source and an electrical current is showing up. Similarly, if $\mu_S > \mu(N+1) > \mu_D$, the current flows in a cycle $N \rightarrow N+1 \rightarrow N$. However in the case none of the chemical potential, $\mu(N)$ and $\mu(N+1)$, are close to the bias window, the transport is inhibited, even if a voltage is applied. The mechanism of discrete charging and discharging of the dot leads to Coulomb blockade oscillations in the conductance as function of the gate voltage, as one can see in Fig. 2.4. The regions of the blocked current form so called Coulomb diamond, revealing many dot characteristics, such as the number of charges involved.

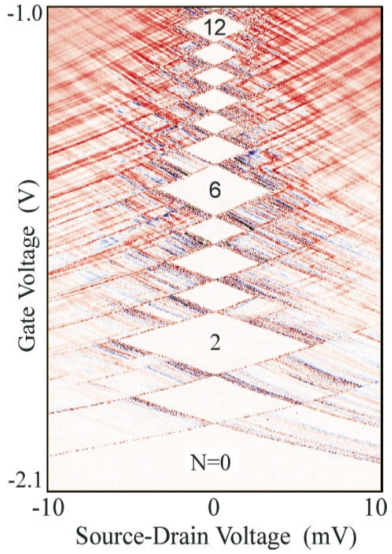

Figure 2.3.: Coulomb diamonds [42]. Differential conductance $\partial I/\partial V_{SD}$ plotted in color scale in the $V_g - V_{SD}$ plane at zero magnetic field. In the white diamond shaped regions $\partial I/\partial V_{SD} = 0$ due to Coulomb blockade. The number of electrons N is fixed in the diamond regions. The lines outside the diamonds running parallel to the sides, identify excited states in the dot or leads.

2.5. Single shot read-out

The spin measurement in quantum dots is important both for fundamental science and for the possible application in quantum computation. We focus on the single-shot read-out of a single electron spin, since the fidelity is close to 100% and only one copy of the state is needed for the measurement [43], [44], [45].

The magnetic moment of the electron spin is tiny, so it is very challenging to measure it directly. The spin state can be determined by a spin-to-charge conversion. Since the spin of the electron depends on the different charge states, measuring the charge on the dot, the spin can be determined. Experimentally two methods have been demonstrated to work. The first is the energy selective read-out (E-RO), where the difference in energy between the spin states is used for spin-to-charge conversion. The second spin-to-charge conversion can be achieved by exploiting the difference in tunnel rates of different spin states to the reservoir (TR-RO).

2.5.1. Energy selective read-out

The first experiment performed to measure a single spin state using the E-RO technique was done in the group of Kouwenhoven in Delft [11]. The measurement takes place in three steps: 1) empty the dot, 2) inject one electron with unknown spin, 3) measure the spin state. The particular steps are controlled by gate voltage pulses and an external perpendicular magnetic fields. The device used in the experiment is shown in Fig. 2.4. The dot is surrounded by a quantum point contact (QPC)

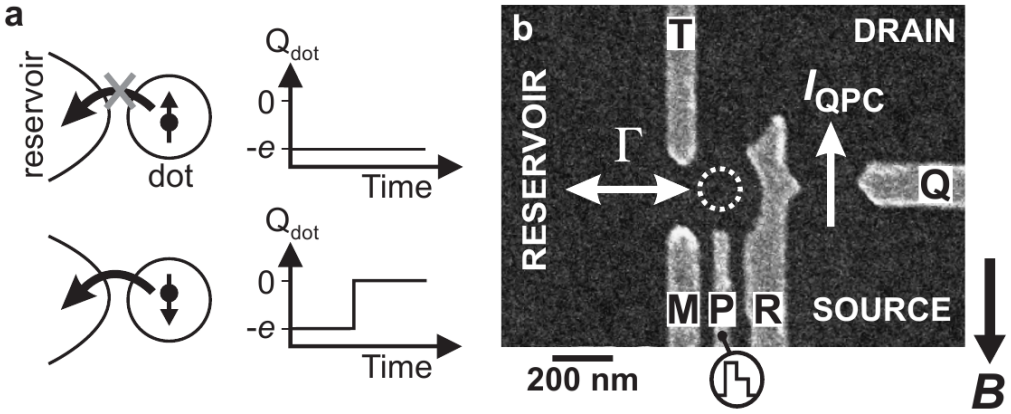

Figure 2.4.: Spin-to-charge conversion in a quantum dot coupled to a quantum point contact. a) Scheme of spin-to-charge conversion. The charge on the quantum dot, Q_{dot}, remains constant if the electron spin is $|\uparrow\rangle$, whereas a spin $|\downarrow\rangle$ electron can escape, thereby changing Q_{dot}. b) Scanning electron micrograph of the metallic gates on the surface of a GaAs/AlGaAs heterostructure. From Ref. [11].

used as charge detector. Since the conductance of the QPC has a step-like behavior depending on the voltage applied to the top gate, transport channels are opened one by one and the charge of the dot can be detected. The scheme of the shifting of the dot's levels is in Fig. 2.5.

Before the pulse, the dot is empty and the two spin states are above the electrochemical potential of the reservoir μ_{res}. When the voltage pulse is applied, the two levels are below μ_{res} and one electron is energetically allowed to tunnel into the dot. The typical time is $\approx \Gamma^{-1}$, where gamma is the tunneling rate. Since the electron is not defined before the tunneling process, the electron can be in either spin-up or spin-down state, as shown in the lower and upper diagram, respectively. During the time t_{wait} the electron is inside the dot and can not escape because of the Coulomb blockade. After that the voltage is reduced and the read-out takes place. As one

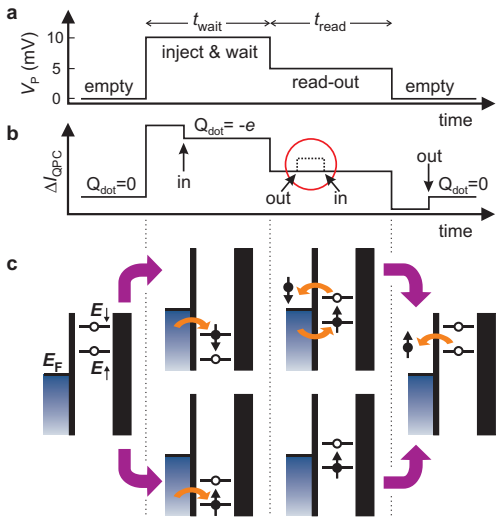

Figure 2.5.: Scheme of single-shot technique to measure the spin state [11]. a) The pulse voltage applied on the gate P. b) The schematic view of the quantum point contact conductance behavior. c) Energy levels of the quantum dot during the different stage of the pulse.

can see from the diagram, if the electron was in the spin-up state, since its energy level is still below μ_{res}, it remains in the dot, whereas the electron in the spin-down state tunnels out after a typical time $\approx \Gamma^{-1}$. After that one electron with spin-up can tunnel from the reservoir. Effectively, the spin on the dot has been flipped by a single electron exchange with the reservoir. After t_{read}, the pulse ends and the dot is empty again.

2.5.2. Tunneling rate selective read-out

The spin read-out scheme we present here is based on spin-to-charge conversion due to the difference in the tunneling rate between spin states [45]. This method is useful to determine singlet $|S\rangle$ and triplet $|T\rangle$ states of a quantum dot. Figure 2.6 shows the scheme of the measurement. The first requirement of that method is a higher difference in the tunneling rates between the two involved states. Let us assume that the tunnel rate, Γ_S, from the singlet state (which corresponds the the ground state in zero magnetic field) to the reservoir is much smaller than the tunnel rate of the higher triplet state, Γ_T, $\Gamma_T \gg \Gamma_S$. The difference in the rates originate in the fact that the triplet state is spatially more extended (being antisymmetric) than singlet, leading to a larger overlap with the states in the lead. Thus this method is not easy in the single electron case.

The first realization of tunneling selective read-out was done in the Delf group [45]. It starts with the situation where both states are above the electrochemical potential of the reservoir, Fig. 2.6. Both electrons are allowed energetically to tunnel out of the dot, regardless their spin. After a time $t = \tau$, where $\Gamma_S^{-1} \gg \tau \gg \Gamma_T^{-1}$, an electron can tunnel off the dot with higher probability, if it was in the triplet state. On the other

hand the electron in the singlet state has less probability to escape. Then, using a quantum point contact, the spin information is converted in charge information and one can determine the original spin state. The method was demonstrated to be flexible, since it works also when the energy splitting between the two states is quite small. Furthermore the relaxation rate can be obtained by fitting the exponential decay of the excited state population as a function of the duration of the waiting time.

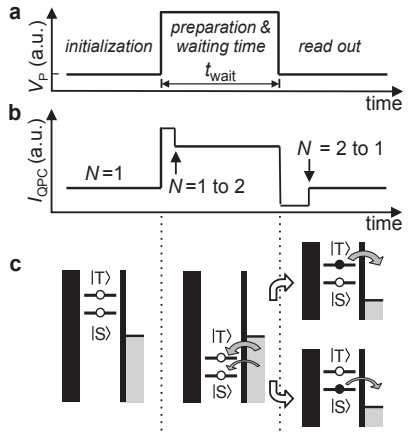

Figure 2.6.: Scheme of single-shot technique to measure the spin singlet $|S\rangle$ and triplet $|T\rangle$ states [45]. a) The pulse voltage applied on the gate P. b) The quantum point contact responce to the pulse. c) Energy diagram of the energy levels of the quantum dot during the different stage of the pulse.

2.6. Gate Operation on Quantum Dots

The manipulation of spins in quantum dots is very important, since it is one of the key elements to realize operations in the quantum computation processes. One has to be able to perform single spin rotation and two-spin swap operation. If a magnetic field is applied, the spin states are split by the Zeeman energy and the single spin rotation can be achieved using the electron spin resonance [46]. On the other hand, a rapid electrical control of the exchange interaction between two electron systems can realize a square-root swap operation [13].

In the experiment [13], a double dot system occupied by two electrons with controllable asymmetry ϵ is considered. The asymmetry parameter ϵ controls the detuning between the dots. Therefore in the case of very large detuning, the system is in the ground state of a single dot $S^{(0,2)}$. Since both electrons occupy one dot, the exchange interaction is high and the occupation of the triplet states can be neglected. On the other hand, if the detuning is small, the double dot configuration is reached and the electrons are each in one dot. The exchange energy is so small that the singlet $S^{(1,1)}$ and the triplets $T_0^{(1,1)}$, $T_+^{(1,1)}$ and $T_-^{(1,1)}$ can be considered as degenerate states. If a magnetic field is applied, the three triplets split. The states $S^{(1,1)}$ and $T_0^{(1,1)}$

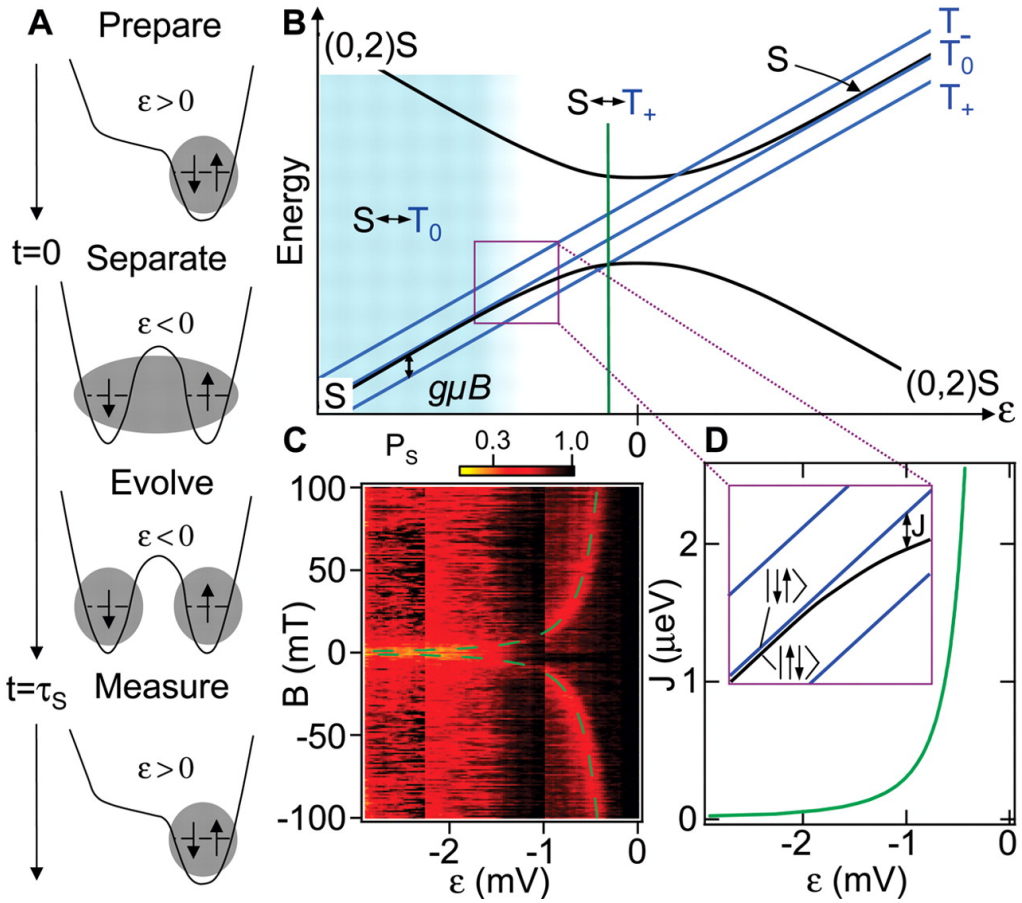

Figure 2.7.: Scheme of the voltage control of the exchange coupling for spin manipulation, according to Ref. [13]. a) Cycles of the experimental control of the spin states. b) Energy diagram near the (1,1)-to-(0,2) charge transition. c) Singlet propability in function of the detuning and the magnetic field. d) Extracted dependence of the exchange on detuning.

can be operated by projecting into/from the single dot singlet $S^{(0,2)}$ by adiabatically changing the detuning, Fig. 2.7. In the $|\uparrow\downarrow\rangle, |\downarrow\uparrow\rangle$ basis, one can operate in the following way. Starting from the state $|\uparrow\downarrow\rangle$ in the condition of zero exchange energy, the application of finite exchange for a time τ_E brings to a spin rotation along the z axis of the Bloch sphere, in the plane containing $|\uparrow\downarrow\rangle$ and $|\downarrow\uparrow\rangle$. The angle reads $\phi = J\tau_E/\hbar$ and in the case of $\phi = \pi$ the SWAP operation is performed, rotating the states from the $|\uparrow\downarrow\rangle$ to the $|\downarrow\uparrow\rangle$ configuration.

3. Single Electron Quantum Dots

In this chapter we give the main results of the influence of the spin-orbit interactions on the energy spectrum and the tunneling Hamiltonian in a single electron quantum dots. We first derive the effective mass approximation and how it is used to calculate the band structure of the GaAs semiconductor and then we introduce the spin-orbit coupling contributions, Bychkov-Rashba and Dresselhaus. The single electron spectrum in presence of a perpendicular magnetic field (Fock-Darwin energies) is studied for single and double quantum dot geometry. Finally the tunneling Hamiltonian, describing the lowest part of the energy spectrum, is presented.

3.1. Effective mass approximation

An electron in a solid is moving in the potential field generated from the positive charges of the ions and and from all other electrons presented in the bulk [47]. This field is called crystal potential. In the independent electron approximation, these interactions are represented by an effective one-electron potential $W(\mathbf{r})$. The problem now turns to find a suitable form for that potential which describes the system. One can deduce one important property in the periodicity of the crystal potential over the lattice distance. Considering the three vectors of the Bravais lattice, $\mathbf{a}_i$, $i = 1, 2, 3$, we have

$$W(\mathbf{r} + \sum_i n_i \mathbf{a}_i) = W(\mathbf{r}), \tag{3.1}$$

where $\mathbf{r}$ is the position vector of a point in the crystal and n_i are integer numbers. The Schrödinger wave equation for a single particle in a periodic potential is

$$H_{cr}\psi(\mathbf{r}) = \left(-\frac{\hbar^2}{2m}\nabla^2 + W(\mathbf{r})\right)\psi(\mathbf{r}) = E\psi(\mathbf{r}), \tag{3.2}$$

where m is the electron free mass and H_{cr} represents the Hamiltonian of the crystal.

Because of the periodicity of the potential, Eq. (3.1), it is possible to show that the wavefunction $\psi(\mathbf{r})$ is in the form (Bloch's theorem)

$$\psi(\mathbf{r}) = e^{-i\mathbf{k}\cdot\mathbf{d}}\psi(\mathbf{r} + \mathbf{d}) = e^{i\mathbf{k}\cdot\mathbf{r}}u_{\mathbf{k}}(\mathbf{r}), \tag{3.3}$$

with

$$u_{\mathbf{k}}(\mathbf{r}) = e^{-i\mathbf{k}\cdot(\mathbf{r}+\mathbf{d})}\psi(\mathbf{r}+\mathbf{d}), \tag{3.4}$$

where $\mathbf{k}$ is a constant vector, $\mathbf{d} = \sum_i n_i \mathbf{a}_i$ is the translation vector over the lattice. One can note that the Bloch functions $u_{\mathbf{k}}(\mathbf{r})$ are periodic and of the type

$$u_{\mathbf{k}}(\mathbf{r}+\mathbf{d}) = u_{\mathbf{k}}(\mathbf{r}). \tag{3.5}$$

Hence, the stationary single particle wave function in the crystal potential is a plane wave modulated by the Bloch function and the period is the lattice spacing. The vector $\mathbf{k}$ is the wave vector of the electron in the lattice. The wave vector is one of the quantum numbers, which characterize the electron state.

Enforcing the boundary conditions to be periodic over the lattice with N_i number of periods along the direction $\mathbf{a}_i$,

$$\psi(\mathbf{r}+N_i\mathbf{a}_i) = \psi(\mathbf{r}) \qquad N_i \to \infty, \tag{3.6}$$

one can find the following condition for the wave vector $\mathbf{k}$:

$$\mathbf{k}\cdot\mathbf{a}_i N_i = 2\pi n_i \qquad n_i = 1, 2, 3, ..., N_i. \tag{3.7}$$

The values of $\mathbf{k}$ form the first Brillouin zone of the crystal. It is important to note that the symmetry of the Brillouin zone is determined by the symmetry of the crystal structure of the solid.

Denoting $E = E(\mathbf{k})$ the single particle energy dispersion corresponding to the wave vector $\mathbf{k}$, when $\mathbf{k}$ changes within the first Brillouin zone, we have a continuous of energy states, which correspond to an energy band. For a fixed value of $\mathbf{k}$, the Hamiltonian Eq. (3.2) has solutions in the Bloch form

$$\psi_{\alpha\mathbf{k}}(\mathbf{r}) = \frac{1}{\sqrt{V}} e^{i\mathbf{k}\cdot\mathbf{r}} u_{\alpha\mathbf{k}}, \tag{3.8}$$

where the index α indicates the energy bands, $V = NV_0$ is the volume of the crystal with $N = N_1N_2N_3$ and V_0 correspond to the number and the volume of the primitive cell, respectively. The normalization condition gives

$$\frac{1}{V_0}\int_{V_0} |u_{\alpha\mathbf{k}}|^2 d\mathbf{r} = 1, \tag{3.9}$$

where the integration is over a primitive cell. The Bloch functions on different band α and wave vector $\mathbf{k}$ are orthogonal. The Bloch functions fulfill the following equation

$$\left[-\frac{\hbar^2}{2m}\nabla^2 - i\frac{\hbar^2}{m}(\mathbf{k}\nabla) + W(\mathbf{r})\right] u_{\alpha\mathbf{k}} = \left[E_\alpha(\mathbf{k}) - \frac{\hbar^2 k^2}{2m}\right] u_{\alpha\mathbf{k}}. \tag{3.10}$$

Due to the periodicity of the crystal, the Bloch function can be computed within the first Brillouin zone.

To find the function $u_{\alpha\mathbf{k}}$ and the energy $E_\alpha(\mathbf{k})$, one should know the effective form of the crystal potential $W(\mathbf{k})$. However most of the electronic properties in a crystal can be obtained knowing these quantities only in a short interval of $\mathbf{k}$ close to the boundary point of the energy band. Choosing $E_\alpha(\mathbf{k})$, $\mathbf{k} = 0$, we can derive from the Eq. (3.10),

$$[H(\mathbf{k}=0) + w(\mathbf{k})]u_{\alpha\mathbf{k}} = E_\alpha(\mathbf{k})u_{\alpha\mathbf{k}}, \tag{3.11}$$

where

$$H(\mathbf{k}=0) = -\frac{\hbar^2}{2m}\nabla^2 + W(\mathbf{r}), \tag{3.12}$$

is the Hamiltonian with eigenfunctions given by $u_{\alpha,0}$,

$$H(\mathbf{k}=0)u_{\alpha 0} = E_\alpha(0)u_{\alpha 0}, \tag{3.13}$$

$$w(\mathbf{k}) = -i\frac{\hbar^2}{m}(\mathbf{k}\nabla) + \frac{\hbar^2\mathbf{k}^2}{2m} \to 0, \qquad \text{for } \mathbf{k} \to 0. \tag{3.14}$$

In this way, for small wave vectors $\mathbf{k}$ the term $w(\mathbf{k})$ can be treated as small perturbation.

The Bloch functions can be expanded in series as follows

$$u_{\alpha\mathbf{k}}(\mathbf{r}) = \sum_{\alpha'} C_{\alpha'}(\mathbf{k})u_{\alpha,0}(\mathbf{r}). \tag{3.15}$$

Placing this expansion in the Eq. (3.10), multiplying by the complex conjugate $u^*_{\alpha,0}(\mathbf{r})$ and integrating over a primitive cell, we have

$$\sum_{\alpha'}\left[\left(E_{\alpha'}(0) - E_\alpha(\mathbf{k}) + \frac{\hbar^2\mathbf{k}^2}{2m}\right)\delta_{\alpha\alpha'} + \frac{\hbar\mathbf{k}}{m}\boldsymbol{\pi}_{\alpha\alpha'}\right]C_{\alpha'}(\mathbf{k}) = 0, \tag{3.16}$$

where

$$\boldsymbol{\pi}_{\alpha\alpha'} = \int_{V_0} u^*_{\alpha 0}(\mathbf{r})(-i\hbar\nabla)u_{\alpha',0}(\mathbf{r}). \tag{3.17}$$

Having a small $\mathbf{k}$, one can calculate the energy correction to the eigenvalue $E_\alpha(0)$ using the perturbation theory. Therefore, choosing $C_{\alpha'}(0) = \delta_{\alpha\alpha'}$,

$$C_{\alpha\neq\alpha'} = \frac{\hbar\mathbf{k}\cdot\boldsymbol{\pi}}{m}\frac{1}{E_\alpha(0) - E_{\alpha'}(0)}, \tag{3.18}$$

$$E_\alpha(\mathbf{k}) = E_\alpha(0) + \frac{\hbar^2k^2}{2m} + \frac{\hbar^2}{m^2}\sum_{\alpha'}\frac{|\mathbf{k}\cdot\boldsymbol{\pi}|^2}{E_\alpha(0) - E_{\alpha'}(0)}. \tag{3.19}$$

The last equation can be rewritten as

$$E_\alpha(\mathbf{k}) = E_\alpha(0) + \frac{\hbar^2}{2}\left(\frac{1}{m^*}\right)_{ik} k_i k_k, \tag{3.20}$$

where a reciprocal tensor of the effective mass has been inserted, $(1/m^*)_{ik}$. This tensor describes the properties of the electronic band α close to the point $\mathbf{k} = 0$. The tensor is symmetry dependent. Indeed for isotropic system, we have

$$\left(\frac{1}{m^*}\right)_{ik} = \frac{1}{m^*}\delta_{ik}, \qquad \frac{1}{m^*} = \frac{1}{m} + \frac{2}{m^2}\sum_{\alpha'}\frac{|\boldsymbol{\pi}|^2}{E_\alpha(0) - E_{\alpha'}(0)}, \tag{3.21}$$

which corresponds to the quadratic dispersion of the electron energy close to the boundary of $E_\alpha(\mathbf{k})$ at $\mathbf{k} = 0$.

The effective mass of the system is determined by the matrix elements in Eq. (3.17) and the distance between the given band and the other bands. Usually the largest contribution is given close to the boundary of the band. In particular, close to a minimum of the band α, the closest band α' is that with $E_{\alpha'}(0) < E_\alpha(0)$. From the Eq. (3.21) follows that the dominant contribution is given by the positive effective mass. For the conduction band with a non-degenerate minimum at $\mathbf{k} = 0$, the electron energy is given by

$$E_e = E_c(0) + \frac{\hbar^2\mathbf{k}^2}{2m^*}, \tag{3.22}$$

where m^* is the effective electron mass. On the other hand, close to the maximum of $E_\alpha(\mathbf{k})$, the main contribution comes from the upper band and it is negative. Therefore the effective electron mass close to a maximum in the energy band is negative.

3.2. Energy dispersion of GaAs semiconductor

GaAs is a III-V compound semiconductor. It has a zincblend crystal structure, composed by two sublattices of FCC type, displaced on the diagonal. The band structure reveals a direct gap semiconductor, where the minimum of the conduction band is over the maximum of the valence band, see Fig 3.1. The electrons in a GaAs quantum dot belong to the conduction band of the semiconductor. The density of the electrons inside this band is quite low, indeed the average distance between them is of order of 10 nm. Accordingly the effects due to the lattice and the other bands can be taken into account using the effective mass approximation. The electrons in the conduction band in a quantum dot form an interacting electron system with effective mass m^*. Furthermore the Coulomb interaction is screened by the core electrons and the ions, so we have to consider also a screened dielectric constant. The quantum

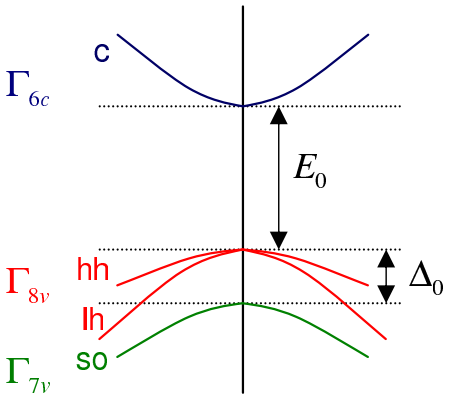

Figure 3.1.: Schematics of a III-V semiconductor band structure. Symbols indicate conduction (c), heavy-hole (hh), light-hole (lh), and spin-off (so) bands. E_0 indicates the band gap of the semiconductor and Δ_0 is the energy shift due to the spin-orbit coupling [48].

dot Hamiltonian, not considering the interaction to the environment, is usually given as a sum of the single dot Hamiltonian and the Coulomb interaction

$$H = \sum_{i=1}^{N} \left(\frac{\hbar^2 \mathbf{K}_i^2}{2m^*} + V(\mathbf{r}_i) \right) + \sum_{i,j=1;\, i<j}^{N} \frac{e^2}{4\pi\varepsilon\varepsilon_0 |\mathbf{r}_i - \mathbf{r}_j|}, \tag{3.23}$$

where $V(\mathbf{r})$ is the confinement potential, m^* is the effective mass and ε is the dielectric constant. Within the effective mass approximation it is possible to describe semiconductor quantum dots made of GaAs or InAs. The band structure has a minimum at $\mathbf{k} = 0$. The dispersion $E(\mathbf{k})$ is approximately parabolic and isotropic for the states with few meV of energy around the conduction band minimum. Indeed we have

$$E(\mathbf{k}) \approx E(0) + \frac{\hbar^2 \mathbf{k}^2}{2m^*}, \tag{3.24}$$

where m^* is the effective mass around the minimum $\mathbf{k} = 0$. In the following table we list the structural parameters for both materials [37].

	m^*	ϵ
GaAs	$0.067m_e$	12.9
InAs	$0.024m_e$	14.6

Table 3.1.: Effective mass and dielectric constant for GaAs and InAs heterostructures. m_e is the free electron mass.

3.2.1. Spin-orbit coupling

In quantum dots the heterostructure confinement is much larger than the dot in-plane confinement. Therefore one can separate the motion into the in-plane and

perpendicular component by averaging along the $\hat{z}$ direction to get the Hamiltonian in Eq. (3.23). Furthermore, since the momentum operator $\hbar\mathbf{K} = -i\hbar\boldsymbol{\nabla} + e\mathbf{A}$ includes the vector potential $\mathbf{A} = -(1/2)\mathbf{r} \times \mathbf{B}$, the in-plane magnetic field has no orbital effects–only the perpendicular magnetic field B_z survives the z averaging in the Hamiltonian.

In a semiconductor the electron feels a relativistic effect due to the motion in an electric field, the spin-orbit interaction. The electric filed is due to the crystal potential generated by the nuclei. The periodic crystal potential felt by the electrons creates a magnetic field, which couples the electron spin via the magnetic moment. In general, the spin-orbit interaction has the following form

$$H_{so} = \frac{\hbar}{4m_e^2c^2}\mathbf{p} \cdot (\boldsymbol{\sigma} \times \nabla V), \tag{3.25}$$

where $\mathbf{p}$ is the momentum operator, m_e is the free electron mass, c is the speed of light, $\boldsymbol{\sigma}$ is the vector of the Pauli matrices and V is the electric potential.

The spin-orbit interaction has a relativistic nature and the correction to the energies are of order of $(1/c^2)$. This is quite small contribution if the electron in moving in the vacuum. In the solid state physics the spin-orbit interaction plays a relevant role, since the band structure can be modified a lot, see Fig. 3.1. In particular the crystal potential causes a large value for $\nabla V(\mathbf{r})$, since it is a periodic oscillating field.

In GaAs and InAs semiconductors, the spin-orbit interaction is due to the bulk inversion asymmetry of the zincblende crystal, called *Dresselhaus* [49]. In other bulk materials, such as silicon or diamond, the Dresselhaus spin-orbit coupling is absent, even if the crystal structure is equivalent, since it consists of two equivalent atoms. For a coordinate system (x, y, z) along the crystallographic axes, the Dresselhaus Hamiltonian is proportional to the third power of the momentum and it is in the form

$$H_D = \gamma_c \boldsymbol{\kappa} \cdot \boldsymbol{\sigma}, \tag{3.26}$$

where γ_c is the strength of the interaction, which depends on the material parameter. The vector $\boldsymbol{\kappa}$ has the following components: $\kappa_x = k_x(k_z^2 - k_y^2)$ (the other components are obtained by cyclical permutations). In a two dimensional electron gases, since we work in a two dimensional approximation, one has to average along $\hat{z}$ also the Hamiltonian in Eq. (3.26). Therefore the Dresselhaus spin-orbit coupling reads as

$$\mathbf{H}_D = \gamma_c\langle K_z^2\rangle(-K_x\sigma_x + K_y\sigma_y), \tag{3.27}$$

$$\mathbf{H}_{D3} = \gamma_c/2(K_xK_y^2\sigma_x - K_yK_x^2\sigma_y) + \text{H.c.}, \tag{3.28}$$

here H.c. denotes the Hermitian conjugate. The two terms differ form the dependence in the momentum, one is linear and the other one is cubic.

In a two dimensional electron gases another contribution to the spin-orbit coupling appears. The quantum well realized between the interface of two semiconductors is not symmetric, giving the *Bychkov-Rashba* spin-orbit coupling [50]. This interaction can be obtained from the Eq. (3.25) assuming ∇V as an electric field along the quantization axis. Furthermore an additional external electric field along the $\hat{z}$ direction influences the coupling. In this way, one is able to tune the strength of the interaction. The Bychkov-Rashba spin-orbit Hamiltonian reads

$$H_{BR} = \alpha_{BR}(K_y\sigma_x - K_x\sigma_y), \tag{3.29}$$

where α_{BR} is the spin-orbit strength. Equations (3.27-3.29) are for x=[100] and y=[010] direction [48].

3.3. Fock-Darwin spectrum

The electronic structure of a quantum dot system in a magnetic field **B** shows quite interesting properties. Now we want to calculate the energy spectrum of one electron confined in a two dimensional parabolic potential. The Hamiltonian, without considering the spin dependent part (Zeeman and spin-orbit interactions) is

$$H = \frac{1}{2m}(\hbar\mathbf{k} + e\mathbf{A})^2 + \frac{\hbar^2}{2ml_0^4}\mathbf{r}^2, \tag{3.30}$$

where m is the effective mass of the electron, l_0 is the confinement length, $\mathbf{k} = -i\boldsymbol{\nabla}$ is the kinetic momentum and $\mathbf{A} = B/2(y, -x, 0)$ is the vector potential. Since the problem has a cylindrical geometry, it is easy to show that $[H, l_z] = 0$, where $l_z = -i\hbar(x\partial_y - y\partial_x)$ is the angular momentum. Therefore the Hamiltonian can be rewritten as

$$H = \frac{(-i\hbar\boldsymbol{\nabla})^2}{2m} + \frac{e}{2m}Bl_z + \left(\frac{e^2B^2}{8m} + \frac{\hbar^2}{2ml_0^4}\right)\mathbf{r}^2. \tag{3.31}$$

Since it is a two dimensional problem, it is useful to represent the Hamiltonian in cylindrical coordinates (r, ϕ). Therefore we have

$$H = \frac{\hbar^2}{2m}\left[\frac{1}{r}\frac{\partial}{\partial r}\left(r\frac{\partial}{\partial r} + \frac{1}{r}\frac{\partial^2}{\partial\phi^2}\right)\right] - \frac{i\hbar eB}{2m}\partial\phi + \frac{\hbar^2}{2ml_B^4}r^2, \tag{3.32}$$

where $l_B = [l_0^{-4} + B^2e^2/4\hbar^2]^{-1/4}$ is the magnetic length. The Schrödinger equation for the Hamiltonian Eq. (3.32) can be separable in the angle and radial coordinates defining the wavefunction

$$\psi_{nl} = \exp(il\phi)R_{nl}(r). \tag{3.33}$$

The eigenfunctions of the Hamiltonian in Eq. (3.32) are called Fock-Darwin states

$$\psi_{nl}(r,\phi) = \frac{1}{\sqrt{\pi} l_B} C_{nl} \left(\frac{r^2}{l_B}\right)^{|l|} e^{-\frac{r^2}{2l_B^2}} \mathcal{L}_n^{|l|}\left(\frac{r^2}{l_B^2}\right) e^{il\phi}, \tag{3.34}$$

where $\mathcal{L}_n^{|l|}$ represents the associated Laguerre polynomials [51] and $C_{ln} = \sqrt{n!/(n+|l|)!}$ is the normalization factor. The states are labeled by the principal quantum number n, a nonnegative integer, and the orbital quantum number l, an integer. This last number corresponds to the value of the z component of the angular momentum. The corresponding Fock-Darwin levels are

$$\epsilon_{nl} = \frac{\hbar^2}{m l_B^2}(2n + |l| + 1) + \frac{\hbar e B}{2m} l. \tag{3.35}$$

The Fock-Darwin energies are shown in Fig. 3.2. In the case of zero magnetic field, the spectrum corresponds to decoupled harmonic oscillators, whose levels are separated by $\hbar^2/ml_0^2$. Increasing the magnetic field, the Landau levels appear. They form groups with the same value of the angular momentum.

3.4. Double-dot states

The confinement potential we use for a double quantum dot is represented by (see Fig. 3.3)

$$V(\mathbf{r}) = \frac{\hbar^2}{2ml_0^4} \min\{(x-d)^2 + y^2, (x+d)^2 + y^2\}. \tag{3.36}$$

Here $2d$ corresponds to the distance between the two minima of the parabolas shifted along the $\hat{x}$ direction. Changing the interdot distance one can turn to a single dot configuration to a double dot. For very large d, the potential Eq. (3.36) represents two isolated quantum dots. We choose such kind of confinement, Eq. (3.36), since with one parameter it is possible to tune the shape of the potential. This can be controlled experimentally by applying a negative potential on the gate between the two dots.

The Schrödinger equation of an electron with this potential does not have analytical solution. This is why we have developed numerically exact method to get the eigenstates. Furthermore, using some analytical approximations, one is able to investigate the main properties of the system, both in the weak and strong coupling regimes.

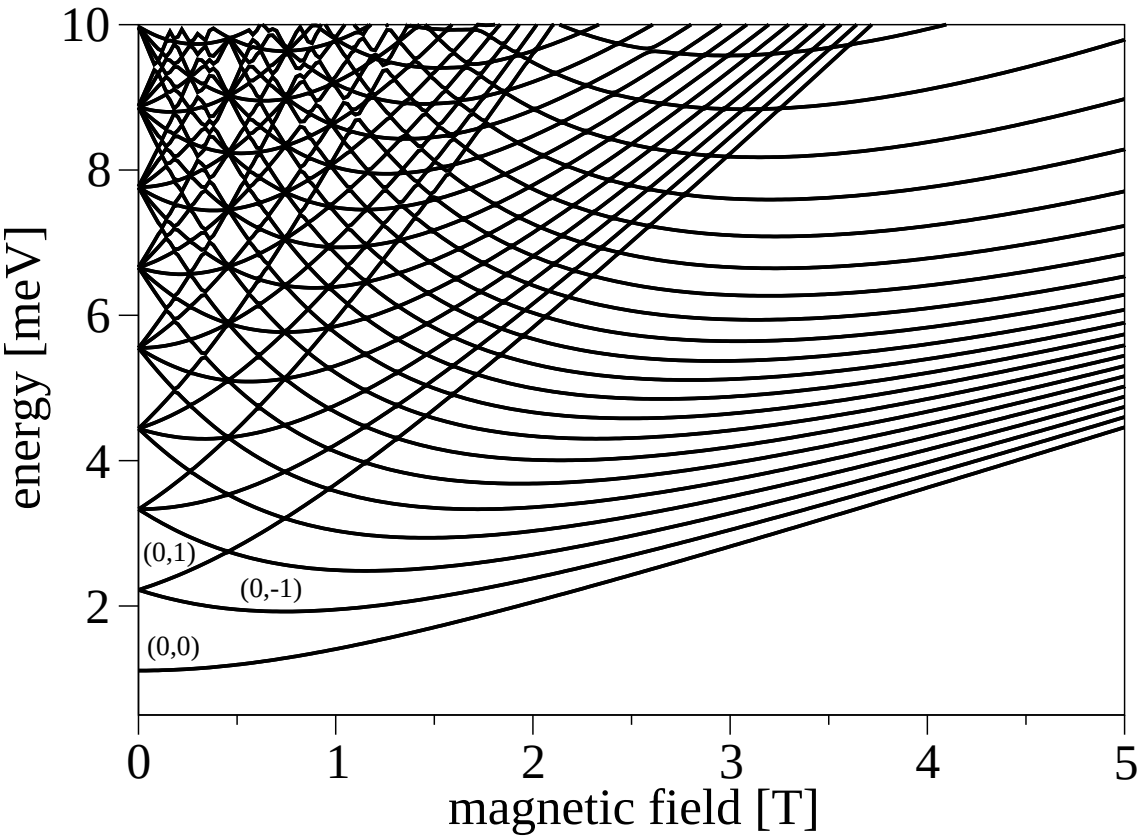

Figure 3.2.: Single particle Fock-Darwin spectrum in a perpendicular magnetic field. The confinement length is $l_0 = 32$ nm. The lowest states are labeled by the quantum number (n, l).

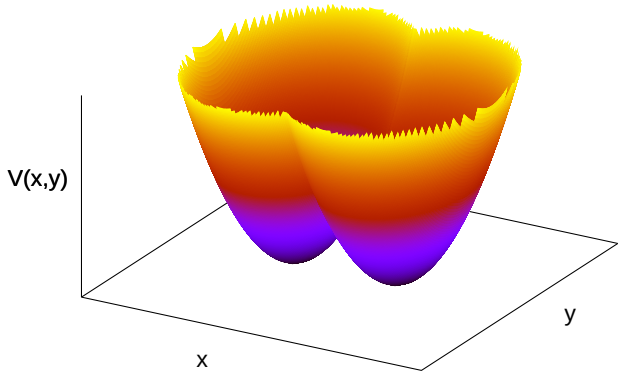

Figure 3.3.: Confinement potential in the double dot model.

3.4.1. LCAO approximation

One of the most used approximations to determine the eigenstates of a molecular system is the LCAO (linear combination of atomic orbitals). The double dot configuration can be thought as a diatomic molecule, whose potential corresponds to the confinement potential Eq. (3.36). Since the solution of the single dot configuration is known as the Fock-Darwin spectrum, for large interdot distance we also know the system eigenstates, corresponding to the Fock-Darwin functions located at potential minima. Each state is twice degenerate, as the left and right isolated dots are identical. In the intermediate regime, but still large compared to the confinement length l_0, we expect that the system eigenstates can be close to a certain combination of the single dot solution. However one can construct quite a good approximation using linear combinations of Fock-Darwin states shifted along $\hat{x}$ direction, $\psi_{00}(x \pm d, y)$.

Our choice of the potential allows us to exploit the symmetries of the double quantum dot structures. This is the symmetry group of the rectangle and is called C_{2v} [52]. This helps us to construct a better combination of the single dot states, according to the symmetry classes. We construct the lowest two double dot electron wavefunctions as the symmetric and the antisymmetric combination of the left and right wavefunction

$$\begin{aligned} \psi_+ &= \frac{1}{\sqrt{2}} \frac{1}{\sqrt{1+\Omega}} (\psi_{00}(x-d, y) + \psi_{00}(x+d, y)), \\ \psi_+ &= \frac{1}{\sqrt{2}} \frac{1}{\sqrt{1-\Omega}} (\psi_{00}(x-d, y) - \psi_{00}(x+d, y)). \end{aligned} \tag{3.37}$$

Here Ω is the overlap between the left and right functions. With the wavefunctions in Eq. (3.37), we can obtain the energy as the expectation value of the Hamiltonian,

$$\epsilon_\pm = \langle \psi_\pm | H | \psi_\pm \rangle. \tag{3.38}$$

In the experiments, one can measure the tunneling energy of the system from the frequency of oscillations of the dots population. In our analytical approximation, we compute the tunneling energy as

$$T = \frac{1}{2}(\epsilon_- - \epsilon_+) = \frac{\hbar^2}{m l_0^2} \frac{2d}{\sqrt{\pi} l_0} e^{-4d^2/l_0^2}, \tag{3.39}$$

where we assume large interdot distance. Figure 3.4 shows the calculated tunneling energy as a function of the interdot distance.

Close to the single dot configuration, the calculated tunneling energy in the simplified LCAO approximation, Eq. (3.39), fails badly with the numerics, while for large interdot distance it is better, as we expected. Furthermore a non-simplified LCAO result is an excellent approximation at all interdot distances.

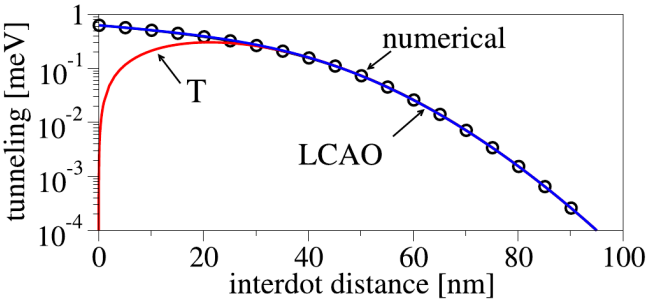

Figure 3.4.: Tunneling energy as a function of the interdot distance for zero magnetic field. The label T corresponds to the Eq. (3.39).

3.4.2. Tunneling Hamiltonian

Considering the qubit space, we are interested in the lowest part of the spectrum. Now we want to derive an effective Hamiltonian, which describes only the region of interest. The important parameter is the tunneling energy T. Therefore, using the results of the LCAO approximation, Eq. (3.37), the Hamiltonian can be written as

$$\begin{aligned} H_T &= \epsilon_+|\psi_+\rangle\langle\psi_+| + \epsilon_-|\psi_-\rangle\langle\psi_-| = \\ &= \frac{1}{2}\left(\frac{\epsilon_+}{1+\Omega} + \frac{\epsilon_-}{1-\Omega}\right)|\psi_L\rangle\langle\psi_L| + |\psi_R\rangle\langle\psi_R| + \\ &+ \frac{1}{2}\left(\frac{\epsilon_+}{1+\Omega} - \frac{\epsilon_-}{1-\Omega}\right)|\psi_L\rangle\langle\psi_R| + |\psi_R\rangle\langle\psi_L|, \end{aligned} \tag{3.40}$$

where $\psi_{R(L)} = \psi_{00}(x \pm d, y)$. Introducing the second quantization formalism, we get the following effective Hamiltonian

$$H_T = T(a_L^\dagger a_R + a_R^\dagger a_L), \tag{3.41}$$

where T is the tunneling energy, $a^\dagger$ is the creation and a the annihilation operators. The tunneling Hamiltonian describes the coupling between the right and left localized states.

The derived tunneling Hamiltonian in Eq. (3.41) does not take into account the influence of the spin-orbit interaction. The lowest part of the spectrum is modified and the spin degree of freedom has a relevant role. Therefore, we do not restrict the description only on the lowest two states, but we consider the first four states, because of the spin degeneracy of the states without the spin-orbit coupling. The eigenstates of the double-dot Hamiltonian are $\Gamma^\sigma_{S(A)}$, where S and A stand for symmetric and antisymmetric state, respectively [52]. The spin is indicated by σ. We introduce the following left and right localized functions:

$$L^\sigma(R^\sigma) = \frac{1}{\sqrt{2}}(\Gamma^\sigma_S \pm \Gamma^\sigma_A). \tag{3.42}$$

In the limit of large interdot distance these functions became solutions of the single dot problem, $\psi_{00}(x \pm d, y)$. The effective Hamiltonian of our system is

$$H = \sum_{\sigma=\uparrow,\downarrow} = E^{\sigma}(n_{L\sigma} + n_{R\sigma}) - T^{\sigma}(a^{\dagger}_{L\sigma}a_{R\sigma} + a^{\dagger}_{R\sigma}a_{L\sigma}), \tag{3.43}$$

where $n = a^{\dagger}a$, $E^{\sigma} = (E^{\sigma}_S + E^{\sigma}_A)/2$ and $T^{\sigma} = (E^{\sigma}_A - E^{\sigma}_S)/2$. Here we allow to have a spin dependent tunneling energy T^{σ}, because of the spin-orbit coupling. Studying the time evolution of localized states of the Hamiltonian in Eq. (3.43) and treating the spin-orbit interaction as a perturbation, one can derive that at finite magnetic field, the tunneling energy for spin up and spin down are different. The difference is caused by spin-orbit terms (Bychkov-Rashba and Dresselhaus) only and it is in the second order in the coupling strengths [52].

4. Two Electron Quantum Dots

In this chapter the influence of the spin-orbit interaction on the energy spectrum of two-electron laterally coupled quantum dots is investigated. Here we perform numerically exact calculations of the isotropic and anisotropic exchange coupling in realistic GaAs coupled quantum dots in the presence of both the Dresselhaus and Bychkov-Rashba spin-orbit interactions [48]. The numerics allows us to make authoritative statements about the exchange. We establish that in zero magnetic field the second-order spin-orbit effects are absent at *all* interdot couplings [29]. Neither is the isotropic exchange affected, nor is the anisotropic exchange present. At finite magnetic fields the anisotropic coupling appears. We derive a spin-exchange Hamiltonian describing this behavior [28], generalizing the existing descriptions; we do not rely on weak coupling approximations such as the Heitler-London one. The model is proven highly accurate by comparison with our numerics and we propose it as a realistic effective model for the two-spin dynamics in coupled quantum dots.

4.1. Two Electron Hamiltonian

Our system is a two-dimensional electron gas confined in a (001) plane of a zincblende semiconductor heterostructure. An additional lateral potential with parabolic shape defines the double quantum dot. We work in the two dimensional approximation, with the electrons described by the single band effective mass approximation. The two-electron Hamiltonian is a sum of the orbital part and the spin dependent part,

$$H_{tot} = H_{orb} + \sum_{i=1,2} H_{so,i} + H_{Z,i} = H_{orb} + H_{so} + H_Z, \tag{4.1}$$

where the subscript i labels the two electrons. The orbital Hamiltonian is

$$H_{orb} = \sum_{i=1,2} (T_i + V_i) + H_C. \tag{4.2}$$

Here, $T = \hbar^2\mathbf{K}^2/2m$ is the kinetic energy with the effective mass m and the kinetic momentum $\hbar\mathbf{K} = \hbar\mathbf{k} + e\mathbf{A} = -i\hbar\boldsymbol{\nabla} + e\mathbf{A}$; e is the proton charge and $\mathbf{A} = B_z/2(-y, x, 0)$ is the vector potential of the magnetic field $\mathbf{B} = (0, 0, B_z)$. The orbital

effects due to the in-plane field $\mathbf{B} = (B_x, B_y, 0)$ are irrelevant due to the confinement in the two-dimensional approximation. The in-plane field only causes Zeeman splitting. The potential V describes the quantum dot geometry

$$V = \frac{1}{2} m\omega_0^2 \min\{(\mathbf{r} - \mathbf{d})^2, (\mathbf{r} + \mathbf{d})^2\}. \tag{4.3}$$

Here $l_0 = (\hbar/m\omega_0)^{1/2}$ is the confinement length, $2d$ measures the distance between the two potential minima, $\mathbf{d}$ is a unit vector which defines the main dot axis with respect to the crystallographic axes and $E_0 = \hbar\omega_0$ is the confinement energy. The Coulomb interaction between the two electrons is

$$H_C = \frac{e^2}{4\pi\epsilon_0\epsilon_r} \frac{1}{|\mathbf{r}_1 - \mathbf{r}_2|}, \tag{4.4}$$

where ϵ_0 is the vacuum dielectric constant and ϵ_r is the dielectric constant of the material.

The lack of the spatial inversion symmetry is accompanied by the spin-orbit coupling. We write it in the following general form

$$H_{so} = \mathbf{w} \cdot \boldsymbol{\sigma}, \tag{4.5}$$

where the vector $\mathbf{w}$ is kinetic momentum dependent, (Eqs. (3.27-3.29)). For the further derivations, we write $\mathbf{w}$ as

$$\begin{aligned} \mathbf{w}_D &= \gamma_c \langle K_z^2 \rangle \left(-K_x, K_y, 0\right), & (4.6)\\ \mathbf{w}_{D3} &= \gamma_c/2 \left(K_x K_y^2, -K_y K_x^2, 0\right) + \text{H.c.}, & (4.7)\\ \mathbf{w}_{BR} &= \alpha_{BR} \left(K_y, -K_x, 0\right), & (4.8) \end{aligned}$$

here H.c. denotes the Hermitian conjugate. The interaction strength γ_c is a material parameter, the angular brackets in $\mathbf{w}_D$ denote the quantum averaging in the $\mathbf{z}$ direction and the magnitude of $\mathbf{w}_D$ depends of the confinement potential details. The strength α_{BR} of the interaction is structure dependent and can be, to some extent, experimentally modulated using top gates potential [53]. Below we use the effective spin-orbit lengths defined as $l_{br} = \hbar^2/2m\alpha_{BR}$ and $l_d = \hbar^2/2m\gamma_c\langle K_z^2\rangle$, where $\langle ...\rangle$ denotes the averaging over the confinement growth direction [52, 48].

The spin is coupled to the magnetic field through the Zeeman interaction

$$H_Z = \frac{g}{2}\mu_B \mathbf{B} \cdot \boldsymbol{\sigma} = \mu \mathbf{B} \cdot \boldsymbol{\sigma}, \tag{4.9}$$

where g is the effective gyromagnetic factor, $\mu_B = e\hbar/2m_e$ is the Bohr magneton, μ is the renormalized magnetic moment and $\boldsymbol{\sigma}$ is the vector of the Pauli matrices.

In lateral quantum dots the Coulomb energy E_C is comparable to the confinement energy and the correlation between the electrons strongly influences the states [54]. One can compare the energies considering

$$\frac{E_C}{E_0} = \frac{e^2}{4\pi\epsilon_0\epsilon_r}\langle\frac{1}{r}\rangle\frac{ml_0^2}{\hbar^2} \sim \frac{l_0^2}{l_C\langle r\rangle}, \tag{4.10}$$

where the Coulomb length $l_C = e^2m/4\pi\epsilon_0\epsilon_r\hbar^2$ is a material parameter and $\langle r\rangle$ is the mean distance between the electrons. In GaAs $l_C \approx 10$ nm, while a typical lateral dot has $l_0 \approx 30$ nm, corresponding to $E_0 \approx 1$ meV. The mean length $\langle r\rangle$ is of the order of the confinement length, if the two electrons are on the same dot, and of the interdot distance, if the electrons are on different dots. In the first case, the Coulomb energy is typically 3 meV. In the second case (one electron per dot) the Coulomb interaction is typically larger than 1 meV.

The strength of the Coulomb interaction precludes the use of perturbative methods. Therefore, to diagonalize the two electron Hamiltonian Eq. (4.1), we use the exact numerical treatment, the Configuration Interaction (CI) method. Details are given in the next chapter. Below we consistently use the notation of Φ for spinor and Ψ for orbital wavefunctions. They fulfil the equations $H_{tot}\Phi = E\Phi$ and $H_{orb}\Psi = E\Psi$, respectively.

We use the GaAs realistic parameters: $m = 0.067m_e$ (m_e is the free electron mass), $g = -0.44$, $\epsilon_r = 12.9$ and $\gamma_c = 27.5$ eVÅ^3. The strength of linear Dresselhaus is $\gamma_c\langle K_z^2\rangle = 4.5$ meVÅ and of the Bychkov-Rashba is $\alpha_{BR} = 3.3$ meVÅ, corresponding to the effective spin-orbit lengths $l_d = 1.26\mu$m and $l_{br} = 1.72\mu$m, according to the recent experiments [52],[55]. The confinement energy $\hbar\omega_0 = 1.1$ meV corresponds to the confining length $l_0 = 32$ nm, in line with the experiment [11].

4.2. Approximative methods for the exchange coupling

In quantum dot spin qubits [9] the exchange interaction implements a fundamental two qubit gate [8],[15]. Compared to single qubit gates [14],[46], the exchange-based gates are much faster [13] and easier to control locally, motivating the solely exchange-based quantum computation [56]. The control is based on the exponential sensitivity of the exchange energy on the inter-particle distance. Manipulation then can proceed, for example, by shifting the single particle states electrically [57],[13],[58] or compressing them magnetically [59].

The practical manipulation schemes require quantitative knowledge of the exchange energy. The Configuration Interaction [60],[61],[62],[63],[64], a numerically

exact treatment, serves as the benchmark for usually adopted approximations. The simplest one is the Heitler-London ansatz, in which one particle in the orbital ground state per dot is considered. The exchange asymptotic in this model differs from the exact [65],[66] and the method fails completely in finite magnetic fields. Extensions of the single particle basis include the Hund-Mullikan [59], Molecular Orbital [61],[67] or Variational method [68],[62]. Other approaches, such as the Hartree-Fock [69],[70],[71], random phase approximation [72] and (spin-)density functional theory [73] were also examined. None of them, however, is reliable in all important regimes [74],[63],[15], which include weak/strong interdot couplings, zero/finite magnetic field and symmetric/biased dot. In the next sections we will briefly review the most used analytical approximations for the isotropic exchange coupling and compare with the exact numerical calculations to investigate the approximation limits.

4.2.1. Heitler-London method

Now we want to consider a double quantum dot system with two electrons. For zero spin-orbit interaction, the eigenstates of the total Hamiltonian Eq. (4.1) are separable in spin and orbital degree of freedom. We get the four lowest states by supplementing $\Psi_\pm$ with spinors, forming singlet and triplets:

$$\{\Phi_i\}_{i=1,\dots,4} = \{\Psi_+ S, \Psi_- T_0, \Psi_- T_+, \Psi_- T_-\}. \tag{4.11}$$

Here $S = 1/\sqrt{2}(|\uparrow\downarrow\rangle - |\downarrow\uparrow\rangle)$ is a singlet spinor built out of two spin-1/2 spinors, $T_0 = 1/\sqrt{2}(|\uparrow\downarrow\rangle + |\downarrow\uparrow\rangle)$, $T_+ = |\uparrow\uparrow\rangle$, $T_- = |\downarrow\downarrow\rangle$ are the three possible triplets; the quantization axis is chosen along the magnetic field. The wavefunctions $\Psi_\pm$ are the lowest two eigenstates of the orbital Hamiltonian, $H_{orb}\Psi_\pm = E_\pm \Psi_\pm$. The exchange energy is then obtained as

$$J_{HL} = \langle \Psi_- | H_{orb} | \Psi_- \rangle - \langle \Psi_+ | H_{orb} | \Psi_+ \rangle = E_- - E_+, \tag{4.12}$$

the difference between the triplet and the singlet energy.

In the Heitler-London approximation (H-L), we consider the configuration in which the interdot distance is large enough to have both electrons sitting at each potential minima. The single particle ground state wavefunction of the Fock-Darwin spectrum is

$$\psi_{00}(x,y) = \frac{1}{l_B\sqrt{\pi}} \exp\left[-\frac{x^2+y^2}{2l_B^2}\right], \tag{4.13}$$

where l_B is the effective confinement length defined by $l_B^2 = l_0^2/\sqrt{1 + B^2 e^2 l_0^4/4\hbar^2}$. The wavefunctions $\psi_{L(R)}$ are obtained shifting the Fock-Darwin ground state to $(\pm l_0 d, 0)$.

In the presence of the magnetic field we have to add a phase factor because of the gauge transformation $\vec{A}' = B/2(-y, x \pm l_0 d, 0) \rightarrow \vec{A} = B/2(-y, x, 0)$; we have

$$\begin{aligned} \psi_{L(R)} &= \exp\left[\pm i d\zeta\vartheta\frac{y}{l_0}\right]\psi_{00}(x \pm l_0 d, y), \\ \zeta = \left(\frac{l_0}{l_B}\right)^2, &\quad \vartheta = \frac{Bel_B^2}{2\hbar}, \quad l_B = l_0(1-\vartheta^2)^{1/4}. \end{aligned} \tag{4.14}$$

Starting from the functions Eq. (4.14), we combine them like

$$\Psi_\pm = \frac{1}{N_\pm}\left(\psi_L(\mathbf{r}_1)\psi_R(\mathbf{r}_2) \pm \psi_R(\mathbf{r}_1)\psi_L(\mathbf{r}_2)\right). \tag{4.15}$$

Here $N_\pm = 2(1 \pm \Omega^2)^{1/2}$ are the normalization factors, where Ω is the overlap between the left and right functions given by

$$\begin{aligned} \Omega &= \frac{1}{\pi l_B^2}\int d\mathbf{r}\exp\left[-\frac{x^2+y^2}{l_B^2}\right]\exp\left[-\zeta d^2\right]\exp\left[2id\zeta\vartheta\frac{y}{l_0}\right] = \\ &= \frac{1}{\pi l_B^2}\exp\left[-\zeta d^2\right]\int d\rho\rho\exp\left[-\frac{\rho^2}{l_B^2}\right]\int d\varphi\exp\left[2id\zeta\vartheta\frac{\rho\sin\varphi}{l_0}\right] = \\ &= \frac{2\pi}{\pi l_B^2}\exp\left[-\zeta d^2\right]\int d\rho\rho\exp\left[-\frac{\rho^2}{l_B^2}\right]J_0\left(2\zeta d\vartheta\frac{\rho}{l_0}\right) = \\ &= \exp\left[-\zeta d^2(1+\vartheta^2)\right]. \end{aligned} \tag{4.16}$$

Now we have to calculate the energies. Since the confinement potential used in Eq. (4.3) is not simply the shifted Fock-Darwin potential, to compute the matrix element of H_{orb} we add and subtract the harmonic potential centered at $x = \mp l_0 d$ for the electron 1(2). The Hamiltonian takes the form

$$H_{orb} = h_{-l_0 d}(\mathbf{r}_1) + h_{l_0 d}(\mathbf{r}_2) + W + H_C. \tag{4.17}$$

Here

$$h_{\pm l_0 d}(\mathbf{r}_i) = \frac{1}{2m}(\hbar\mathbf{k}_i + e\mathbf{A}_i)^2 + \frac{1}{2}m\omega_0^2[(x_i \pm l_0 d)^2 + y_i^2], \tag{4.18}$$

$$W = -m\omega_0^2 l_0 d\left(|x_1| + x_1 + |x_2| - x_2\right). \tag{4.19}$$

In order to calculate the two-electron energies of the states Ψ_+ and Ψ_-, we begin with the expression

$$\begin{aligned} E_\pm &= \frac{1}{N_\pm}\int d\mathbf{r}_1 d\mathbf{r}_2\left(\psi_L\psi_R \pm \psi_R\psi_L\right)H_{orb}\left(\psi_L\psi_R \pm \psi_R\psi_L\right) = \\ &= 2\hbar\omega_0\zeta + \frac{1}{N_\pm}(E_{RI} + E_{W_{RI}}) \pm \frac{1}{N_\pm}(E_{CE} + E_{W_C E}), \end{aligned} \tag{4.20}$$

where $\hbar\omega_0$ is the confinement energy and

$$E_{RI} + E_{W_{RI}} = \int d\mathbf{r}_1 d\mathbf{r}_2 |\psi_L(\mathbf{r}_1)|^2 |\psi_R(\mathbf{r}_2)|^2 \left(\frac{e^2}{4\pi\varepsilon_0\varepsilon_r} \frac{1}{|\mathbf{r}_1 - \mathbf{r}_2|} + W \right), \tag{4.21}$$

$$E_{CE} + E_{W_{CE}} = \int d\mathbf{r}_1 d\mathbf{r}_2 \psi_R(\mathbf{r}_1)^* \psi_L(\mathbf{r}_2)^* \left(\frac{e^2}{4\pi\varepsilon_0\varepsilon_r} \frac{1}{|\mathbf{r}_1 - \mathbf{r}_2|} + W \right) \psi_L(\mathbf{r}_1)\psi_R(\mathbf{r}_2). \tag{4.22}$$

The term E_{RI} can be interpreted as the Coulomb interaction between two classical charge distributions localized in the two dots, with the electron density $|\psi_{L/R}|^2$. The exchange integral E_{CE} represents the Coulomb interaction energy between the two electrons, but not computed using the normal charge density, but rather the exchange energy. This integral is therefore referred to as the Coulomb-exchange interaction. Furthermore the total contribution to the energy involves the integrals over the potential W with the same charge densities.

The isotropic exchange energy reads

$$J = \frac{2\Omega^2}{1 - \Omega^4} \left(E_{RI} + E_{W_{RI}} - \frac{E_{CE} + E_{W_{CE}}}{\Omega^2} \right). \tag{4.23}$$

In the case there is no overlap between the two functions, the exchange energy is influenced only by the Coulomb exchange integral. The integrals E_{RI} and E_{CE} can be calculated simply using the Fourier Transform method. The details of the calculations are given in the Appendix.

Using the previous results, we obtain for the exchange coupling in the Heitler-London approximation

$$\begin{aligned} J_{HL} &= \frac{\hbar\omega_0}{\sinh[2\zeta d^2(1+\vartheta^2)]} \Big\{ c_s\sqrt{\zeta} \left(\exp\left[-\zeta d^2\right] I_0(\zeta d^2) - \exp\left[\zeta d^2\vartheta^2\right] I_0(\zeta d^2\vartheta^2) \right) + \\ &+ \frac{2d}{\sqrt{\pi\zeta}} \left(1 - \exp\left[-\zeta d^2\right] \right) + 2d^2 \left(1 - \mathrm{Erf}(d\sqrt{\zeta}) \right) \Big\}, \end{aligned} \tag{4.24}$$

where I_0 is the zeroth-order modified Bessel function of first kind. The factor c_s is the ratio between the Coulomb strength and confining energy, $c_s = e^2\sqrt{\pi/2}/4\pi\varepsilon_0\varepsilon_r l_0\hbar\omega_0$. In the natural units, we can write $c_s = \sqrt{\pi/2}\alpha\hbar c/\varepsilon_r$ where α is the fine-structure constant. The result of J versus the magnetic field and the interdot distance are plotted in the Fig. 4.1 and Fig. 4.2. Similar formula can be found in Ref.[36] for a quartic confinement potential. The formula in the Eq. (4.24) has been derived in Ref.[63] (in the original paper there is a typo that we correct).

4.2.2. Hund-Mullikan method

In the molecular physics, another method is used to give an improvement to the exchange energy. Considering the Fock-Darwin ground state, there are two more

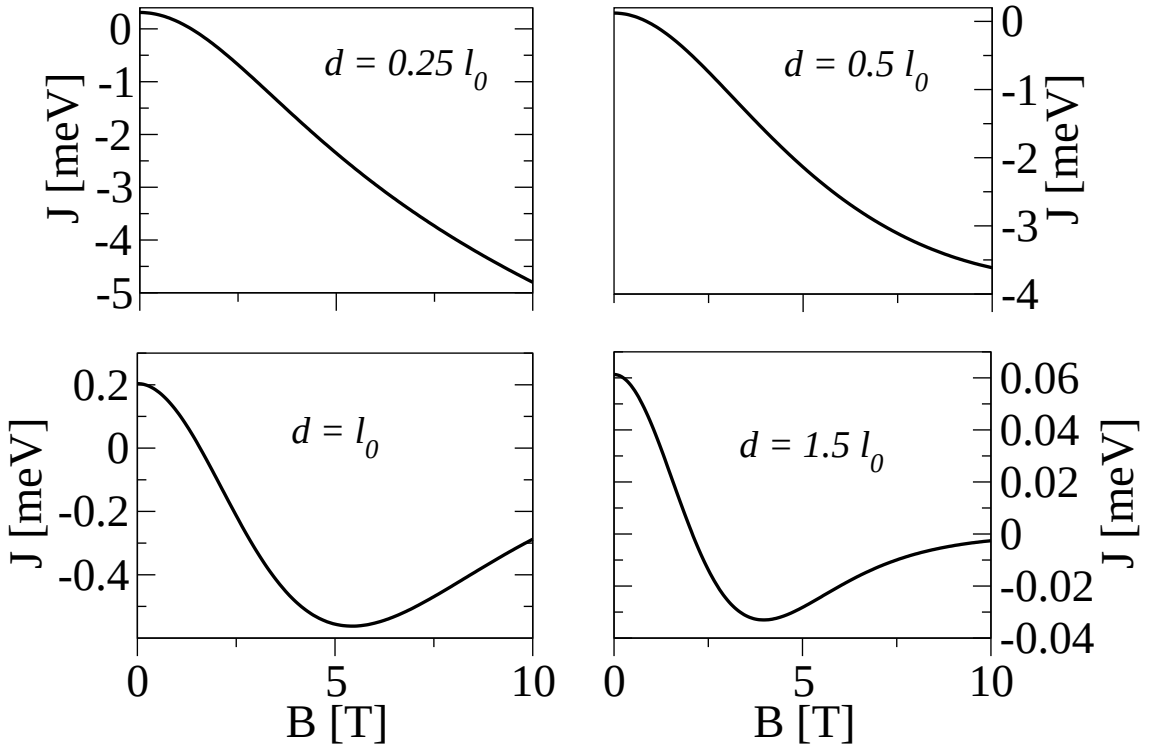

Figure 4.1.: Exchange energy J versus the magnetic field perpendicular to the dot plane for different interdot distance. The confining energy is $\hbar\omega_0 = 6$ meV that corresponds to $l_0 = 13.78$ nm.

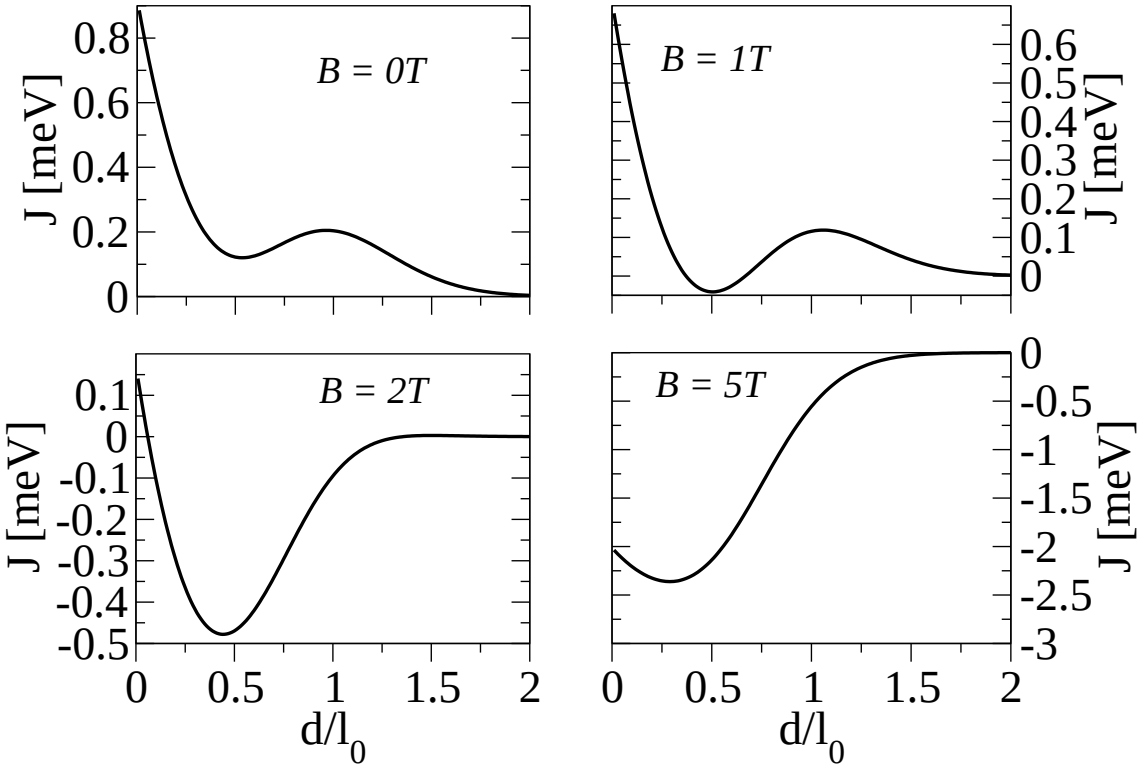

Figure 4.2.: Exchange energy J versus the interdot distance for different values of the magnetic field perpendicular to the plane. The confining energy is $\hbar\omega_0 = 6$ meV that corresponds to $l_0 = 13.78$ nm.

two-electron states that one has to consider. If we allow to have a double occupancy of the dot, we can built

$$\begin{aligned} \Psi_L &= \psi_L(\mathbf{r}_1)\psi_L(\mathbf{r}_2), \\ \Psi_R &= \psi_R(\mathbf{r}_1)\psi_R(\mathbf{r}_2). \end{aligned} \tag{4.25}$$

We did not consider this before, since here both electrons occupy the same dot, leading to a higher Coulomb interaction energy. These new states extend the orbital Hilbert space from two to four dimensions and they are both singlet states. This is the new basis in which the two electron Hamiltonian is diagonalized. The Hund-Mullikan approximation improves the calculated exchange energy only in the strong coupling regime, where the interdot distance is small.

4.2.3. Variational method

The variational method is a simple approach which provides a quantitative improvement on the calculation of the ground state energy. The method consists in choosing an appropriate trial function, ansatz, which approximates the exact wavefunction. Then, since the trial wavefunction depends on some parameters, using the variational principle one is able to find (at least) an upper bound for the ground state energy. In the double quantum dots the Heitler-London functions are very good approximation to the exact eigenstates at large interdot distance. One could expect that getting the distance smaller, the Heitler-London approximation fails and the electron can sit not exactly at the minima of the dot potential, mainly in the case of zero distance. However, using the interdot distance d as a variational parameter of the functions Eq. (4.14), one can get a better approximation. The variational ansatz reads

$$\Psi_{\pm}(D) = \frac{1}{\sqrt{N_{\pm}(D)}}(\psi_L(D)\psi_R(D) \pm \psi_R(D)\psi_L(D)), \tag{4.26}$$

where the displacement D of the Fock-Darwin functions is a variational parameter which we allow to be different from the potential minima displacement d.

The isotropic exchange J_{Var} is defined as the difference between the minima of the variational energy for the corresponding symmetric and antisymmetric states,

$$J_{Var} = \min_D\langle\Psi_-|H_{orb}|\Psi_-\rangle - \min_D\langle\Psi_+|H_{orb}|\Psi_+\rangle. \tag{4.27}$$

The exchange energies computed according the discussed approximations are given in Fig. 4.3, for zero magnetic field. The different approximations predict an exponential behavior of the isotropic exchange versus the interdot distance. They quantitatively differ for zero interdot distance, while they are quite close in larger dots.

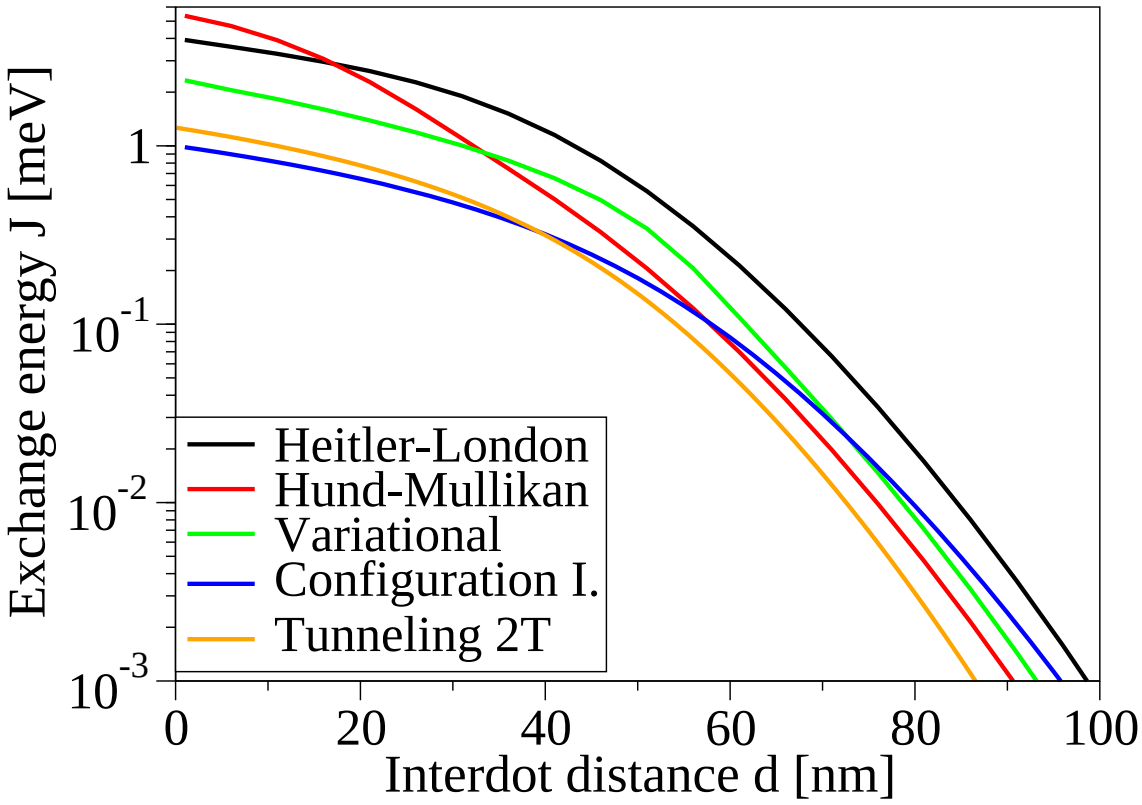

Figure 4.3.: Exchange energy J as a function of the interdot distance for different approximations at zero magnetic field. (Courtesy of Peter Stano).

4.2.4. Numerical calculation

The numerical calculation we have performed gives a better understanding and prediction of the exchange coupling. Since our method is based on CI, the precision of the energy spectrum strongly depends on the number of states involved to construct the two-electron Slater determinant. In Fig. 4.4 we compare the exchange coupling with the numerical results taken from the work of Pedersen et *al.* [63]. The difference is on the number of the single electron functions used to build the two-electron space. We use 21 states, while in the work [63] only 7 states are considered. For $d = 0$ we see that the Heitler-London prediction deviates significantly from the numerical results. In particular for d around 6 nm it shows a minimum that is not present in the exact calculation. For very large distances, the prediction is better, because it is a good approximation to consider the eigenfunctions situated in two different dots. For all values of d our prediction is close to the Pedersen *et.al* work, even if they differ from the number of single electron states. We can conclude that there is no a substantial difference in the two approximations. In Fig. 4.5 we show numerical results for the exchange energy as a function of the magnetic field perpendicular to the dot plane with $d = 0.25\ l_0$ as the interdot distance. The result shows that in the entire range of parameters the H-L approximation fails. This is because of the presence of the magnetic field. It predicts a zero exchange at $B = 1$ T, which means that there is a crossing point between the singlet and triplet state. But this value from our data is 6 T, completely different from the H-L prediction. Again the difference between our and Pedersen et *al.* approximation is not important in this range; it is of the order of 10%. For very high magnetic field $B = 10$ T, the blue curve shows that there is another crossing point, which we do not have in our results. The two predictions are different. We believe that there is no crossing point from that value of B, as we can see from our numerics. The conclusion is that if we want to investigate exchange energies close to zero and want to see the spin-orbit effects on the crossing points, we need more precision on the energy spectrum. So it is better to increase the number of single electron states until a good precision is reached. Our precision in the data is of order of 10^{-5} meV, while the Pedersen *et al.* is two orders of magnitude smaller.

4.3. Unitarily transformed model

We will analyze analytically the role of the spin-orbit coupling in the two-electron spectrum using the perturbation theory. This approach is appropriate since the spin-orbit energy corrections are small compared to the typical confinement energy. For a GaAs quantum dot the ratio between the confinement length and the strength of the

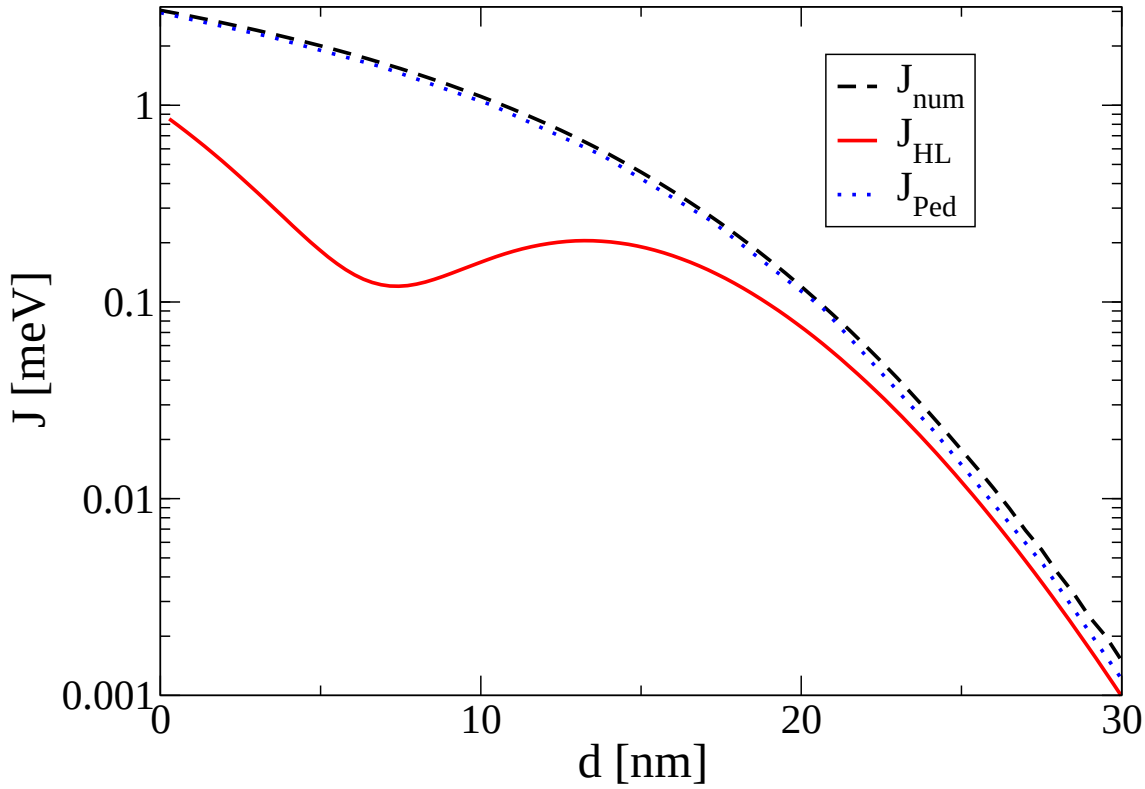

Figure 4.4.: Exchange coupling versus the interdot distance for a quantum dot size $l_0 = 14$ nm. The red line is the analytical exchange coupling in the Heitler-London approximation. The dashed curves are our numerical results and the Pedersen *et.al* data [63].

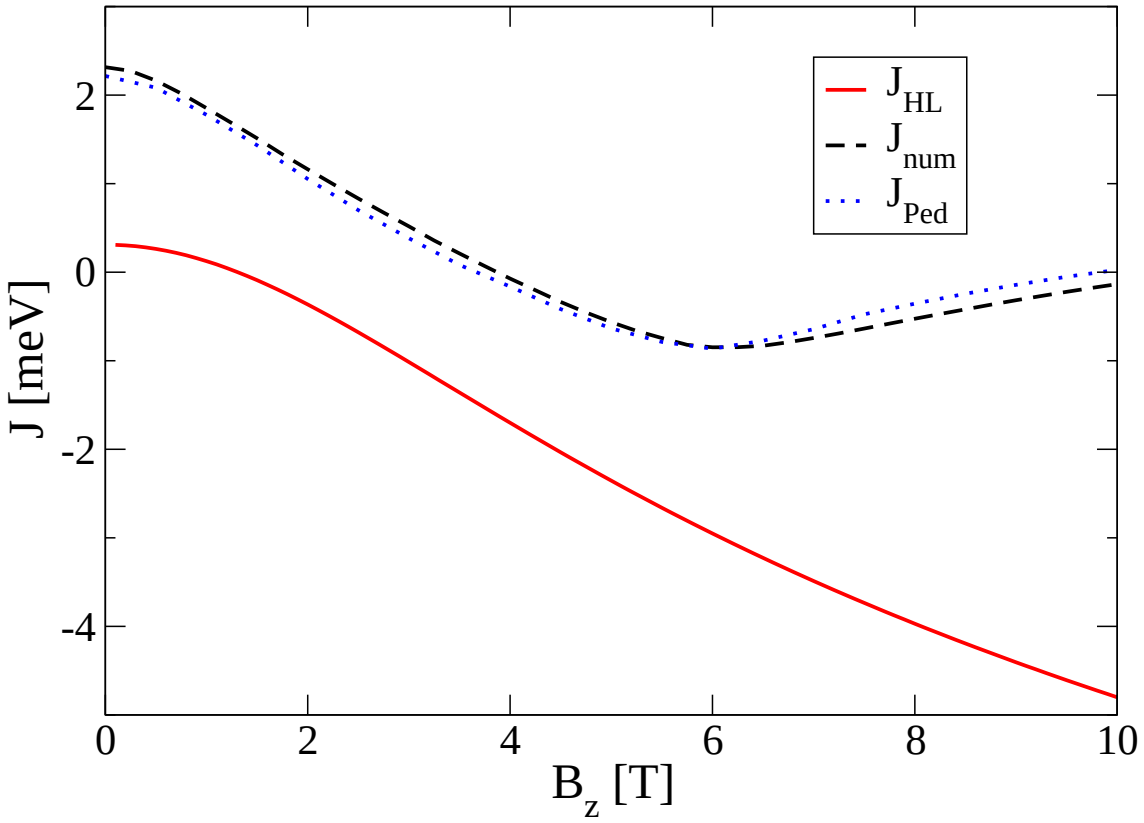

Figure 4.5.: Exchange coupling versus orthogonal magnetic field B_z for a double dot system of size $d = 0.25\ l_0$. For the notation see Fig. 4.4.

spin-orbit coupling $l_0/l_{so} \sim 10^{-2} \div 10^{-3}$. Furthermore, for a magnetic field of 1 T, the ratio between the Zeeman energy and the confinement energy is $\mu B/E_0 \sim 10^{-2}$. Therefore the spin-orbit interaction is a small perturbation, comparable in strength to the Zeeman term at $B = 1$ Tesla.

We consider the perturbative solution of the Hamiltonian Eq. (4.1). We transform the Hamiltonian to remove the linear spin-orbit terms, (we neglect the cubic Dresselhaus contribution in the analytical models)

$$H_{tot} \to U H_{tot} U^\dagger = H_{orb} + H_Z + \overline{H}_{so} \tag{4.28}$$

using the operator [75],

$$U = \exp\left(-\frac{\mathrm{i}}{2}\mathbf{n}_1 \cdot \boldsymbol{\sigma}_1 - \frac{\mathrm{i}}{2}\mathbf{n}_2 \cdot \boldsymbol{\sigma}_2\right), \tag{4.29}$$

where

$$\mathbf{n} = \left(\frac{x}{l_d} - \frac{y}{l_{br}}, \frac{x}{l_{br}} - \frac{y}{l_d}, 0\right). \tag{4.30}$$

Keeping only terms up to the second order in the spin-orbit strengths and the Zeeman coupling, we get the following effective spin-orbit interactions $\overline{H}_{so} = H_{so}^{(2)} + H_Z^{(2)}$, where

$$H_{so}^{(2)} = \sum_{i=1,2} \left(-K_+ + K_- L_{z,i}\sigma_{z,i}\right), \tag{4.31}$$

$$H_Z^{(2)} = \sum_{i=1,2} -(\mu\mathbf{B} \times \mathbf{n}_i) \cdot \boldsymbol{\sigma}_i. \tag{4.32}$$

Here, $L_z = xK_y - yK_x$, and

$$K_\pm = \left(\frac{\hbar^2}{4ml_d^2} \pm \frac{\hbar^2}{4ml_{br}^2}\right). \tag{4.33}$$

Equation (4.32) describes the mixing between the Zeeman and spin-orbit interactions, which is linear in the spin-orbit strengths. It disappears in zero magnetic field, where only the terms in Eq. (4.31) survive – a sum of an overall constant shift of $2K_+$ and the spin-angular momentum operators. Both of these are quadratic in the spin-orbit couplings.

4.3.1. Orbital wavefunctions symmetry

The symmetry of the two-electron wavefunctions Ψ has important consequences, for example, in the form of selection rules for the couplings between the states due to

the spin-orbit interactions. The choice of the potential in Eq. (4.3) is motivated by the fact that for small ($d \to 0$) and large ($d \to \infty$) interdot distance and in the absence of the Coulomb interaction, the wavefunction ϕ, solution of the single particle Hamiltonian, converges to the single dot solution centered at $d = 0$ and $x = \pm 2d$, respectively. For zero magnetic field, since the double dot potential does not have the rotational symmetry around the axis z, the inversions of the coordinate along axes of the confinement potential (x and y) are the symmetries involved. Indeed, the orbital Hamiltonian Eq. (4.2) commutes with the inversion operator I_x and I_y, $[H_{orb}, I_{x,y}] = 0$. Furthermore $[H_{orb}, I] = 0$, where $I = I_x I_y$ is the inversion of both axes simultaneously. All these operations belong to the C_{2v} group (Tab. 4.1). Accordingly, the wavefunctions transform as the functions 1, x, xy, y, which repre-

representation	under I_x, I_y transforms as
Γ_1	1
Γ_2	x
Γ_3	xy
Γ_4	y

Table 4.1.: Notation and transformation properties of C_{2v} representations.

sent this group. If a perpendicular magnetic field is applied, only the total inversion operation, $I = I_x I_y$, commutes with the Hamiltonian and the wavefunction is symmetric or antisymmetric with respect to the total inversion – this is due to the lack of I_x and I_y symmetry of the kinetic energy operator. The Slater determinants (the two-electron basis that we use in the diagonalization procedure) have also definite symmetries, if they are built from single particle states of definite symmetry (see next chapter).

We define the functions $\Psi_\pm$ to be the lowest eigenstates of the orbital part of the Hamiltonian, $H_{orb}\Psi_\pm = E_\pm \Psi_\pm$ with the following symmetry,

$$P\Psi_\pm = \pm\Psi_\pm, \tag{4.34}$$

where P is the particle exchange operator. We observe that $\Psi_\pm$ have, in addition to the previous symmetry, also a definite spatial symmetry. In what follows we will assume they fulfill

$$I_1 I_2 \Psi_\pm = \pm\Psi_\pm, \tag{4.35}$$

where $I_{1(2)}$ stands for the particle 1(2). We point out that while Eq. (4.34) is a definition, Eq. (4.35) is an assumption based on an observation. In zero magnetic field

$I_1 I_2 \Psi_+ = +\Psi_+$, follows from the Mattis-Lieb theorem [76]. However, we confirmed from numerics that Eq. (4.35) holds, without exception in all the cases we studied.

Figure 4.6 shows the calculated double dot spectrum at zero magnetic field without the spin-orbit interactions. The two lowest states, $\Psi_\pm$ discussed previously, are split

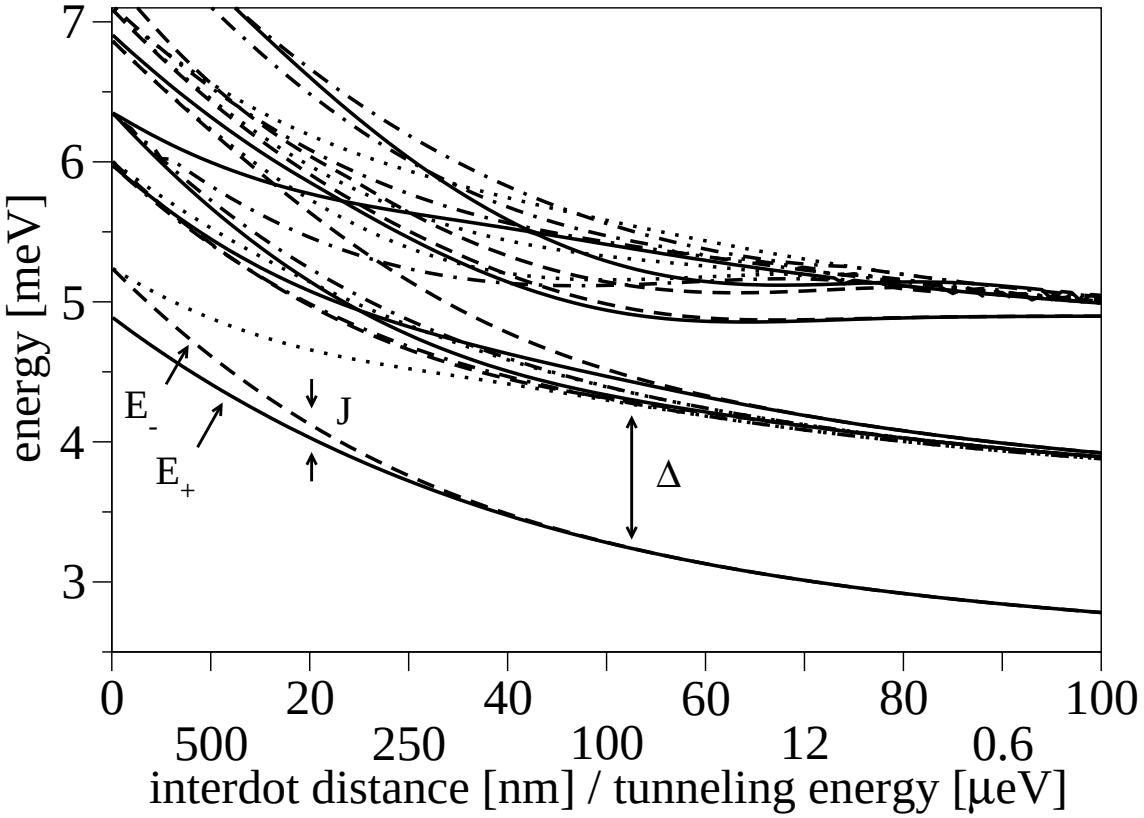

Figure 4.6.: Two-electron energy spectrum of a double dot at zero magnetic field as function of the interdot distance and the tunneling energy. The spatial symmetries of wavefunctions, 1, x, xy, y are denoted as solid, dashed, dotted-dashed and dotted line, respectively. The two lowest energies are labeled; they are split by the isotropic exchange energy J. The energy separation between the lowest states and the higher exited states is denoted by Δ. The confinement length is $l_0 = 32$ nm.

by the exchange energy J. In the single dot case ($d = 0$), the ground state is non degenerate, while the first exited state is doubly degenerate. Increasing the interdot distance, this degeneracy is removed, as the two states have different spatial symmetry (x and y). The energy of the states $\Psi_\pm$ is separated from the higher states by an energy gap Δ. This gap allows us to consider only the two lowest orbital states when studying the spin-orbit influence on the lowest part of the two-electron spectrum. Indeed, in the double dot Δ is of the order of 1 meV, while the spin-orbit

interactions are two order of magnitude smaller. In the case of $\Delta = 0$, the two orbital states approximation can be improved including more states.

The symmetry properties of the Hamiltonian lead to certain selection rules for the matrix elements between the two electron states. In zero magnetic field, because the angular momentum operator L_z operator transforms as xy, the singlet and triplets are not coupled, up to the second order in the spin-orbit interactions, $\langle\Phi_1|\overline{H}_{so}|\Phi_{2,3,4}\rangle = 0$. The only contribution is due to the constant K_+. For non zero magnetic field, the singlet and triplet are coupled only if the orbital states belong to the different spatial symmetry. Indeed, in the transformed Hamiltonian the term in Eq. (4.32) leads to the coupling between the singlet and the triplets and $\langle\Psi_+|\mathbf{n}|\Psi_-\rangle \neq 0$. The coupling arises only if the orbital states Ψ have the opposite inversion symmetry. The non-vanishing matrix elements are listed in Table 4.2.

$\hat{O}$	zero field	non zero field
L_z	never	$i_1 = i_2$
$\mathbf{n}$	$i_1 \neq i_2$	$i_1 \neq i_2$

Table 4.2.: The matrix elements $\langle\Psi_1|\hat{O}|\Psi_2\rangle$ are non-zero if the orbital symmetries fulfill the conditions given in the table. The symmetries are $I\Psi_{1,2} = i_{1,2}\Psi_{1,2}$.

4.3.2. Effective Hamiltonians

Here we derive effective four-level Hamiltonians, which provide understanding for the numerical results. We follow two different approaches:

- restriction of the total Hamiltonian, Eq. (4.1), to the spin basis in Eq. (4.11);
- inclusion of higher excited states through a sum rule using the Schrieffer-Wolff transformation with the unitary operator, Eq. (4.29).

Then we compare the two models, including their simplifications using the Heitler-London approximation, to demonstrate the quality of their description of the two-qubit subspace.

We restrict the Hilbert space of the double dot to the four lowest functions Eq. (4.11) to describe the qubit pair. We start with the case of zero spin-orbit interactions. In the external magnetic field, the two triplets T_+ and T_- are split by twice the Zeeman energy $E_Z = 4\mu B_z$. The restriction of the Hamiltonian Eq. (4.1) to the basis in Eq. (4.11) produces a diagonal matrix

$$H_{iso} = \mathrm{diag}(E_+, E_-, E_- - E_Z, E_- + E_Z). \tag{4.36}$$

The standard notation is to refer only to the spinor part of the basis states. The matrix Eq. (4.36) can be rewritten in a more compact way using the basis of the sixteen sigma matrices, $\{\sigma_{\alpha,1}\sigma_{\beta,2}\}_{\alpha,\beta=0,1,2,3}$ (see Appendix). The result is the so-called isotropic exchange Hamiltonian (where the constant $E_- - J$ was subtracted)

$$H_{\text{iso}} = (J/4)\boldsymbol{\sigma}_1 \cdot \boldsymbol{\sigma}_2 + \mu\mathbf{B} \cdot (\boldsymbol{\sigma}_1 + \boldsymbol{\sigma}_2). \tag{4.37}$$

The singlet and triplets are separated by the isotropic exchange energy $J = E_- - E_+$, the only parameter of the model.

The Hamiltonian in Eq. (4.37) describes the coupling of the spins in the Heisenberg form. With this form, the SWAP gate can be performed as the time evolution of the system, assuming the exchange coupling J is controllable. The isotropic exchange has already been studied analytically, in the Heitler-London, Hund-Mullikan, Hubbard, variational and other approximations, as well as numerically using the finite-difference method. Usually analytical methods provide a result valid within certain regime of the external parameters only and a numerical calculation is needed to assess the quality of various analytical models.

When the spin-orbit interaction is included, additional terms in the effective Hamiltonian appear, as the matrix elements due to the spin-orbit interaction $(H'_{aniso})_{ij} = \langle\Phi_i|H_{so}|\Phi_j\rangle$. Selection rules in Tab. 4.2 restrict the non-zero matrix elements to those between a singlet and a triplet,

$$H'_{aniso} = \begin{pmatrix} 0 & 2\overline{w}_z & -\sqrt{2}u & \sqrt{2}v \\ 2\overline{w}_z^* & 0 & 0 & 0 \\ -\sqrt{2}u^* & 0 & 0 & 0 \\ \sqrt{2}v^* & 0 & 0 & 0 \end{pmatrix}. \tag{4.38}$$

Here $u = (\overline{w}_x + \mathrm{i}\overline{w}_y), v = (\overline{w}_x - \mathrm{i}\overline{w}_y)$ and

$$\overline{\mathbf{w}} = \langle\Psi_+|\mathbf{w}_1|\Psi_-\rangle, \tag{4.39}$$

where vector $\mathbf{w}$ is defined by the spin-orbit interaction Eq. (4.5). Using the sigma matrix notation, Eq. (4.38) can be written as

$$H'_{aniso} = \mathbf{a}' \cdot (\boldsymbol{\sigma_1} - \boldsymbol{\sigma_2}) + \mathbf{b}' \cdot (\boldsymbol{\sigma_1} \times \boldsymbol{\sigma_2}), \tag{4.40}$$

where the $\mathbf{a}'$ and $\mathbf{b}'$ are the spin-orbit vectors defined as

$$\mathbf{a}' = \mathrm{Re}\langle\Psi_+|\mathbf{w}_1|\Psi_-\rangle, \tag{4.41a}$$
$$\mathbf{b}' = \mathrm{Im}\langle\Psi_+|\mathbf{w}_1|\Psi_-\rangle. \tag{4.41b}$$

We denote the derived standard exchange Hamiltonian as

$$H'_{ex} = H_{iso} + H'_{aniso}. \tag{4.42}$$

Note that we repeated the derivation of Ref. [26] including the external magnetic field. The Hamiltonian in Eq. (4.42) treats the spin-orbit interactions in the first order, which shows inadequate comparisons with numerical calculations (see below).

To remove this discrepancy, we derive a more suitable model following the same approach but using the unitarily transformed Hamiltonian Eq. (4.28). In this way, the linear spin-orbit terms are removed and the resulting effective Hamiltonian treats the spin-orbit interactions in the second order in small quantities (the spin-orbit and the Zeeman couplings). The transformation asserts the original Schrödinger equation $H_{tot}\Phi = E\Phi$ can be equivalently solved in terms of the transformed quantities $\overline{H}_{tot}(U\Phi) = E(U\Phi)$, with the Hamiltonian $\overline{H}_{tot} = UH_{tot}U^{\dagger}$. The transformed Hamiltonian $\overline{H}$ is the same as the original, Eq. (4.1), except for the linear spin-orbit interactions, appearing in an effective form $\overline{H}_{so}$. We again restrict the basis to the lowest four states and for the spin-orbit contributions we get

$$(\overline{H}_{aniso})_{ij} = \langle\Phi_i|\overline{H}_{so}|\Phi_j\rangle. \tag{4.43}$$

Using the selection rules and the algebra of the Pauli matrices, we get the exchange Hamiltonian

$$H_{ex} = (J/4)\boldsymbol{\sigma}_1\cdot\boldsymbol{\sigma}_2 + \mu(\mathbf{B}+\mathbf{B}_{\rm so})\cdot(\boldsymbol{\sigma}_1+\boldsymbol{\sigma}_2) + \mathbf{a}\cdot(\boldsymbol{\sigma}_1-\boldsymbol{\sigma}_2) + \mathbf{b}\cdot(\boldsymbol{\sigma}_1\times\boldsymbol{\sigma}_2) - 2K_+. \tag{4.44}$$

Compared to the model in Eq. (4.40), the functional form of the Hamiltonian is the same, except for the effective spin-orbit magnetic field

$$\mu\mathbf{B}_{so} = \hat{\mathbf{z}}(K_-/\hbar)\langle\Psi_-|L_{z,1}|\Psi_-\rangle, \tag{4.45}$$

which appears due to an inversion symmetric part of $\overline{H}_{so}$, see Eq. (4.31), and the spin-orbit vectors, which are qualitatively different,

$$\mathbf{a} = \mu\mathbf{B}\times{\rm Re}\langle\Psi_+|\mathbf{n}_1|\Psi_-\rangle, \tag{4.46a}$$
$$\mathbf{b} = \mu\mathbf{B}\times{\rm Im}\langle\Psi_+|\mathbf{n}_1|\Psi_-\rangle. \tag{4.46b}$$

We remind that the effective Hamiltonian Eq. (4.44) refers to the four functions in Eq. (4.11) unitarily transformed $\{U\Phi_i\}_{i=1,\ldots,4}$. The agreement between the effective model and the numerical data is very good, as we will see.

4.3.3. Effective Hamiltonian H'_{ex} in zero field

In this section we give H'_{ex} explicitly for zero B and diagonalize it. This is the only case for which it is possible to give an analytical solution. For zero magnetic field, one can choose the functions $\Psi_\pm$ to be real. Therefore the matrix elements of the spin-orbit operator $\mathbf{w}$ in Eq. (4.5) are purely imaginary and $\mathbf{a}' = \mathbf{0}$. With the spin quantization axis chosen along the vector $\mathbf{b}'$, the 4x4 matrix, in Eq. (4.42), takes the form

$$H'_{ex} = \begin{pmatrix} -2J & 2\mathrm{i}b & 0 & 0 \\ -2\mathrm{i}b & 2J & 0 & 0 \\ 0 & 0 & 2J & 0 \\ 0 & 0 & 0 & 2J \end{pmatrix}. \tag{4.47}$$

The upper left 2×2 block of this matrix is a Hamiltonian of a spin 1/2 particle in a magnetic field $\tilde{\mathbf{B}} = (0, 2b', 2J)$. The eigenstates of this Hamiltonian are spins oriented along the magnetic field $\tilde{\mathbf{B}}$. Since the matrix in Eq. (4.47) is block diagonal, it is easy to see it can be diagonalized with the help of the following matrix

$$\Sigma = \begin{pmatrix} 0 & 1 & 0 & 0 \\ 1 & 0 & 0 & 0 \\ 0 & 0 & 0 & 0 \\ 0 & 0 & 0 & 0 \end{pmatrix}. \tag{4.48}$$

In the notation of the Pauli matrices, (see Appendix),

$$\Theta = \exp\left(-\mathrm{i}\frac{\Sigma\theta}{2}\right) = \exp\left(-\frac{\mathrm{i}}{4}\theta(\sigma_{z,1} - \sigma_{z,2})\right), \tag{4.49}$$

where $\tan\theta = b'/J$. The Hamiltonian in Eq. (4.47) can be diagonalized by $H_{diag} = \Theta H'_{ex}\Theta^\dagger$,

$$H_{diag} = \begin{pmatrix} -J - \sqrt{(b')^2 + J^2} & 0 & 0 & 0 \\ 0 & -J + \sqrt{(b')^2 + J^2} & 0 & 0 \\ 0 & 0 & 2J & 0 \\ 0 & 0 & 0 & 2J \end{pmatrix}. \tag{4.50}$$

The unitary transformation Θ in Eq. (4.49) performs the rotation of the two spins in the opposite sense. The Hamiltonian can be interpreted as a rotation of the electron around a spin-orbit field when transfered from one dot to the other [26]. As already discussed, this eigenspectrum qualitatively differs from the numerics, showing that the assumptions leading to the construction of H'_{ex} are invalid.

4.4. Single Dot

We start with the single dot case, corresponding in our model to $d = 0$. The analytical solution of the single particle Hamiltonian $T + V$ is known as the Fock-Darwin spectrum. The corresponding wave functions ψ and the energies ε are in Eqs. (3.34-3.35).

Let us consider now the orbital two-electron states Ψ, eigenstates of H_{orb}, Eq. (4.2). The Coulomb operator H_C commutes with the rotation of both electrons around the z axis by an angle φ, $R_z^{(1)}(\varphi) \otimes R_z^{(2)}(\varphi)$ – the Coulomb interaction couples only states with the same total angular momentum. This allows us to label the states with the quantum number L, the total angular momentum. Furthermore, the Hamiltonian H_{orb} commutes with any spin rotation of any of the electrons $U_{\mathbf{n},i}(\psi)$, which express the fact that the Coulomb interaction conserves spin. Therefore, we can consider the full two-electron wavefunctions obtained by supplementing the orbital part Ψ with a spinor, respecting the overall wavefunction symmetry, similarly as in Eq. (4.11).

The two-electron spectrum, without the Zeeman and the spin-orbit interactions, is shown in Fig. 4.7. Focusing on the first two lowest states, which are the most relevant for the qubit pair, we note that they cross at $B \approx 0.43$ T, so one can turn the ground state from the singlet to the triplet by applying an external magnetic field. In the presence of spin-orbit interaction, the crossing is turned into anticrossing, as described below.

For zero magnetic field the ground state is $L = 0$, a singlet non-degenerate state. The first exited state is six-fold degenerate, corresponding to two different values of the angular momentum $L = \pm 1$. The total spin is $S_t = 1$ and reflects the fact that each state is a threefold degenerate triplet state. Increasing B the ground state energy raises and crosses the line with $L = -1$. For the first exited state the degeneracy in L is removed: the state with angular momentum $L = -1$ drops in energy and crosses the singlet state, while the state $L = 1$ increases the energy. After the crossing point the ground state of the system turns to a triplet state.

4.4.1. Spin-orbit corrections to the energy spectrum in finite magnetic field

Suppose some parameter, such as the magnetic field, is being changed. It may happen at some point that the states of the opposite spin became degenerate. Such points are called spin hot spots. Here, because of the degeneracy, a weak spin-orbit coupling has strong effects. For the spin relaxation, spin hot spots play often a dominant role [77].

We are interested in the changes to the spectrum due to the spin-orbit interaction.

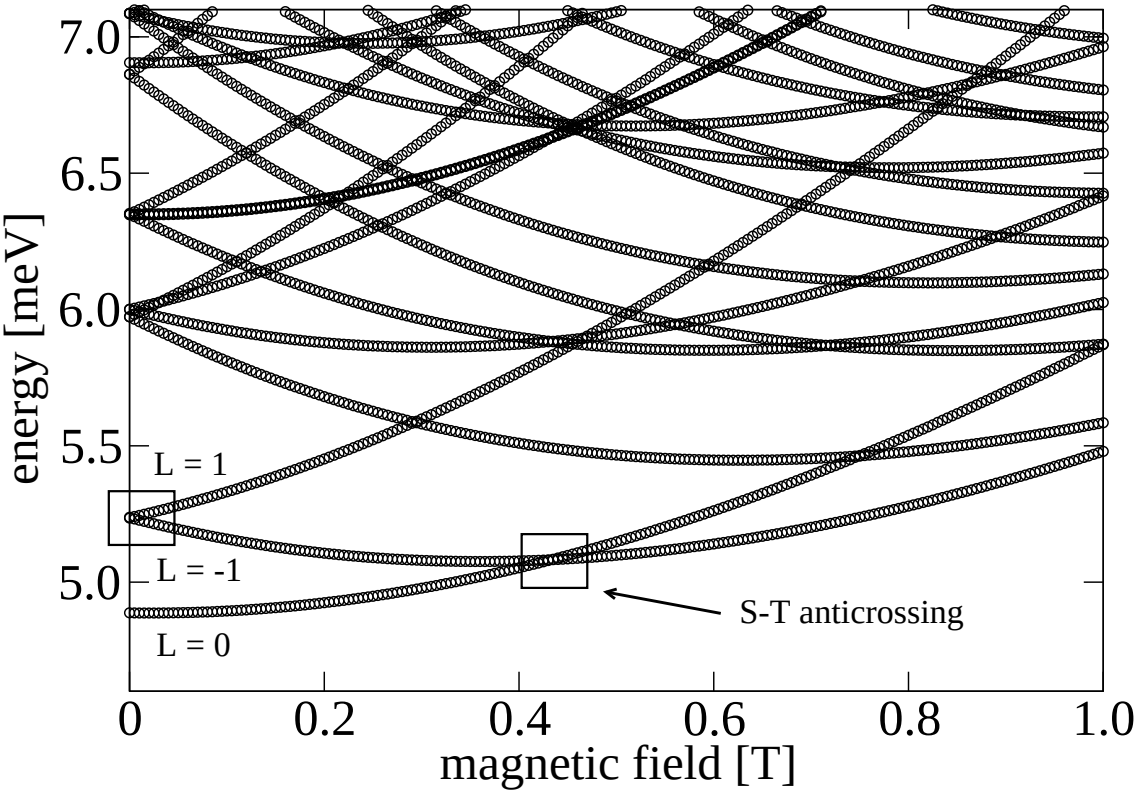

Figure 4.7.: Two-electron energy spectrum of a single dot in magnetic field. The states are labelled by the total angular momentum L. A singlet-triplet crossing point is showed. Zeeman and spin-orbit interactions are neglected and the confinement length is $l_0 = 32$ nm. The insets are magnified on Fig. 4.8 and Fig. 4.9.

Let us neglect the cubic Dresselhaus in this section. To understand the spin-orbit influence, it is important to note the following commutation relations for the linear spin-orbit terms

$$\begin{aligned}[\mathbf{w}_{BR,1}\cdot\boldsymbol{\sigma}_1+\mathbf{w}_{BR,2}\cdot\boldsymbol{\sigma}_2,\hat{J}_+]=0,\\ [\mathbf{w}_{D,1}\cdot\boldsymbol{\sigma}_1+\mathbf{w}_{D,2}\cdot\boldsymbol{\sigma}_2,\hat{J}_-]=0,\end{aligned} \tag{4.51}$$

where $\hat{J}_\pm=\hat{L}\pm\hat{S}_z$. These commutation rules hold for any magnetic field B. Since the Hamiltonian Eq. (4.2) commutes with the operator $\hat{J}_\pm$, we can label the states using the quantum numbers $J_+=L+S_z$ and $J_-=L-S_z$. The spin-orbit interactions couple only the states with the same quantum numbers J_+ and J_-, for Bychkov-Rashba and Dresselhaus terms, respectively.

Let us focus on the part of the spectrum close to $B=0$ and on the states with $L=\pm1$, Fig. 4.7. The degeneracy of the states is removed by the spin-orbit interaction, as shown in Fig. 4.8.

Let us now use the Hamiltonian in Eq. (4.28), to understand the influence of the spin-orbit interactions. The degeneracy of the states with angular momenta $L=\pm1$ makes the description with the lowest two orbital states questionable. Therefore now we take three orbital states and repeat the derivation of H_{ex}, obtaining a 7×7 Hamiltonian matrix. The basis functions are

$$\{\Phi_i\}_{i=1,\dots,7}=\{\Psi_+S,\Psi_-T_0,\Psi_-T_+,\Psi_-T_-,\Psi'_-T_0,\Psi'_-T_+,\Psi'_-T_-\}, \tag{4.52}$$

where Ψ_+ is the electron wavefunction with angular momentum $L=0$, Ψ_- and Ψ'_- have angular momentum $L=\pm1$, respectively. Since the magnetic field is negligible with respect to the spin-orbit strengths, the Hamiltonian in Eq. (4.32) is negligible. Because of the selection rules, Tab. 4.2, the contributions from Eq. (4.31) in the basis Eq. (4.52), gives non-zero matrix elements only for the states $\langle\Psi_-T_\pm|\overline{H}_{so}|\Psi_-T_\pm\rangle=\pm K_-$. For the GaAs parameters, $K_-=0.16\mu$eV. The same conclusion stays for $\langle\Psi'_-T_\pm|\overline{H}_{so}|\Psi'_-T_\pm\rangle=\pm K_-$. In the region of small magnetic field, the states with $J_\pm=0$ are coupled by the spin-orbit interaction and the lifting is in the second order in the spin-orbit strengths. The other states are not coupled since they have different values of $J_\pm$. Therefore we conclude that the two-orbital state approximation can be used also for the single dot case (or strongly coupled double dots), because the spin-orbit interactions do not mix states with $L=+1$ and $L=-1$.

Figure 4.9 shows the region of the ground state anticrossing from Fig. 4.7. The spin-orbit interaction induces two anticrossings. The first is due to the Bychkov-Rashba term, since the crossing states have different J_-, but the same $J_+=0$ and couples the singlet S and triplet T_+ spins. The second is due to the Dresselhaus term which couples states with $J_-=0$, the singlet S and the triplet T_-. The central point is a

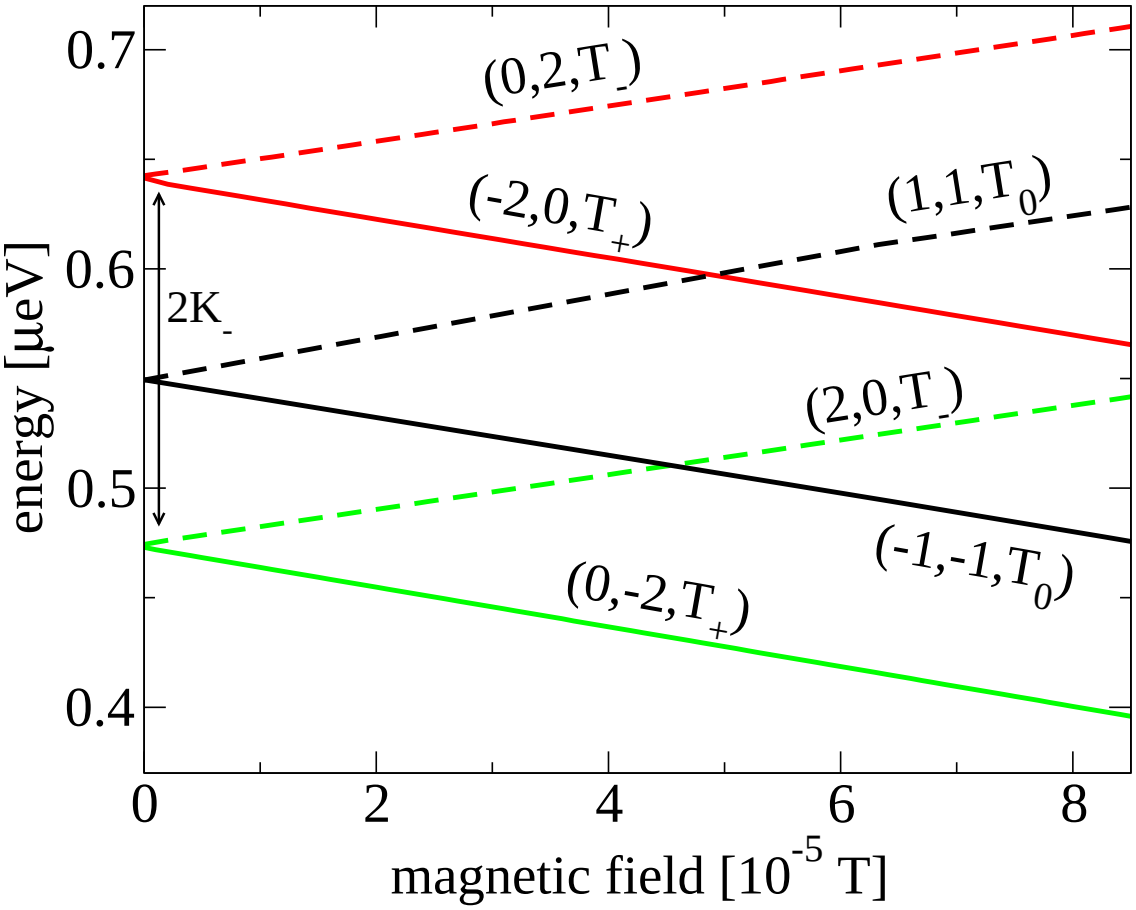

Figure 4.8.: Magnified region from Fig. 4.7. Energy spectrum of a single dot close to magnetic field $B = 0$. Only the states with the total angular momentum $L = \pm 1$ are plotted. A constant shift is removed from the spectrum. Each state is labeled by the quantum numbers (J_+, J_-, T_i).

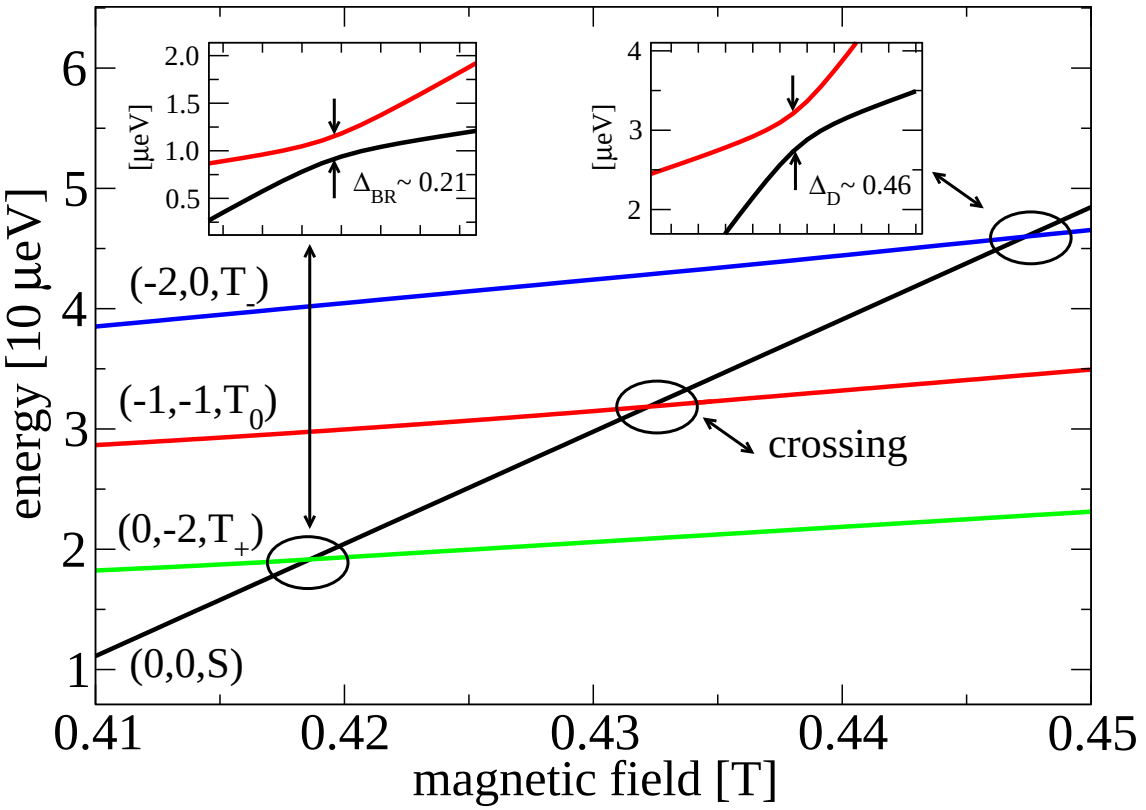

Figure 4.9.: Lowest energy levels close to the anticrossing point Fig. 4.7. A constant shift is removed from the spectrum. The quantum numbers (J_+,J_-,Σ_i) are used to label the states. Insets show the anticrossing regions. The units of Δ_{BR} and Δ_D are μeV.

crossing point, because the crossing state differ in both J_+ and J_-. The splitting energy can be evaluated using the unitarily transformed Hamiltonian Eq. (4.28). Using the degenerate perturbation theory, one can estimate analytically, using Eq. (4.31) and Eq. (4.32), the value of the two gaps to be $\Delta_{BR} \approx 4\sqrt{2}\mu B l_0/l_{BR} = 0.15\mu eV$ and $\Delta_D \approx 4\sqrt{2}\mu B l_0/l_D = 0.58\mu eV$. These values are consistent with the numerical values (0.21 μeV and 0.46 μeV, respectively).

4.5. Double Dot

The double dot case can be obtained by choosing different from zero interdot distance in the confined potential in Eq. (4.3). This kind of structure is useful for quantum computation applications. A universal quantum gate can be obtained by changing the exchange coupling J between the electrons. In our model, we can tune J by the external magnetic field $\mathbf{B}$ and the interdot distance $\mathbf{d}$. In the next sections we discuss our derived model, see Eq. (4.44), in the limit of the Heitler-London approximation and how one can improve it to predict the spin-orbit induced energy shifts.

4.5.1. Heitler-London approximation

The shape of the double dot potential does not allow to have a closed analytical form of the two electron wavefunctions. We consider here the Heitler-London ansatz since it is a good approximation at large interdot distances and we can work out the spin-orbit influence on the spectrum analytically. For this purpose, we compute the spin-orbit vectors, Eq. (4.41) and Eq. (4.46), for our models.

In the Heitler-London ansatz, the two electron eigenfunctions are given by

$$\Psi_\pm = \frac{1}{\sqrt{2(1 \pm |\langle\psi_L|\psi_R\rangle|^2)}}(|\psi_L\rangle|\psi_R\rangle \pm |\psi_R\rangle|\psi_L\rangle) \tag{4.53}$$

where $|\psi_{L(R)}\rangle$ is a single electron Fock-Darwin state centered in the left (right) dot. With this ansatz, the spin-orbit vectors, Eq. (4.41), follow as

$$\mathbf{a}' = \frac{1}{\sqrt{1 - |\langle\psi_L|\psi_R\rangle|^4}}\langle\psi_L|\mathbf{w}|\psi_L\rangle, \tag{4.54a}$$

$$\mathbf{b}' = \frac{\mathrm{i}}{\sqrt{1 - |\langle\psi_L|\psi_R\rangle|^4}}\langle\psi_L|\mathbf{w}|\psi_R\rangle\langle\psi_R|\psi_L\rangle. \tag{4.54b}$$

For the explicit form of the vectors in Eq. (4.54) see Appendix.

Similarly we get the spin-orbit vectors, in Eq. (4.46), as

$$\mathbf{a} = \frac{\mu}{\sqrt{1-|\langle\psi_L|\psi_R\rangle|^4}}\langle\psi_L|\mathbf{B}\times\mathbf{n}|\psi_L\rangle, \tag{4.55a}$$

$$\mathbf{b} = \frac{\mathrm{i}\mu}{\sqrt{1-|\langle\psi_L|\psi_R\rangle|^4}}\langle\psi_L|\mathbf{B}\times\mathbf{n}|\psi_R\rangle\langle\psi_R|\psi_L\rangle, \tag{4.55b}$$

and the spin-orbit induced magnetic field (see Appendix for more details)

$$\mu\mathbf{B}_{\mathrm{so}} = \hat{\mathbf{z}}\frac{K_-/\hbar}{1-|\langle\psi_L|\psi_R\rangle|^2}\Big(\langle\psi_L|L_z|\psi_L\rangle - \langle\psi_L|L_z|\psi_R\rangle\langle\psi_R|\psi_L\rangle\Big). \tag{4.56}$$

Differently from the spin-orbit vectors in Eq. (4.54), the vectors in Eq. (4.55) reveal explicitly the anisotropy with respect to the magnetic field and dot orientation [78] (note that x and y in the definition of $\mathbf{n}$, in Eq. (4.30) are the crystallographic coordinates).

4.5.2. Spin-orbit correction to the energy spectrum in zero magnetic field

To quantify the spin-orbit contributions to the energy spectrum, we analyze the difference between a state energy if the spin-orbit interactions are considered and artificially set to zero. We consider only the lowest four states, relevant for a qubit pair.

In the previous sections, we have derived two effective Hamiltonians, H'_{ex} and H_{ex}, which differ in the order in which we treat the spin-orbit interactions. Employing the Heitler-London approximation, we have four candidates to explain the exact numerical data:

- H'_{ex} and the vectors $\mathbf{a}'$ and $\mathbf{b}'$ are computed within the Heitler-London approximation according to Eqs. (4.54);
- H'_{ex} and the vectors $\mathbf{a}'$ and $\mathbf{b}'$ are computed by Eqs. (4.41) using $\Psi_\pm$ extracted from the numerics;
- H_{ex} and the vectors $\mathbf{a}$ and $\mathbf{b}$ are computed within the Heitler-London approximation according to Eqs. (4.55);
- H_{ex} and the vectors $\mathbf{a}$ and $\mathbf{b}$ are computed by Eqs. (4.46) using $\Psi_\pm$ extracted from the numerics.

We will compare the four models with the exact results. The models $H_{ex}^{\prime HL}$ and $H_{ex}^{\prime}$ are based on the generalized and corrected Hamiltonian proposed in the Ref. [29]. The only difference is in the calculation of the spin-orbit vectors: in the first case we use the analytical Heitler-London to calculate them, while in the second case a numerical evaluation based on the exact wavefunctions is done. The same approach is repeated for models H_{ex}^{HL} and H_{ex}. Apart from the energies, we compare also the spin-orbit vectors. Since they are defined up to the relative phase of states Ψ_+ and Ψ_-, the observable quantity is $c'^2 = (a')^2 + (b')^2$ and analogously for $c^2 = (a)^2 + (b)^2$. We refer to these quantities as the anisotropic part of the exchange coupling. The isotropic exchange J is also a given parameter for the models presented before. Therefore we compute it in the Heitler-London approximation and numerically for the models $H_{ex}^{\prime HL}$ and $H_{ex}^{\prime}$, respectively. The same applies for H_{ex}^{HL} and H_{ex}.

Figure 4.10 shows the spin-orbit induced energy shift as a function of the interdot distance. For each of the four states, we plot the result of numerics and models $H_{ex}^{\prime}$ and H_{ex}. The numerical result is a constant and equal shift for all 4 spin states, with value -0.54μeV. Let us consider the result of the model H_{ex}^{HL} and H_{ex}, Eq. (4.44). For zero magnetic field, all spin-orbit vectors are zero, as is the effective magnetic field. The only contribution comes from the constant term $2K_+ = -0.54\mu$eV that is equal for all states. Our derived spin-model, Eq. (4.44), accurately predicts the spin-orbit contributions to the energy spectrum. On the other hand, the models $H_{ex}^{\prime HL}$ and $H_{ex}^{\prime}$ are completely off on the scale of the spin-orbit contributions. The exchange Hamiltonian $H_{ex}^{\prime}$ does not predict the realistic spin-orbit influence on the spectrum, even in the simple case when the magnetic field is zero. The reason is that in the $H_{ex}^{\prime}$, the spin-orbit interactions are present in the linear order only, while in H_{ex} the second order contributions appear.

Figure 4.11 shows the non zero parameters for all four models. The exact isotropic exchange J decays exponentially with the interdot distance. The same behavior is predicted in the Heitler-London approximation. It decays exponentially, but deviates from the numerical results. As for the anisotropic exchange, $H_{ex}^{\prime}$ gives exponentially falling spin-orbit vectors, which are an order of magnitude smaller than J. In contrast, H_{ex} predicts zero spin-orbit parameters. The first main result, proven numerically and justified analytically by the Hamiltonian H_{ex}, is that *at zero magnetic field the spin-orbit vectors vanish at any interdot distance*, up to the second order in spin-orbit couplings. In the transformed basis, there is no anisotropic exchange at zero magnetic field due to the spin-orbit interactions. This is an important result for quantum computation applications. Indeed, since the exchange energy can be used to perform a SWAP operation, this means that the spin-orbit interactions do not induce any significant errors on the gate operation. The only difference is the computational

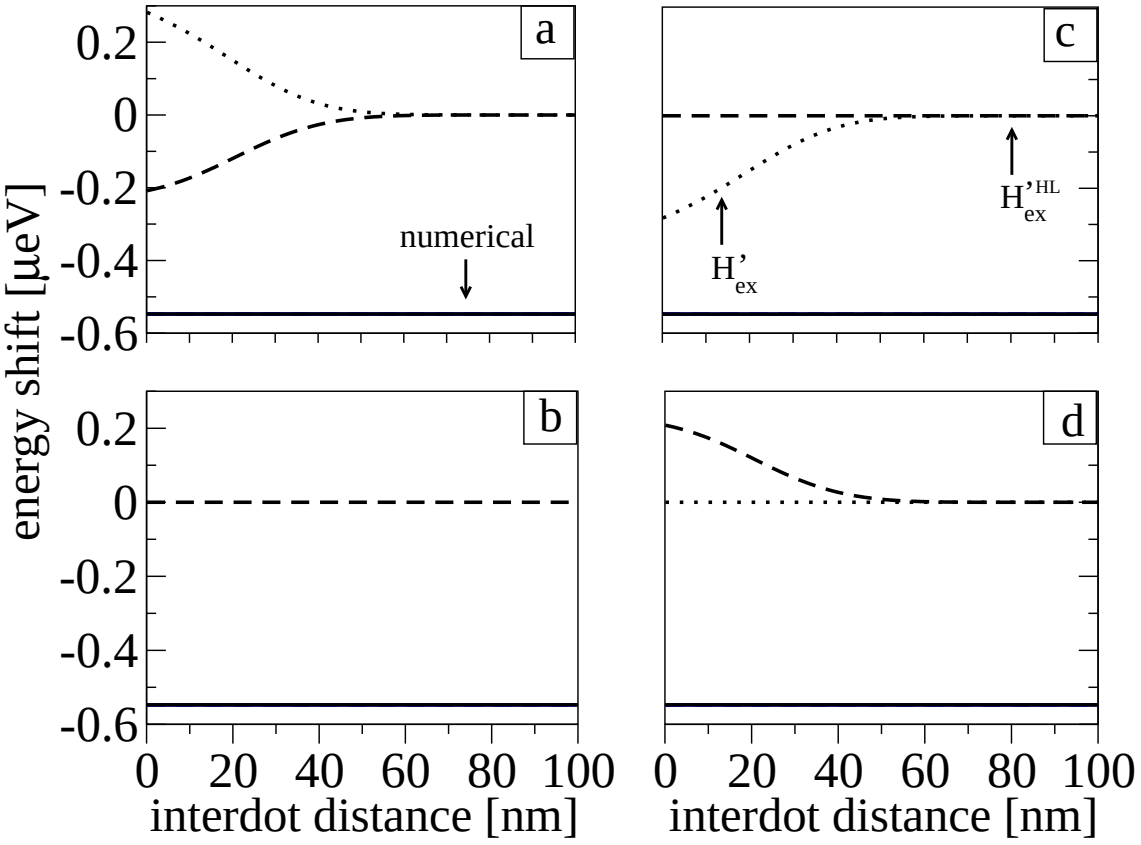

Figure 4.10.: Spin-orbit contributions to the energy at zero magnetic field as a function of the interdot distance. Comparison of the model H'_{ex} and numerics. a) Singlet, b) triplet T_+, c) triplet T_0, d) triplet T_-. The results of H_{ex}^{HL} and H_{ex} are indiscernible from exact numerical data.

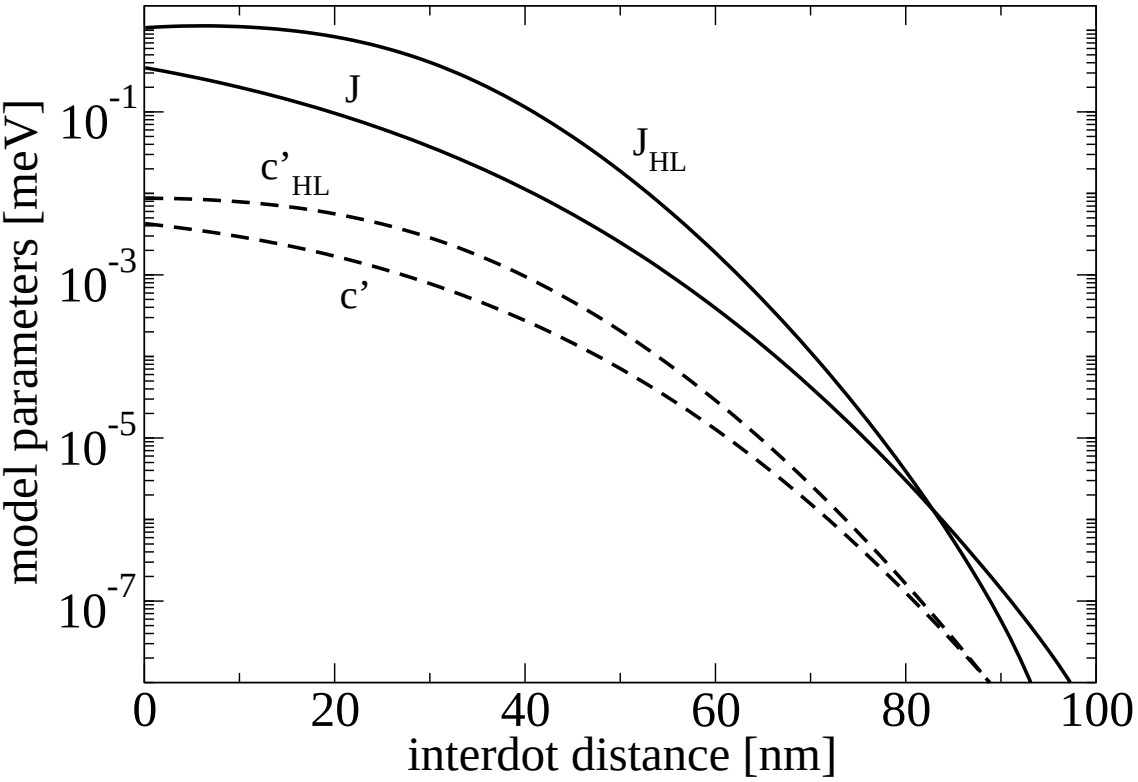

Figure 4.11.: Spin-orbit parameters at zero magnetic field as function of the interdot distance. Isotropic exchange (solid) and the anisotropic vectors (dashed) of the H'_{ex} model.

basis, which is unitarily transformed with respect to the usual singlet-triplet basis.

4.5.3. Finite magnetic field

In the presence of the perpendicular magnetic field the structure of the spin-orbit contributions are quite different with respect to the zero field case. First of all, anticrossing points appear, where the energy shift is enhanced. Figure 4.12 shows the spin-orbit contributions to the magnetic field of 1 T. We plot only the anticrossing states, the singlet, and the triplet T_+. The prediction of the models $H_{ex}^{\prime HL}$, $H_{ex}^{\prime}$ are

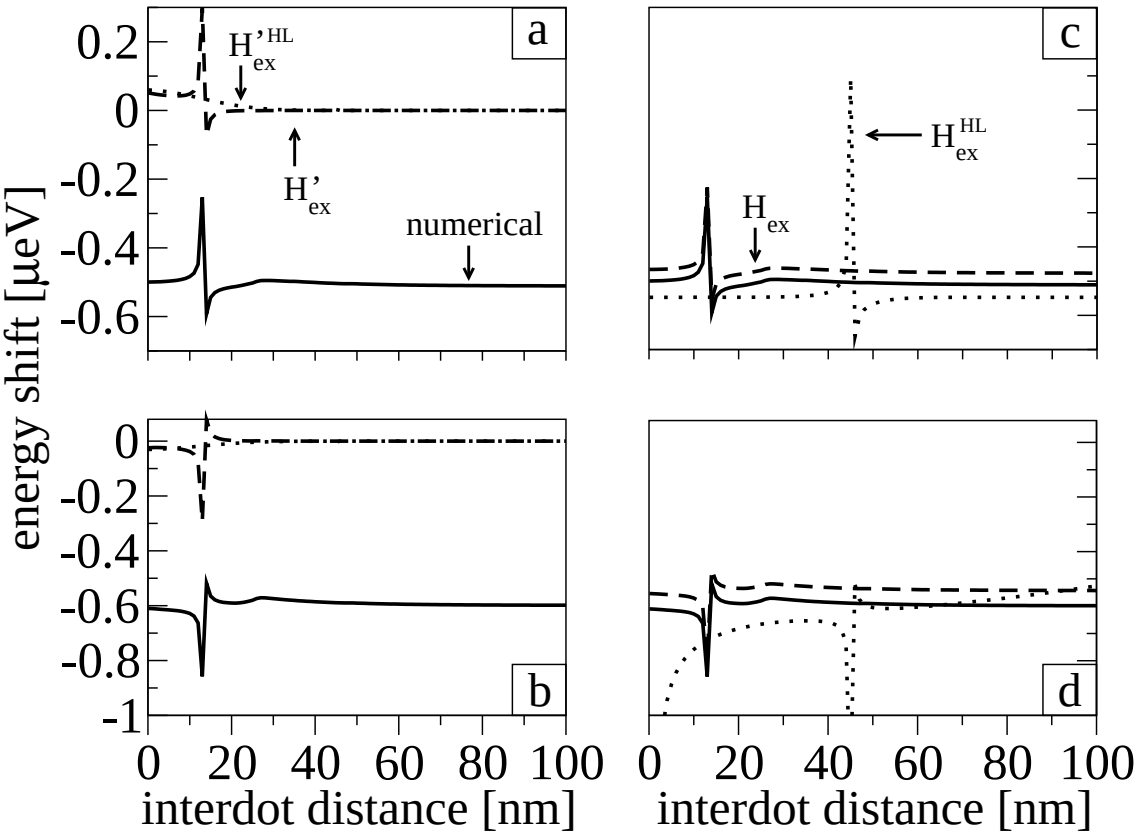

Figure 4.12.: Spin-orbit contributions for a perpendicular magnetic field of 1 T versus the interdot distance. a) and c) Singlet S; b) and d) triplet T_+.

in Fig. 4.12a,b. As in the case of zero magnetic field, these models are off from

the numerical results. In particular, H'_{ex} still predicts a zero contribution for the states. The only non zero contributions are close to the anticrossing point. We note the discrepancy is not due to (a failure of) the Heitler-London approximation, as using the exact numerical two-electron wavefunctions does not improve the model predictions.

In Fig. 4.12c,d, the comparison between the models H_{ex}^{HL}, H_{ex} and the numerics is provided. We observe that the two models are very close to the numerical calculations, even if the model H_{ex}^{HL} predicts the crossing point in a different position. The predictions of the model H_{ex} is consistent with the exact numerics. The only discrepancy is due to the influence of the cubic Dresselhaus term, as we will see in the next section.

We observe two peaks due to the anticrossing point between the singlet S and the triplet T_+ state. Here the spin-orbit contributions are enhanced, since around the anticrossing region the spin is not very well defined due to the spin-orbit interaction. The position of the anticrossing point is the same as in the numerical results, since in the H_{ex}, the isotropic exchange J is taken from numerics. The spin-orbit contributions to the energy are still in accordance with the exact results.

To get more insight, in Fig. 4.13 we have plotted the parameters of the models. Fig. 4.13a shows the anisotropic exchange for the four models. The H'_{ex} model predicts the anisotropic exchange decreasing with the interdot distance, similar to the isotropic exchange energy. For large interdot distance the anisotropic exchange c' vanishes. This means that there is no influence on the energy due to the spin-orbit interaction. This is because the spin-orbit parameter c' is two order of magnitude smaller than the isotropic exchange J. On the other hand, for the model H_{ex} the conclusion is different. For large interdot distances c^{HL} and c are linear in d. Furthermore the anisotropic exchange vector computed in the Heitler-London ansatz is very close to the numerical one. We made a very important observation here: surprisingly, *the Heitler-London is quite a good approximation for all interdot distances.* Therefore, despite its known deficiencies to evaluate the isotropic exchange J, it grasps the anisotropic exchange even quantitatively, rendering the spin-orbit part of the effective Hamiltonian H_{ex} fully analytically.

Figure 4.13b shows the isotropic exchange J, and the effective magnetic field induced by the spin-orbit interaction μB_{so} compared to the Zeeman energy μB. We see the failure of the Heitler-London approximation for J. Although the numerical calculation and the analytical prediction have the same sign (this means that the ground state is the triplet) they differ by an order of magnitude. The Zeeman energy is constant and always much larger than the effective spin-orbit induced magnetic field μB_{so}. Consequently, the effective field can be always neglected. The point

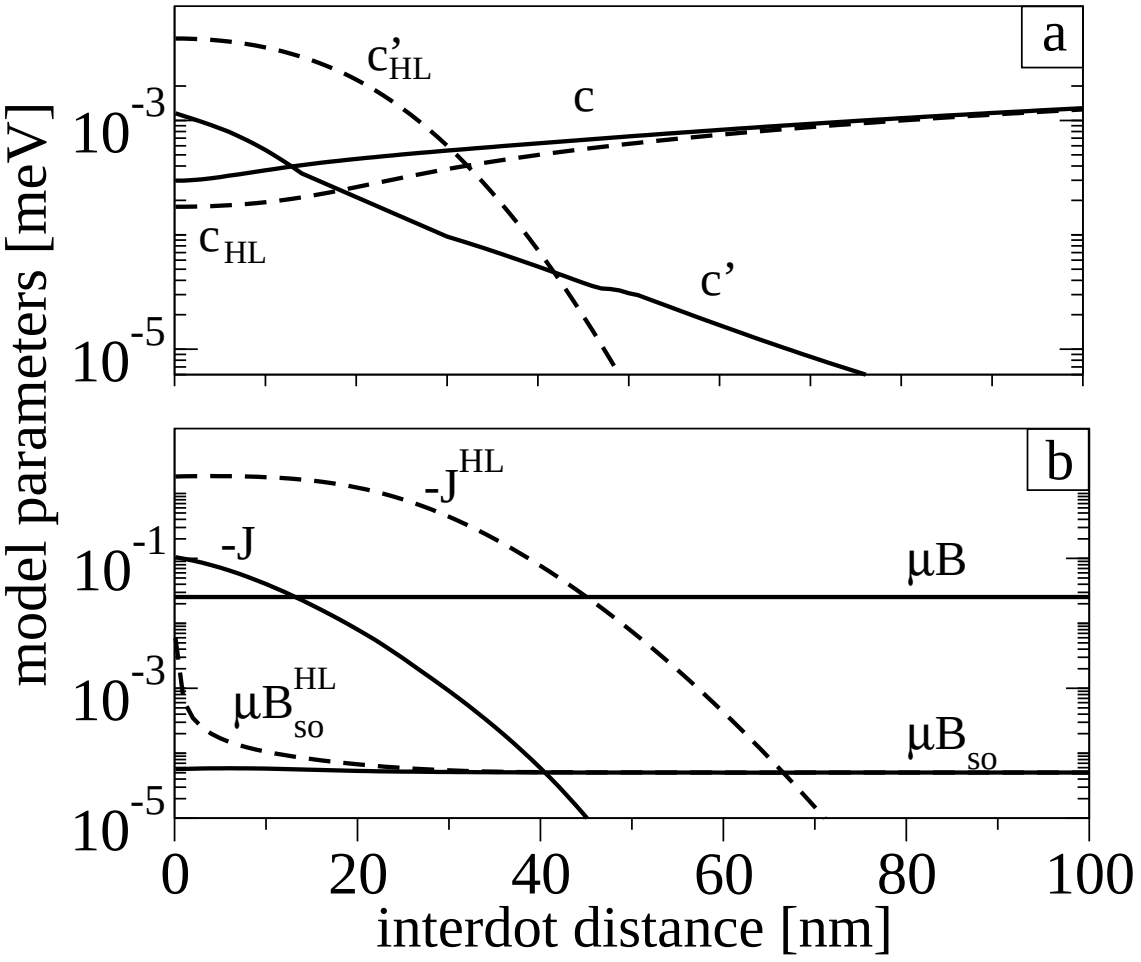

Figure 4.13.: Spin-orbit parameters for a perpendicular magnetic field of 1 T. a) Anisotropic exchange. b) Isotropic exchange, Zeeman energy and the effective induced magnetic field.

where the Zeeman energy equals to the isotropic exchange (close to $d = 18$ nm) is the anticrossing point, where the spin-orbit contributions are strongly enhanced, as one can see in Fig. 4.12.

Let us consider a double dot system at fixed interdot distance of $d = 55$ nm, corresponding to zero field isotropic exchange of 1μeV. In Fig. 4.14 the spin-orbit contributions versus the magnetic field are plotted. The only spin-orbit contributions

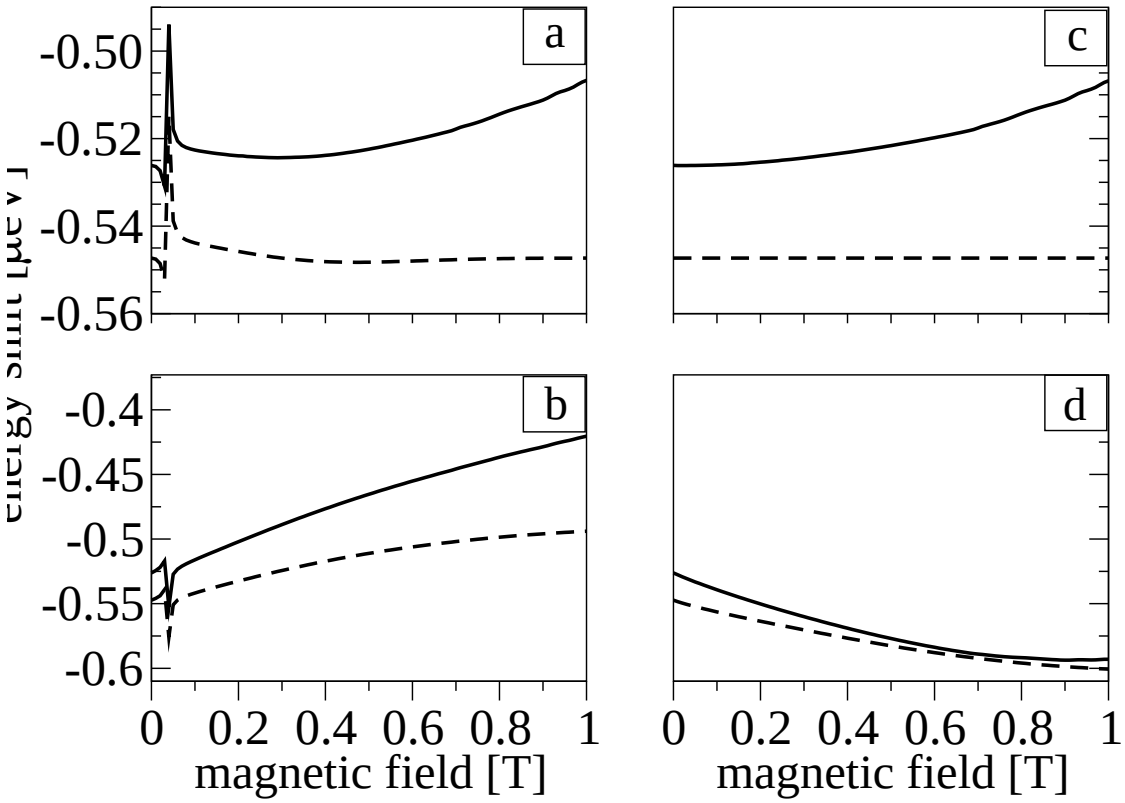

Figure 4.14.: Spin-orbit contribution of a double dot system with interdot distance of 55 nm versus the magnetic field. a) singlet S, b) triplet T_+, c) triplet T_0, d) triplet T_-.

coming from the model H_{ex} are considered. The position of the crossing point is the same as the exact model and also the prediction of the spin-orbit contributions. We can conclude that to describe the spin-orbit influence on the states in a double-dot system it is important to use the Hamiltonian H_{ex}.

In Fig. 4.15 the spin-orbit parameters versus the magnetic field are plotted. Figure 4.15 shows again that the main influence on the states is due to the Zeeman

interaction in all range of B, since μB_{so} is several orders of magnitude smaller than the Zeeman energy. Close to the anticrossing point, the isotropic exchange coupling is close to zero, while the anisotropic exchange c is finite. Since it is two order of magnitude smaller than the Zeeman energy, it does not influence the spin-orbit induced energy shifts.

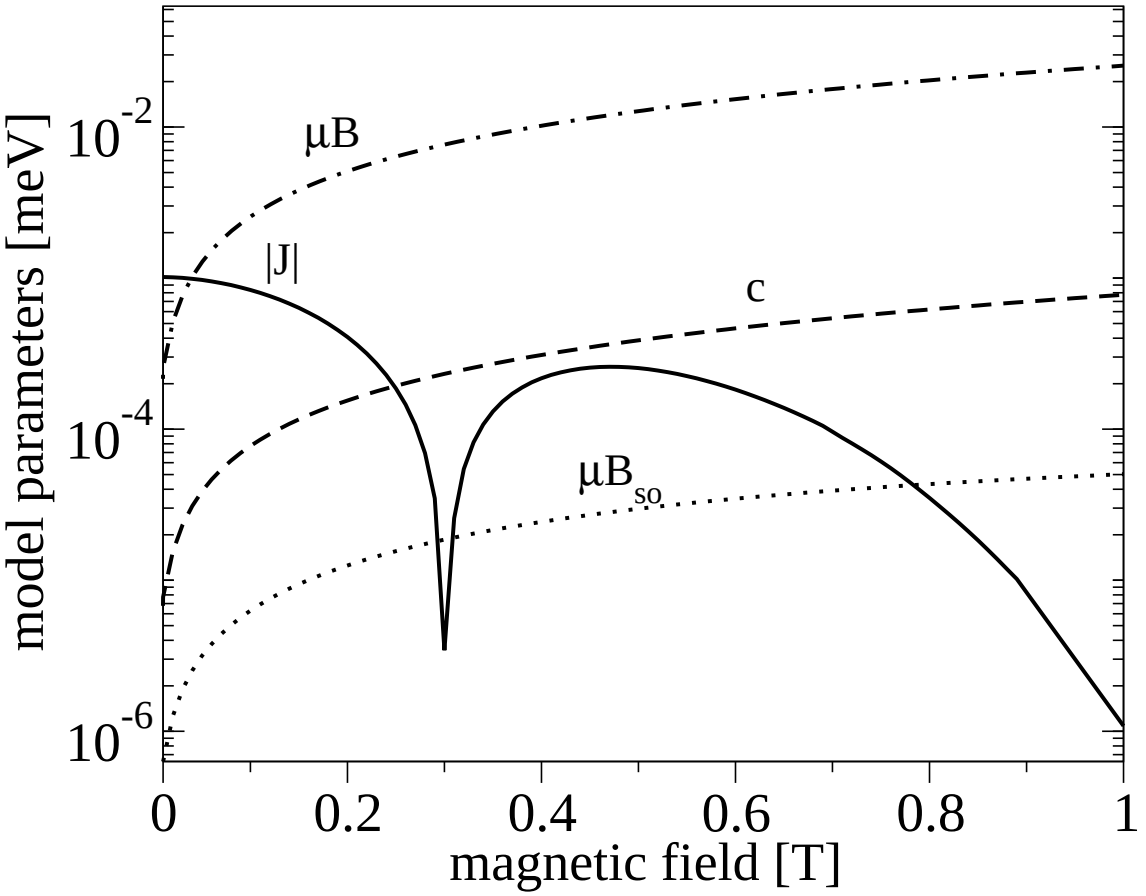

Figure 4.15.: Spin-orbit parameters of a double dot system with interdot distance of 55 nm versus the magnetic field.

4.5.4. Cubic Dresselhaus contributions

Finally we consider the role of the cubic Dresselhaus term. The Schrieffer-Wolff transformation does not remove it in the linear order. Figure 4.16 shows the energy shifts induced by the spin-orbit interactions also in the case where we do not take into account the cubic term. For each of the four states, we compare the result of the numerics with and without the cubic Dresselhaus. One can see a very good agreement

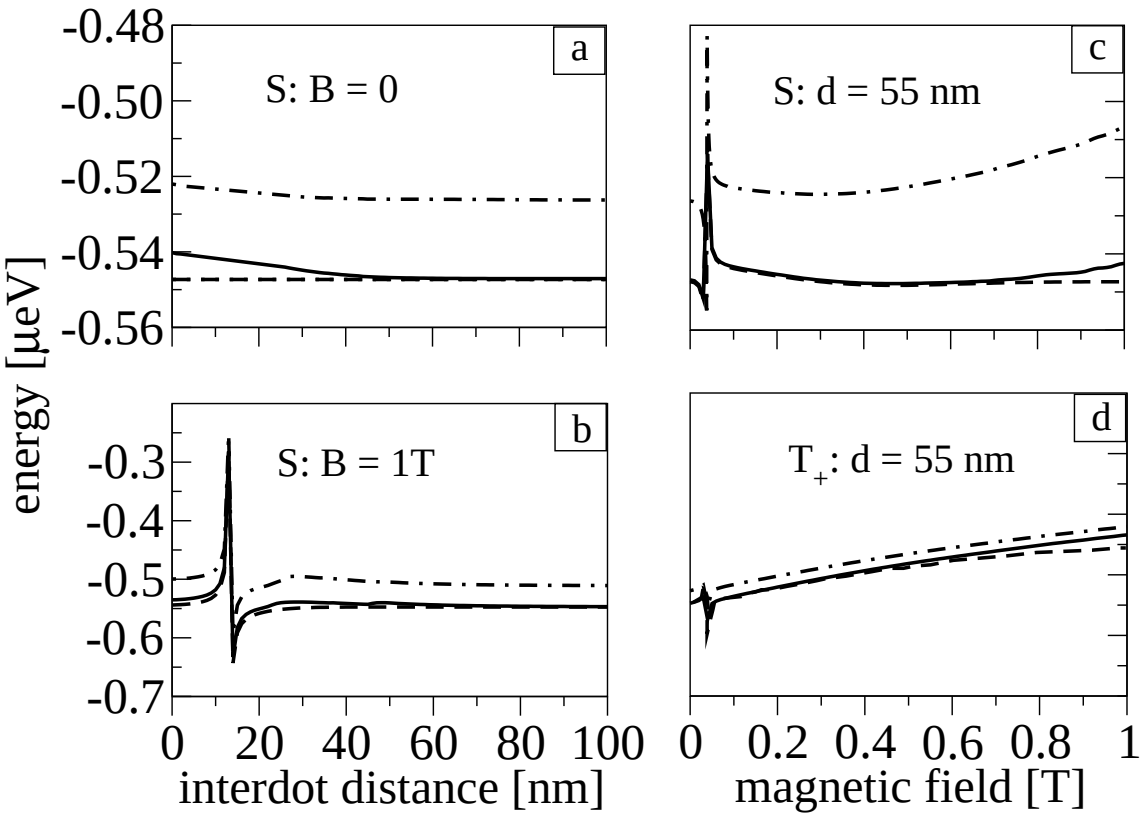

Figure 4.16.: The spin-orbit shift as function of interdot distance (left panel) and perpendicular magnetic field (right panel). a) Singlet in zero magnetic field, b) singlet at 1 T field, c) and d) singlet and triplet T_+ at 55 nm. The exchange model H_{ex} (dashed line), numerics (dot-dashed line) and numerics without the cubic spin-orbit terms (solid line) are compared.

between the prediction of the model H_{ex} and the exact numerics. Therefore we can conclude that the main part of *the discrepancy we see in the spin-orbit induced energy shift are due to the cubic Dresselhaus term.*

4.6. Comparison between models for anisotropic exchange

At zero magnetic field, only the first and the last term in Eq. (4.44) survive. This is the result of Ref. [27], where primed operators were used to refer to the fact that the Hamiltonian H_{ex} refers to the transformed basis, $\{U\Phi_i\}$. Note that if a basis separable in orbital and spin part is required, undoing U necessarily yields the original Hamiltonian in Eq. (4.1), and the restriction to the four lowest states gives H'_{ex}. Replacing the coordinates (x, y) by mean values $(\pm d, 0)$ [19] visualizes the Hamiltonian H_{ex} as an interaction through rotated sigma matrixes, but this is just an approximation, valid if $d, l_{so} \gg l_0$.

One of our main numerical results is establishing the validity of the Hamiltonian in Eq. (4.44) for $B = 0$, confirming recent analytic predictions and extending their applicability beyond the weak coupling limit. *In the transformed basis, the spin-orbit interactions do not lead to any anisotropic exchange, nor do they modify the isotropic one.* In fact, this result could have been anticipated from its single-electron analog: at zero magnetic field there is no spin-orbit contribution to the tunneling energy [52], going opposite to the intuitive notion of the spin-orbit coupling induced coherent spin rotation and spin-flip tunneling amplitudes. Figure 4.18a summarizes this case, with the isotropic exchange as the only nonzero parameter of model $H_{\rm ex}$. In contrast, model $H'_{\rm ex}$ predicts a finite anisotropic exchange.

From the concept of dressed qubits [79] it follows that the main consequence of the spin-orbit interaction, the transformation U of the basis, is not a nuisance for quantum computation. We expect this property to hold also for a qubit array, since the electrons are at fixed positions without the possibility of a long distance tunneling. However, a rigorous analysis of this point is beyond the scope of this thesis. If electrons are allowed to move, U results in the spin relaxation [80].

Figure 4.18b shows model parameters in perpendicular magnetic field of 1 Tesla. The isotropic exchange again decays exponentially. As it becomes smaller than the Zeeman energy, the singlet state anticrosses one of the polarized triplets (seen as cusps on Fig. 4.17). Here it is T_+, due to the negative sign of both the isotropic exchange and the g-factor. Because the Zeeman energy always dominates the spin-dependent terms and the singlet and triplet T_0 are never coupled (see below), the anisotropic exchange influences the energy in the second order [19]. Note the differ-

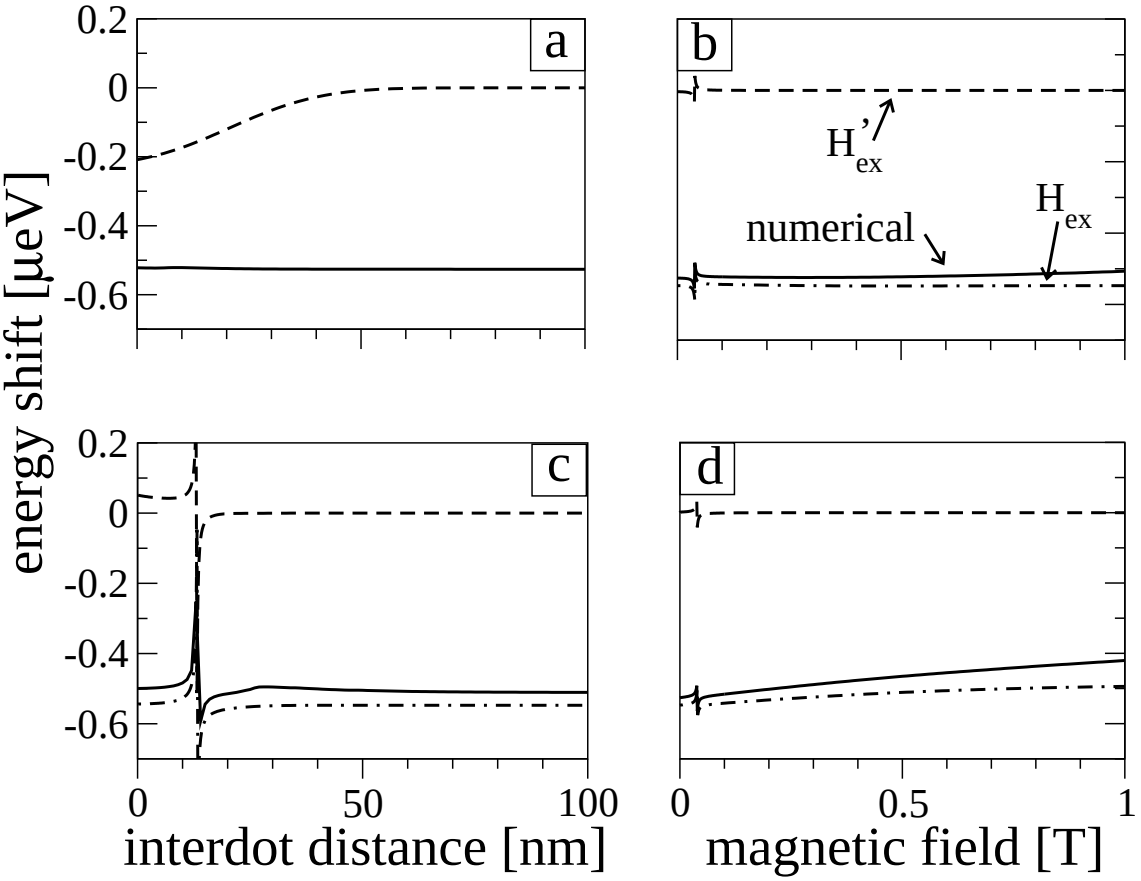

Figure 4.17.: The spin-orbit induced energy shift as a function of the interdot distance (left) and perpendicular magnetic field (right). a) Singlet in zero magnetic field, c) singlet at 1 Tesla field, b) and d) singlet and triplet T_+ at the interdot distance 55 nm corresponding to the zero field isotropic exchange of 1 μeV. The exchange models $H'_{\rm ex}$ (dashed) and $H_{\rm ex}$ (dot-dashed) are compared with the numerics (solid).

ence in the strengths. In $H'_{\rm ex}$ the anisotropic exchange falls off exponentially, while $H_{\rm ex}$ predicts non-exponential behavior, resulting in spin-orbit effects larger by orders of magnitude. The effective magnetic field $B_{\rm so}$ is always much smaller than the real magnetic field and can be neglected in most cases.

Figure 4.18c compares the analytical models. In zero field and no spin-orbit interactions, the isotropic exchange Hamiltonian $H_{\rm iso}$ describes the system. Including the spin-orbit coupling in the first order, $H'_{\rm ex}$, gives a nonzero coupling between the singlet and triplet T_0. Going to the second order, the effective model $H_{\rm ex}$ shows there are no spin-orbit effects (other than the basis redefinition).

The Zeeman interaction splits the three triplets in a finite magnetic field. Both $H'_{\rm ex}$ and $H_{\rm ex}$ predict the same type of coupling in a perpendicular field, between the singlet and the two polarized triplets. Interestingly, in in-plane fields the two models differ qualitatively. In $H'_{\rm ex}$ the spin-orbit vectors are fixed in the plane. Rotation of the magnetic field "redistributes" the couplings among the triplets. (This anisotropy with respect to the crystallographic axis is due to the C_{2v} symmetry of the two-dimensional electron gas in GaAs, imprinted in the Bychkov-Rashba and Dresselhaus interactions [48]). In contrast, the spin-orbit vectors of $H_{\rm ex}$ are always perpendicular to the magnetic field. Remarkably, aligning the magnetic field along a special direction (here we allow an arbitrary positioned double dot, with δ the angle between the main dot axis and the crystallographic x axis),

$$[l_d - l_{br}\tan\delta, l_{br} - l_d\tan\delta, 0], \tag{4.57}$$

all the spin-orbit effects disappear once again, as if B were zero. This has strong implications for the spin-orbit induced singlet-triplet relaxation. Indeed, $S \leftrightarrow T_0$ transitions are *ineffective at any magnetic field*, as these two states are never coupled in our model. Second, $S \leftrightarrow T_\pm$ transitions will show strong (orders of magnitude) anisotropy with respect to the field direction, reaching minimum at the direction given by Eq. (4.57). This prediction is testable in experiments on two-electron spin relaxation.

Our derivation was based on the inversion symmetry of the potential only. What are the limits of our model? We neglected third order terms in $\overline{H}_{so}$ and, restricting the Hilbert space, corrections from higher excited orbital states. (Among the latter is the non-exponential spin-spin coupling [19]). Compared to the second order terms we keep, these are smaller by (at least) d/l_{so} and c/Δ, respectively. Apart from the analytical estimates, the numerics, which includes all terms, assures us that both of these are negligible. Based on numerics we also conclude our analytical model stays quantitatively faithful even at the strong coupling limit, where $\Delta \to 0$. More involved is the influence of the cubic Dresselhaus term, which is not removed by the unitary transformation. This term is the main source for the discrepancy of the model and

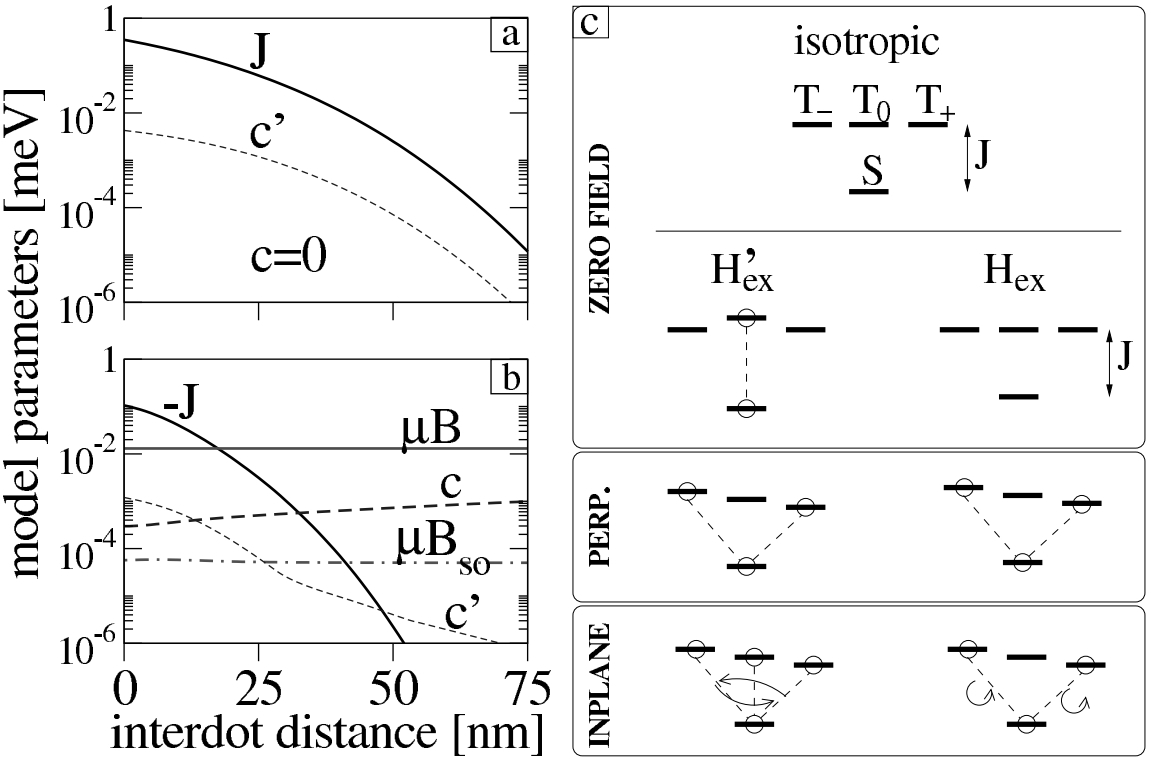

Figure 4.18.: a) The isotropic and anisotropic exchange as functions of the interdot distance at zero magnetic field. b) The isotropic exchange J, anisotropic exchange c/c', the Zeeman splitting μB, and its spin-orbit part μB_{so} at perpendicular magnetic field of 1 Tesla. c) Schematics of the exchange-split four lowest states for the three models, $H_{\rm iso}$, $H'_{\rm ex}$, and $H_{\rm ex}$, which include the spin-orbit coupling in the first, and second order, respectively, at zero magnetic field (top). The latter two models are compared in perpendicular and in-plane magnetic fields as well. The eigenenergies are indicated by the solid lines. The dashed lines show which states are coupled by the spin-orbit coupling. The arrows indicate the redistribution of the couplings as the in-plane field direction changes with respect to the crystallographic axes (see the main text).

the numerical data in finite fields. Most importantly, it does not change our results for $B = 0$.

4.7. Discussion

We analyzed the spin-orbit influence on two electrons confined in a lateral double quantum dot. We focused on the lowest part of the Hilbert space, which corresponds to a qubit pair. In Ref. [29] a Hamiltonian for such pair was proposed, with the spin-orbit interactions giving raise to an anisotropic exchange interaction. Within a unitarily transformed basis, this interaction is encoded into two real three dimensional spin-orbit vectors. These, together with the isotropic exchange energy and the magnetic field vector, completely parameterize an effective two qubit Hamiltonian. In this thesis, we examined the quantitative validity of this effective Hamiltonian.

In addition to a numerical study, we also provided the details of the effective Hamiltonian derivation. We noted that it can be diagonalized in the case of zero magnetic field and aligned spin-orbit vectors, the only exactly solvable case (apart from the trivial case of no spin-orbit interactions present). We also evaluated the spin-orbit vectors in the Heitler-London approximation and compared the analytical results with their exact numerical counterparts [28].

There are three possible sources for a discrepancy between the model and the exact data: the higher excited orbital states of the quantum dot, the higher orders of the effective (unitary transformed) spin-orbit interaction and the cubic Dresselhaus term. Elucidation of their importance is one of the main results of this thesis. i) We find the cubic Dresselhaus term is the main source of the discrepancy. In a typical double dot regime and a moderate field of 1 Tesla, it brings an error of $\sim 0.1\mu$eV for the energies, while the two other mentioned corrections have an order of magnitude smaller influence. ii) We find the effective Hamiltonian describes both the weak and the strong coupling regimes (the single dot represents the strongest possible coupling). iii) Surprisingly, the spin-orbit vectors obtained within the Heitler-London approximation are faithful even at a finite magnetic field. Overall, we find the anisotropic exchange Hamiltonian to be generally reliable, providing a realistic and yet simple description for an interacting pair of spin qubits realized by two coupled quantum dots.

5. Numerical Method

Here we describe the numerical method we use to diagonalize the two electron Hamiltonian Eq. (4.1). We proceed in three steps. We first solve the single particle Schrödinger equation $H = T + V$ numerically, using finite differences method with the Dirichlet boundary condition (vanishing of wave function at boundaries). We do not take into account the spin-dependent part (Zeeman and spin-orbit interactions) of the Hamiltonian at this stage. This allows us to exploit symmetries of the confinement potential, as we explain below. In the second step, using the single electron eigenstates, we construct the two electron states. In this new basis we compute the two electron Hamiltonian, including the matrix elements of the Coulomb interaction numerically. Then in the last step we add the spin dependent parts in the Hamiltonian and diagonalize it. We have performed a detailed analysis of the two proposed approaches for the two-electron diagonalization and studied the numerical precision of the Coulomb integrals.

5.1. Introduction

In the study of the quantum dot physics, one realizes that the Coulomb interaction term can not be treated in the perturbative way. The problem is similar to the atomic physics, where the electrons are moving in a confinement potential energy of the Coulomb type. In the atoms, the electron-electron interaction plays not a relevant role, since it is quite small compared to the field generated by the nuclei. In the absence of external fields, the atomistic spin-independent Hamiltonian of Z electrons is

$$H = \sum_{i=1}^{Z} \left(\frac{p_i^2}{2m} - Z \frac{e^2}{4\pi\epsilon_0 r_i} \right) + \frac{1}{2} \sum_{i=1}^{Z} \sum_{j \neq i}^{Z} \frac{e^2}{4\pi\epsilon_0 |\mathbf{r}_i - \mathbf{r}_j|}. \tag{5.1}$$

Except for one electron ($Z = 1$), the eigenvalues problem for the Hamiltonian Eq. (5.1) is not analytically solvable. The simplest approach to many-body physics is the Hartree-Fock method. For few electrons systems, the perturbation theory and the variational calculus lead to results rather satisfactory. Comparing the energies

involved in the problem, we get

$$\frac{\sum_{i=1}^{Z} Z\frac{e^2}{r_i}}{\frac{1}{2}\sum_{i=1}^{Z}\sum_{j\neq i}^{Z}\frac{e^2}{|\mathbf{r}_i-\mathbf{r}_j|}} \simeq 2Z, \tag{5.2}$$

and then for atomic systems with large Z, the interaction energy between the electrons can be treat as a perturbation.

For quantum dots, the problem is not so simple, since the confinement potential of the two-electron gas does not depend on the number of particles involved. In this systems, the usual approximation methods can not be applied. The recent methods use numerical techniques, which gives us a better understanding of strong correlated systems.

In lateral quantum dots the Coulomb energy E_C is comparable to the confinement energy and the correlation between the electrons strongly influence the states. The validity regimes of application in which one should apply a numerical approach, can be classified naively introducing a dimensionless parameter λ. This is defined as the ratio between the Coulomb interaction and a typical confinement energy

$$\lambda = \frac{E_C}{E_0} = \frac{e^2}{4\pi\epsilon_0\epsilon_r}\langle\frac{1}{r}\rangle\frac{ml_0^2}{\hbar^2} \sim \frac{l_0^2}{l_C\langle r\rangle}, \tag{5.3}$$

where the Coulomb length $l_C = e^2m/4\pi\epsilon_0\epsilon_r\hbar^2$ is a material parameter.

In the case of a quantum dot where the correlation between the electrons is quite small, $\lambda \sim 0$, it is possible to use the perturbative methods and analyze the confinemet potential effects on the energy spectrum. When E_C becomes larger, in the regime of small coupling, $\lambda \sim 1$, one can use the Hartree-Fock method with very good results. In typical GaAs quantum dots, $l_C \approx 10$ nm, while a typical lateral dot has $l_0 \approx 30$ nm, corresponding to $E_0 \approx 1$ meV. The mean length $\langle r\rangle$ is of the order of the confinement length, if the two electrons are on the same dot, and of the interdot distance, if the electrons are on different dots. In the first case, the Coulomb energy is typically 3 meV. In the second case (one electron per dot) the Coulomb interaction is typically larger than 1 meV. In this case $\lambda \sim 2 \div 4$ and the strength of the Coulomb interaction precludes the use of perturbative methods. Therefore, to diagonalize the two electron Hamiltonian Eq. (4.1), we use the exact numerical treatment, the Configuration Interaction method.

5.2. Finite differences

The finite differences is a numerical method to calculate the solution of a differential equation, where the derivatives are replaced by finite differences approximations.

This gives a large algebraic system of equations to be solved in place of the differential equation, something that is easily solved on a computer.

Now we want to solve the Schrödinger partial differential equation

$$H_1\psi(\mathbf{r}) = \epsilon\psi(\mathbf{r}), \quad H_1 = T_1 + V_1, \tag{5.4}$$

where H_1 is the single particle Hamiltonian, see Eq. (4.2). We proceed by the discretization of the position variables. Therefore we do not consider them as continuous variables, but as a set of discrete points defined on a two-dimensional grid

$$\{\mathbf{r}_{ij} = id_x\hat{x} + jd_y\hat{y}\}, \quad i = 1, ..., N_x; \;\; i = 1, ..., N_y. \tag{5.5}$$

The total number of points on the grid is $N = N_x \times N_y$, where $N_{x(y)}$ is the number of points along the $x(y)$ direction. The distance between two points is defined by $d_{x(y)}$ and determines the accuracy of the numerical solution. The wavefunction is also discretized as an array of N points

$$\psi(\mathbf{r}) \to \{\psi(\mathbf{r}_{ij})\}_{i,j}. \tag{5.6}$$

Now we derive the discretized form of the Schrödinger equation. It can be written as

$$H(\mathbf{r}, -i\hbar\nabla)\psi(\mathbf{r}) = \epsilon\psi(\mathbf{r}) \to H_{ij,kl}\psi_{kl} = \epsilon\psi_{kl}, \tag{5.7}$$

where $H_{ij,kl}$ is a $N \times N$ matrix that one has to compute depending of the operators involved in the Hamiltonian. In the single particle Hamiltonian we have two kind of operators that need to be represented in discrete form. One is a non-differential operator, the confinement potential, which corresponds to a diagonal matrix $V_{ij,kl} = \delta_{ik}\delta_{jl}V(\mathbf{r}_{ij})$. The second one is a differential operator, the kinetic energy. We use the finite differences approximation to write it in discrete form. As an example, we consider a first derivative operator as ∂_x. Using the Taylor expansion of the wavefunction at points $\mathbf{r}_{i\pm1,j}$,

$$\psi_{i\pm1,j} = \psi(\mathbf{r}_{ij} \pm d_x\hat{x}) = \psi_{i,j} \pm (\partial_x\psi)_{ij}d_x + (1/2!)(\partial^2_{xx}\psi)_{ij}d_x^2 \pm O(d_x^3), \tag{5.8}$$

we can derive the lowest order discrete representation of the first partial derivative

$$(\partial_x\psi)_{ij} = \frac{1}{2d_x}(\psi_{i+1,j} - \psi_{i-1,j}). \tag{5.9}$$

The operator matrix definition given in Eq. (5.7) for the differential operator is

$$(\partial_x)_{ij,kl} = \frac{1}{2d_x}(\delta_{i+1,k}\delta_{jl} - \delta_{i-1,k}\delta_{jl}). \tag{5.10}$$

The order of the approximation for the derivatives gives the precision of the numerical solution. One can increase the precision just adding more terms in the Taylor expansion.

Let us consider to have a magnetic field applied to the system. The kinetic operator changes in $-i\hbar\nabla = -i\hbar\nabla + e\mathbf{A}$, where $\mathbf{A}$ is the vector potential. The orbital effects due to the magnetic field can be easily incorporated via the Peierls phase. This gives

$$H\psi(\mathbf{r}, -i\hbar\nabla + e\mathbf{A}) \rightarrow H'_{ij,kl} = H_{ij,kl} \exp\left(i(e/\hbar \int_{\mathbf{r}_{ij}}^{\mathbf{r}_{kl}} \mathbf{A} \cdot d\mathbf{r})\right), \tag{5.11}$$

where only a simple numerical integration has to be performed. Once we have the Hamiltonian matrix, we diagonalize it by the Lanczos method.

5.3. Lanczos diagonalization

To compute the eigenvalues and the eigenvectors of a given Hamiltonian, one can simply represent the Hamiltonian in a certain basis $|\psi_n\rangle$ (with $n = 1...N$),

$$H_{nn'} = \langle\psi_n|H|\psi_{n'}\rangle, \tag{5.12}$$

which gives a $N \times N$ matrix to diagonalize. There are a lot methods and packages which accomplish this aim (for example LAPACK package [81]). This approach can be useful in the cases where the matrix to be diagonalized can be hold completely in the memory. In a many body problem, the matrix can be very large, depending on the number of basis functions and the electrons. In general the dimension of the Hilbert space increases exponentially in the number of the single electron functions used to construct the Slater determinants. Indeed, for a given number of basis functions N and spin up and down electrons, $n_\uparrow$ and $n_\downarrow$ respectively, the Hilbert space dimension is

$$N_H = \frac{N!}{n_\uparrow!(N-n_\uparrow)!} \times \frac{N!}{n_\downarrow!(N-n_\downarrow)!}. \tag{5.13}$$

For example for $N = 20$, 4 electrons and considering the degeneracy in the spin, we have $N_H = (4845)^2 = 23474025$. This means that the matrix dimension to diagonalize is 23474025×23474025, quite large number to manage. Furthermore we have $\sim 2 \cdot 10^7 \times 2 \cdot 10^7 = 4 \cdot 10^{14}$ matrix elements to store and then we would need 400 TBytes of memory. To avoid this problem, we will use the Lanczos method, which is an iterative method which constructs only the matrix element we need.

The Lanczos method is one of the exact diagonalization techniques [82]. It is a recursive method which gives the information on the lowest part of the spectrum,

with very high precision (usually chosen by the user). This is frequently used for very large sparse matrices.

The main purpose is to find a particular basis where the matrix has a tridiagonal form. The procedure is quite straightforward. Let us consider a matrix H and a given arbitrary vector $|\phi_0\rangle$, belonging to the Hilbert space of the system we are going to study. The dimension of the vector $|\phi_0\rangle$ is N where N is the dimension of the matrix H. The normalization condition gives $\langle\phi_0|\phi_0\rangle = 1$. We apply the matrix H to the initial vector $|\phi_0\rangle$ such that we have a new vector orthogonal to the previous

$$\beta_1|\Psi_1\rangle = H|\phi_0\rangle - \alpha_0|\phi_0\rangle. \tag{5.14}$$

The orthogonality condition requires

$$\beta_1\langle\phi_0|\Psi_1\rangle = \langle\phi_0|H|\phi_0\rangle - \alpha_0\langle\phi_0|\phi_0\rangle, \tag{5.15}$$

and since $|\phi_0\rangle$ is normalized, we have

$$\alpha_0 = \langle\phi_0|H|\phi_0\rangle. \tag{5.16}$$

The coefficient α_0 is the mean value of the energy on the state $|\phi_0\rangle$. The value for β_1 can be obtained requiring

$$\beta_1 = \langle\Psi_1|H|\phi_0\rangle. \tag{5.17}$$

We note that using the Eq. (5.14), we have

$$\beta_1^2 = \langle\phi_0|(H-\alpha_0)(H-\alpha_0)|\phi_0\rangle = \langle\phi_0|H^2|\phi_0\rangle - \alpha_0^2, \tag{5.18}$$

which corresponds to the mean square value on the state $|\phi_0\rangle$. The next step is to proceed applying the H operator on the state $|\Psi_1\rangle$ to get a new vector $|\Psi_2\rangle$ orthogonal to the two previous. Hence

$$\beta_2|\Psi_2\rangle = H|\Psi_1\rangle - \alpha_1|\Psi_1\rangle - C|\phi_0\rangle. \tag{5.19}$$

The orthogonality conditions force

$$\langle\Psi_1|\Psi_2\rangle = 0 \;\Rightarrow\; \alpha_1 = \langle\Psi_1|H|\Psi_1\rangle \tag{5.20}$$

$$\langle\phi_0|\Psi_2\rangle = 0 \;\Rightarrow\; \langle\phi_0|H|\Psi_1\rangle - C = 0 \Rightarrow C = \beta_1, \tag{5.21}$$

and making $|\Psi_2\rangle$ normalized we obtain

$$\beta_2 = \langle\Psi_2|H|\Psi_1\rangle. \tag{5.22}$$

Now we show how a step further in this iterative procedure leads to an important consequence for the Lanczos process, i.e. a tridiagonal matrix. We define the next vector $|\Psi_3\rangle$ in the similar way of the previous

$$\beta_3|\Psi_3\rangle = H|\Psi_2\rangle - \alpha_2|\Psi_2\rangle - C_1|\Psi_1\rangle - C_0|\phi_0\rangle. \tag{5.23}$$

The orthogonality conditions give

$$\langle\Psi_2|\Psi_3\rangle = 0 \;\Rightarrow\; \alpha_2 = \langle\Psi_2|H|\Psi_2\rangle \tag{5.24}$$
$$\langle\Psi_1|\Psi_3\rangle = 0 \;\Rightarrow\; \langle\Psi_1|H|\Psi_2\rangle - C_1 = 0 \Rightarrow C_1 = \beta_2 \tag{5.25}$$
$$\langle\phi_0|\Psi_3\rangle = 0 \;\Rightarrow\; C_0 = \langle\phi_0|\Psi_2\rangle = 0, \tag{5.26}$$

where we have used $H|\phi_0\rangle = \beta_1|\Psi_1\rangle + \alpha_0|\phi_0\rangle$, and then

$$C_0 = \langle\phi_0|H|\Psi_2\rangle = \beta_1\langle\Psi_1|\Psi_2\rangle + \alpha_0\langle\phi_0|\Psi_2\rangle = 0. \tag{5.27}$$

Therefore we note that constructing the vector $|\Psi_3\rangle$ in that way, orthogonal to the two previous vectors, automatically ensure the orthogonality to the first vector $|\phi_0\rangle$. This important statement yields the Lanczos method very efficient, since it is enough to construct the vector at the step n orthogonal only to the vectors at the two previous steps. This ensure the orthogonality even to the other vectors. The recurrence law for the basis is

$$\beta_n|\Psi_n\rangle = H|\Psi_{n-1}\rangle - \alpha_{n-1}|\Psi_{n-1}\rangle - \beta_{n-1}|\Psi_{n-2}\rangle, \tag{5.28}$$

with $n = 1, 2, ...$ and the coefficients are given by

$$\alpha_{n-1} = \langle\Psi_{n-1}|H|\Psi_{n-1}\rangle \tag{5.29}$$
$$\beta_{n-1} = \langle\Psi_{n-1}|H|\Psi_{n-2}\rangle \tag{5.30}$$
$$\beta_n = \langle\Psi_n|H|\Psi_{n-1}\rangle. \tag{5.31}$$

The three terms in the Eq. (5.28) are all those needed to generate the orthonormal basis where H has a tridiagonal form

$$H = \begin{pmatrix} \alpha_0 & \beta_1 & 0 & 0 & \dots \\ \beta_1 & \alpha_1 & \beta_2 & 0 & \dots \\ 0 & \beta_2 & \alpha_2 & \beta_3 & \dots \\ 0 & 0 & \beta_3 & \alpha_3 & \dots \\ \vdots & \vdots & \vdots & \vdots & \ddots \end{pmatrix}.$$

Once in this form, the matrix can be easily diagonalized by using package library like LAPACK [81], which are optimized for this aim. In our calculations we have used

the ARPACK [83] package, a collection of subroutines designed to solve large scale eigenvalue problems.

One of the benefits of this procedure is that one can obtain information sufficiently accurate on the ground state and the first exited states. The number of iterations is quite small (typically less then 100) and we do not have to construct the whole matrix. Indeed after 100 steps, the Lanczos procedure has produced a 100×100 matrix, which requires only 10^4 bytes to store. The direct diagonalization of the matrix is not necessary since we really do not need to know the whole spectrum, but only few states. The only disadvantage of this method is the increasing number of basis vectors for each iteration. But one can even reduce it by using the symmetry property of the system.

5.4. Basis for the two electron diagonalization

We write the Hamiltonian of the two electron system as

$$H_{tot} = H_C(\mathbf{r}_1, \mathbf{r}_2) + \sum_{i=1,2} H_{0,i}(\mathbf{r}_i, \mathbf{K}_i) + H_{so,i}(\mathbf{K}_i, \boldsymbol{\sigma}_i) + H_{Z,i}(\boldsymbol{\sigma}_i), \tag{5.32}$$

where the first term is the two particle Coulomb interaction and the second is the sum of the single electron double dot Hamiltonians for each electron. A single electron Hamiltonian consists of the kinetic energy and confinement part, $H_0 = T + V$, spin-orbit interaction H_{so}, and the Zeeman term H_Z.

The question we will be concerned in the following is: which approach should we choose to obtain the two electron eigenstates of H_{tot}? There are quite many possibilities and we will not list here all. We will compare only two – our current strategy and its small modification, which is much more precise and suitable for the reasons we will explain. The two approaches differ in which basis we choose to diagonalize the single particle Hamiltonian.

In the first approach, the diagonalization of H_{tot} proceeds in two steps: first, the single electron states are obtained as solutions of the full single particle Hamiltonian including spin-orbit and Zeeman terms. The two particle states are then created as antisymmetric combinations of the single particle states (Slater determinants). The two particle Hamiltonian Eq. (5.32) is then diagonalized in this basis – single particle energies appear on the diagonal, while the Coulomb matrix elements appear both on the diagonal and off the diagonal. The advantage of this approach is that it is simpler. The disadvantage is that due to the strength of the Coulomb interaction, the expected error using a computationally feasible basis is several percent for the energies.

In the second approach, we first diagonalize the single particle Hamiltonian consisting of only the kinetic energy and the double dot confinement potential – the spin does not have to be considered at this stage. Once we have the single particle states, we build the two particle states of two kinds – an antisymmetric combination of orbital single particle wavefunctions times one of the three spin triplets, and a symmetric combination of orbital wavefunctions times spin singlet. In this basis the orbital part of the Hamiltonian is diagonalized. The advantage of this approach is in this step – due to the spatial and spin symmetries, the matrix being diagonalized, $H_{0,1} + H_{0,2} + H_C$, is block diagonal. This allows to use approximately twice as many single particle states in the basis and get an order of magnitude better precision. The spin dependent part of Eq. (5.32) is taken into account in the third diagonalization. Since this part of the Hamiltonian is a small perturbation, just a few two particle states will suffice to be included in the basis – there will be negligible overhead in computation time. The price is that the algorithm is more complex. We have implemented this last approach. A flow chart of the two presented algorithms is given in the Fig. 5.1.

5.4.1. Relative strengths of parts of the Hamiltonian

First let us look at the hierarchy of the interactions' strengths. We take the confinement energy $E_0 = \hbar^2/ml_0^2$ as the scale. A typical confinement energy of a single GaAs lateral electrostatic quantum dot is a few meV. For example, for a harmonic confinement, a confinement length of $l_0 = 30$ nm corresponds to 1.3 meV. The confinement energy equals the excitation energy, that is the energy difference of two neighbor orbital excited states. The perpendicular magnetic field makes the excitation energy inside a Landau level smaller, while increasing the distance between different Landau levels. The interdot distance has large influence on the energy differences of levels that are degenerate for zero or very large interdot distance, but the energy differences between different such groups are still roughly given by the confinement energy. The Coulomb energy in units of confinement energy is given in Eq. (5.3). The strengths of the interactions of the model are compared in Tab. 5.1. To treat the Coulomb interaction as a perturbation does not have to be as catastrophic as it seems from the Tab. 5.1, if a large part of the Coulomb energy would be the classical charging energy (constant) and just a small part would be dependent on the actual electron wavefunction. Let us therefore look at the variation of the Coulomb energy. In Fig. 5.2 there are Coulomb energies of two electron states built as symmetric combinations of single particle Fock Darwin states from the low part of the spectrum. From there one can see that the classical charging energy is ~ 1.5, if higher excited single particle states are forbidden (energy at which one can cut the basis is defined

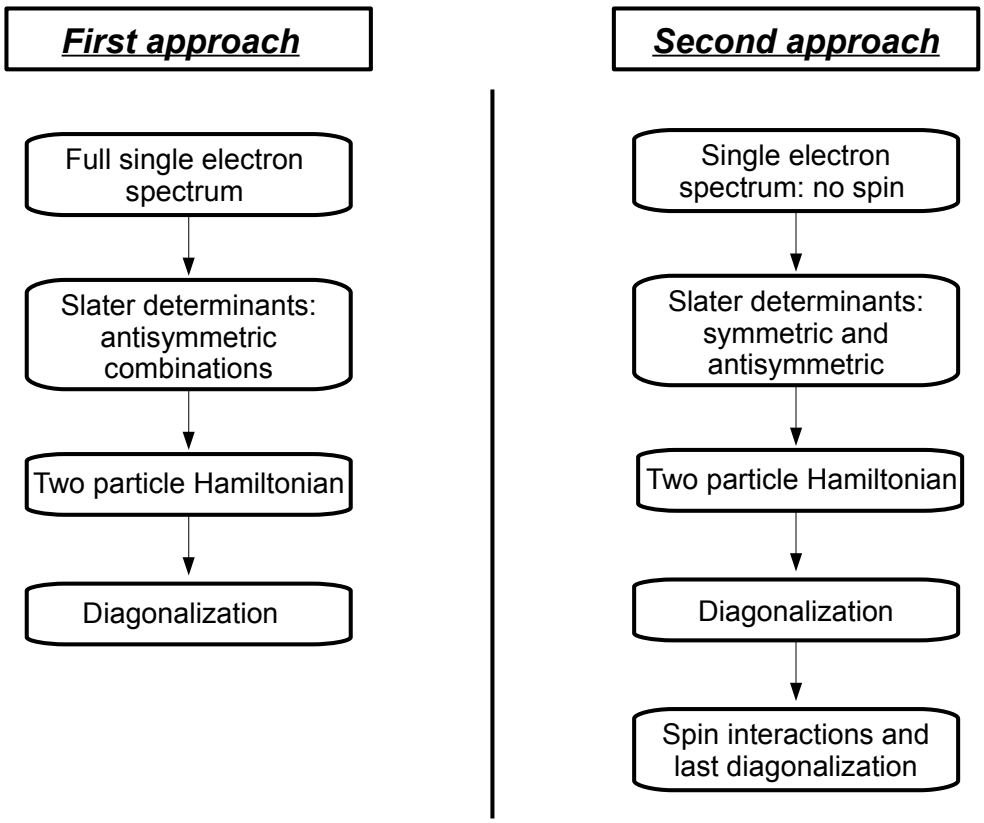

Figure 5.1.: Flow chart scheme of the two approaches investigated for the numerical procedure.

confinement energy	$\hbar^2/ml_0^2$	1 (=1.3 meV)
Coulomb (both electrons in one dot)	l_0/l_C	3
Coulomb (electrons in different dots)	l_0^2/dl_C	1
spin-orbit (linear)	l_0/l_{so}	10^{-2}
spin-orbit (cubic)	$l_0^3/l_{so}l_z^2$	10^{-3}
Zeeman (at 1 Tesla)	$g\mu_B B/E_0$	2.10^{-2}

Table 5.1.: Relative strengths of interactions in the model (order of magnitude values).

by the confining potential). More importantly, the variation of the Coulomb energies between different two particle states is substantial on the scale of confinement energy.

$$\begin{pmatrix}
7.37 & 1.84 & 1.84 & 2.53 & 3.23 & 2.53 & 1.67 & 1.79 & 1.79 & 1.67 & 2.48 \\
1.84 & 5.07 & 3.23 & 1.32 & 1.73 & 1.79 & 2.35 & 2.38 & 2.2 & 2.17 & 1.6 \\
1.84 & 3.23 & 5.07 & 1.79 & 1.73 & 1.32 & 2.17 & 2.2 & 2.38 & 2.35 & 1.6 \\
2.53 & 1.32 & 1.79 & 4.21 & 2.38 & 2.48 & 1.09 & 1.5 & 1.6 & 1.65 & 1.83 \\
3.23 & 1.73 & 1.73 & 2.38 & 4.41 & 2.38 & 1.48 & 1.41 & 1.41 & 1.48 & 2.29 \\
2.53 & 1.79 & 1.32 & 2.48 & 2.38 & 4.21 & 1.65 & 1.6 & 1.5 & 1.09 & 1.83 \\
1.67 & 2.35 & 2.17 & 1.09 & 1.48 & 1.65 & 3.72 & 2.02 & 1.92 & 2.12 & 1.42 \\
1.79 & 2.38 & 2.2 & 1.5 & 1.41 & 1.6 & 2.02 & 3.66 & 2.29 & 1.92 & 1.36 \\
1.79 & 2.2 & 2.38 & 1.6 & 1.41 & 1.5 & 1.92 & 2.29 & 3.66 & 2.02 & 1.36 \\
1.67 & 2.17 & 2.35 & 1.65 & 1.48 & 1.09 & 2.12 & 1.92 & 2.02 & 3.72 & 1.42 \\
2.48 & 1.6 & 1.6 & 1.83 & 2.29 & 1.83 & 1.42 & 1.36 & 1.36 & 1.42 & 3.41
\end{pmatrix}$$

Figure 5.2.: Coulomb energies of 121 two particle states. Entry at row i, column j is the Coulomb matrix element $\langle ij|C|ij\rangle$, where i, j denote single particle states from the set$\{\psi_{00}, \psi_{01}, \psi_{0\bar{1}}, \psi_{02}, \psi_{10}, \psi_{0\bar{2}}, \psi_{03}, \psi_{11}, \psi_{1\bar{1}}, \psi_{0\bar{3}}, \psi_{20}\}$, and in the set ψ^{nm} denotes a single particle state with principal quantum number n and angular momentum quantum number m.

5.4.2. First approach

Here we describe the method where the single particle states are obtained by diagonalization of the full single particle Hamiltonian. Looking at the single particle spectrum, Fig. 5.3, at large interdot distances, we see that to include the two lowest orbital (each of them degenerate) "levels" in the double dot configuration we need to consider six orbital (that is 12, including the spin) single particle wavefunctions at minimum. Out of 12 single particle states, one can build 12*11/2=66 Slater determinants, and we need to calculate 66*67/2=2211 Coulomb elements. If one element costs 50 milliseconds, we get $\sim$ 2 minutes for the Coulomb elements evaluation. If we would like to include just the next degenerate level (comprising 6 additional orbital states), the computation time would be half an hour – it scales with the fourth power of the number of single particle states.

A crude estimate of the error from cutting the single particle basis can be obtained from Fig. 5.4, where the total Hamiltonian (neglecting the spin, which is not important for the energies) is listed in the basis of several Slater determinants, each with zero total orbital moment.

The first six states are built from single particle states from the lowest part of the Fock-Darwin spectrum (up to the sixth level), while the last three states contain ∼20th, ∼40th, and ∼60th level, respectively. The (relative) contribution to the energy of the approximate ground state (second line of the table) coming from these three states is approximately $2 \cdot 10^{-2}$, $6 \cdot 10^{-3}$, $1 \cdot 10^{-3}$, respectively. Concluding, the error from taking only several single particle states is, due to the strong Coulomb interaction, quite large.

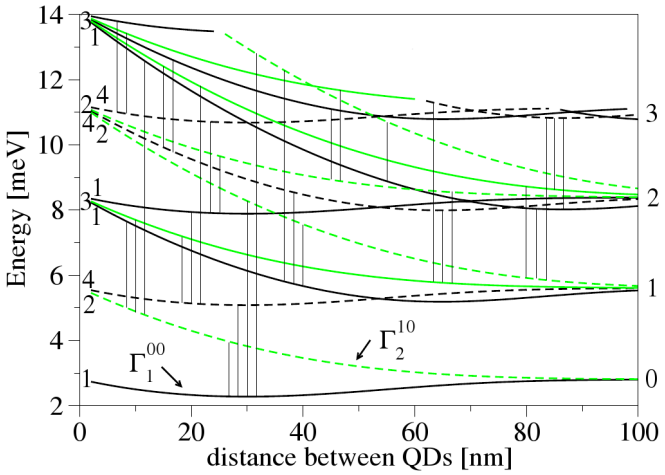

Figure 5.3.: Spectrum of a single dot at zero perpendicular magnetic field.

5.4.3. Second approach

Now we describe the method we are using to get the two-electron spectrum. We use single particle states without considering the spin-orbit interaction.

The idea in this approach is to exploit all the symmetries of the problem, what enables to block diagonalize the two particle Hamiltonian containing the Coulomb interaction. It goes as follows (see the Appendix for the notation and more details):

1 obtain the single particle states $|i\rangle$ with definite orbital symmetries diagonalizing the Hamiltonian H_0, without the spin;

2 build symmetric and antisymmetric combinations of these to obtain $|ij\rangle_p$-states;

3 identify the blocks in the two particle (no spin-orbit, no Zeeman) Hamiltonian according to the spatial symmetry;

4 diagonalize each block, obtaining $|a\rangle$-states;

5 choose certain number of the lowest $|a\rangle$-states as the new basis and add the spin, obtaining $|b\rangle$-states;

$$\begin{pmatrix}
9.37 & 1.84 & -1.84 & -0.98 & 0.69 & 0.69 & 0.29 & 0.13 & 0.06 \\
1.84 & 7.23 & 0.46 & -0.57 & -0.52 & 1.32 & 0.68 & 0.36 & 0.19 \\
-1.84 & 0.46 & 7.23 & 0.57 & -1.32 & 0.52 & 0.36 & 0.22 & 0.13 \\
-0.98 & -0.57 & 0.57 & 8.2 & 0.23 & 0.23 & 0.36 & 0.31 & 0.23 \\
0.69 & -0.52 & -1.32 & 0.23 & 8.48 & -0.28 & -0.08 & 0.01 & 0.04 \\
0.69 & 1.32 & 0.52 & 0.23 & -0.28 & 8.48 & 1.13 & 0.65 & 0.38 \\
0.29 & 0.68 & 0.36 & 0.36 & -0.08 & 1.13 & 10.12 & 1.01 & 0.62 \\
0.13 & 0.36 & 0.22 & 0.31 & 0.01 & 0.65 & 1.01 & 11.89 & 0.94 \\
0.06 & 0.19 & 0.13 & 0.23 & 0.04 & 0.38 & 0.62 & 0.94 & 13.73
\end{pmatrix}$$

Figure 5.4.: Part of the total Hamiltonian, where the off-diagonal terms are due to the Coulomb interaction for several two particle states with zero total angular moment. Entry at position k, l denotes the Coulomb matrix element $\langle k|C|l\rangle$, where k, l are from the set of two particle states $\{|\psi_{00}\psi_{00}\rangle_+, |\psi_{00}\psi_{10}\rangle_+, |\psi_{01}\psi_{0\bar{1}}\rangle_+, |\psi_{01}\psi_{1\bar{1}}\rangle_+, |\psi_{02}\psi_{0\bar{2}}\rangle_+, |\psi_{00}\psi_{20}\rangle_+, |\psi_{00}\psi_{30}\rangle_+, |\psi_{40}\psi_{00}\rangle_+, |\psi_{00}\psi_{50}\rangle_+\}$, where + stays for the symmetric combination of the two states.

6 diagonalize the total Hamiltonian including the single particle Zeeman and spin-orbit interactions in this basis, getting the final result as $|f\rangle$-states.

This is certainly more complicated compared to the previous approach, but there are two advantages. First, for equal computational time we can include more than twice as many single particle states (more precisely quantified below), which lowers the error due to the large Coulomb interaction by an order of magnitude. More importantly, here we are directly led to the two particle analog of Fig. 5.3 for two particles. Namely, after the diagonalization of the Coulomb interaction (step 4 in the previous list), the $|a\rangle$-states have definite spatial symmetry (the same four classes as the single particle states - 1, x, y, xy). Even without further numerics including the spin-orbit, we can repeat the analysis from the single dot case using the x and y symmetry of the unitary transformed spin-orbit interactions. The only question, which can not be answered in advance, is what is the spatial symmetry of the ground, the first excited state and so on. It also will depend on the details of the spectrum, whether, for example, anticrossing(s) will dominate relaxation. Another example, the proportionality constant of the anisotropic exchange will be possible to read from the figure directly just knowing the spatial symmetry of the lowest states. Of course, the same figure could be obtained also in the first approach by setting the spin-orbit to zero, but here we will obtain it automatically in each computation.

5.5. Symmetries of the two electron states

To reduce the number of Coulomb matrix elements, we identify the symmetries of the Coulomb operator

$$H_C \sim \frac{1}{|\mathbf{r_1} - \mathbf{r_2}|} = \frac{1}{\sqrt{(x_1 - x_2)^2 + (y_1 - y_2)^2}}. \tag{5.33}$$

This operator commutes with the following symmetry operations:

- shift of both electrons by a vector $\mathbf{R}$, $S_1(\mathbf{R}) \otimes S_2(\mathbf{R})$. This allowes to reduce the dimensions of the integration using the Fourier transform, but since the dot potential is not translationally invariant, it will not play role here;

- rotation of both electrons around z axis by an angle, $R_{z,1}(\phi) \otimes R_{z,2}(\phi)$. This allows to block diagonalize the total two electron Hamiltonian (without spin-orbit) in the parabolic potential – the Coulomb interaction couples only states with the same total orbital momenta in the single dot case;

- inversions of both electrons along axes of the confinement potential (x and y), $I_{x,1} \otimes I_{x,2}$ and $I_{y,1} \otimes I_{y,2}$. These are the crucial symmetries which will determine the spatial symmetry of the two electron wavefunctions – there will be four symmetry classes – 1, x, xy, y. If a perpendicular magnetic field is present, only the composite inversion survives $I_1 \otimes I_2$ and the wavefunction is symmetric or antisymmetric with respect to the inversion – this is due to the lack of I_x and I_y symmetry of the kinetic energy operator, not the Coulomb;

- permutation of the two particles P_{12}, which is a general property originating in the indistinguishability of the electrons;

- any spin rotation of any of the electrons $U_{\mathbf{n},i}(\psi)$, which expresses the fact that the Coulomb interaction conserves spin and therefore we can consider the spin separately;

- time reversal symmetry $T = \mathrm{i}C_1\sigma_{y,1} \otimes \mathrm{i}C_2\sigma_{y,2}$, which implies that the wavefunction can be chosen real (also only in the zero orbital magnetic field, due to the lack of this symmetry of the kinetic energy in finite field).

The Slater determinants (and similarly $|ij\rangle_p$ states) have also definite symmetries, if they are build from single particle states of definite symmetry. Suppose the single particle Hamiltonian commutes with certain set of operators, $\{O_\alpha\}$, and therefore

the single particle states ψ_i can be chosen such that they have definite symmetries (they form a representation of the group O of the symmetry operators), such that

$$O_\alpha \psi_i = o_\alpha^i \psi_i. \tag{5.34}$$

For example, since the double dot potential has inversion symmetry along x axis, I_x is in the group O, while $o_x^i = \pm 1$ – the states are symmetric or antisymmetric with respect to x inversion. Now consider the two electron states $|\Psi_{s/t}^{(i,j)}\rangle$ – these states also have definite symmetry if a certain operator from O acts simultaneously on both particles

$$O_{\alpha,1} \otimes O_{\alpha,2} \Psi_{i,j} = o_\alpha^i o_\alpha^j \Psi_{i,j}. \tag{5.35}$$

For our case of the symmetry group C_{2v}, since $o_\alpha^i = \pm 1$, the set of all possible results of multiplication of two characters is the same as the set of characters for a single particle, $\{o_\alpha^i o_\alpha^j\}_{i,j} = \{o_\alpha^i\}_i$. This means two particle states will form the same symmetry classes as single particle states, with the same characters.

5.6. Spin as an additional degree of freedom

Since we choose the single particle Hamiltonian as spin independent, as is also the Coulomb interaction, we can consider the spin and the orbital part of the wavefunction decoupled, meaning the two electron states are product states of the orbital part and spin part. Let us have N orbital single particle states each double spin degenerate. One possibility is not to consider the spin and the orbital parts separately. Then the two electron basis contains

$$2N(2N-1)/2 = N(2N-1) \tag{5.36}$$

Slater determinants (that is all states $\Psi_{i,j}$ possible to build from 2N single particle states ψ_i).

Another possibility is to consider the spin and orbital part separately. Since the total wavefunction has to be antisymmetric with respect to particle exchange, one part (out of spin and orbital) has to be symmetric, and the other antisymmetric. Out of N orbital states $|i\rangle$ one can build $N(N-1)/2$ antisymmetric states $|ij\rangle_-$, which can be combined with three symmetric spin states $|T_x\rangle$, where $x = 0, +, -$, and $N(N+1)/2$ symmetric states $|ij\rangle_+$, which can be combined with just one spin state $|S\rangle$. All together we get the same number as before,

$$N(N+1)/2 + 3N(N-1)/2 = N(N+1+3N-3)/2 = N(2N-1). \tag{5.37}$$

If we write the two particle states in the latter way, then the states $|ij\rangle_p$ split into s sets of different spatial symmetry ($s = 4$ if both I_x and I_y commute with the Hamiltonian $H_0 + H_C$), and two different kinds with respect to the particle exchange ($p = +$ and $p = -$). Together we have $2s$ different groups, which are not interconnected by the Coulomb interaction – we need to diagonalize the Coulomb interaction only inside each of the groups.

5.6.1. Number of needed Coulomb elements

Let us say we have $2N$ single particle states $|i\rangle$ – here we quantify how many Coulomb elements are needed in both approaches. In the first approach, there is only one "symmetry group", since the states do not have any definite symmetry. Therefore we need to compute Coulomb elements between all possible pairs of Slater determinants, that is

$$\#C = N(2N-1) * [N(2N-1)+1]/2 = 2N^4 - 2N^3 + 3N^2/2 - N/2. \qquad (5.38)$$

In the second approach, the single particle states are separable into orbital and spin part - since the Coulomb operator H_C, Eq (5.33), commutes with any spin operator, we consider only the orbital part of the wavefunction, taking the basis to consist of states $|ij\rangle_p$. We have $N(N+1)/2$ symmetric (with respect to the particle exchange) states $|ij\rangle_+$ and $N(N-1)/2$ antisymmetric states $|ij\rangle_-$. Each group splits into s subsets with different spatial symmetries (If all symmetries are present, $s = 4$. If the perpendicular magnetic field is non zero, or the dot is biased, $s = 2$). We suppose, that each spatial symmetry subset contains the same number of terms (for small number of single particle states some deviations can occur, like there will be more x-like states than y-like, but we expect these deviations to be small, especially for a larger number of states). Then we need to compute Coulomb elements inside $2s$ blocks of the total Hamiltonian. The number of Coulomb elements is

$$\begin{aligned} \#C &= s\{[N(N-1)/2/s][N(N-1)/2/s+1]/2 + [N(N+1)/2/s] \times \\ &\times [N(N+1)/2/s+1]/2\} = N^4/4s + N^2(1/4s + 1/2). \end{aligned} \qquad (5.39)$$

Compared to the previous, it is still fourth order with respect to N, but the coefficient at the leading term is $8s$ times smaller. The number of Coulomb elements for several number of the single particle states N is in Fig. 5.5.

5.6.2. Finite width along growth direction (z)

Now we look how the finite width of the electron wavefunction along the growth direction influences the results in the two electron case. The most important message

N	#1	s=2	s=4
5	1035	94	53
10	18145	1312	681
15	94830	6469	3291
20	304590	20250	10225
25	750925	49219	24766
30	1567335	101812	51131

Figure 5.5.: N, number of needed Coulomb elements in the first approach, in the second for a reduced symmetry, and for the full symmetry, respectively.

is that the finite width preserves the symmetries, therefore qualitative results will be still valid. The finite width can be roughly taken into account by renormalization (diminishing) the interdot distance.

The three dimensional single electron wavefunction, in the limit of much smaller perpendicular confinement length than the inplane one, $l_z \ll l_0$, is

$$|ij\rangle = \Psi_{ij}(\mathbf{r}_1, \mathbf{r}_2)\psi_0(z_1)\psi_0(z_2), \tag{5.40}$$

and the Coulomb matrix element between two such states is

$$\begin{aligned}\langle ij|H_C|kl\rangle &= \int d^2\mathbf{r_1}d^2\mathbf{r_2}dz_1dz_2\Psi^\dagger_{ij}\frac{|\psi_0(z_1)|^2|\psi_0(z_2)|^2}{\sqrt{(\mathbf{r_1}-\mathbf{r_2})^2+(z_1-z_2)^2}}\Psi_{kl} \approx \\ &\approx \int d^2\mathbf{r_1}d^2\mathbf{r_2}\Psi^\dagger_{ij}\frac{1}{\sqrt{(\mathbf{r_1}-\mathbf{r_2})^2+\overline{z}^2}}\Psi_{kl},\end{aligned} \tag{5.41}$$

where

$$\overline{z}^2 = \int dz_1dz_2|\psi_0(z_1)|^2(z_1-z_2)^2|\psi_0(z_2)|^2. \tag{5.42}$$

This leads to a correction of the order of l_z^2/l_0^2, with a dimensionless numerical prefactor a bit less than 1 due to the term $(z_1 - z_2)$ and the fact that the ψ_0 is the ground state and has no nodes. For example, for the lowest Fock Darwin state, the numerical prefactor is 1/2 (for the sine function, it is almost the same). Since $l_z/l_0 \approx 1/4$, we expect that neglecting the finite width overestimates the Coulomb integrals by several percent. This is a lot, but further observation is that in the double dot, the Coulomb energy for two electrons on the same dot is diminished by the finite width along z. If the electrons are located on different dots, their Coulomb energy is much less sensitive to the finite width in z. The same effect has a slight enlargement of the confining length and reduction of the interdot distance. By such effective parameter renormalization, one can suppress the error due to the finite width. The error that stays is the variation of the Coulomb energies due to the finite width among states where the two electron are located on the same dot. We cannot do anything with that without sacrificing the simplicity of the two dimensional model. Most important thing is that both the three dimensional wavefunctions (even if not only ground

state in the z dimension plays role) and the three dimensional Coulomb operator preserve the inplane inversion symmetries and therefore a finite width does not cause a qualitative change.

5.7. Configuration Interaction

The Configuration Interaction (CI) method is one of the most general ways to go beyond the Hartree-Fock theory by adding a description of the correlations between electron motions. The word "configuration" means that we consider the states as linear combination of the Slater determinants and compute the interactions matrix elements in this basis set [84]. Using the eigenstates of the single electron Hamiltonian $\{(\psi_i, \epsilon_i)\}$, we construct the two electron states. We use them as a basis where the two electron orbital Hamiltonian Eq. (4.2) is diagonalized. We choose $n_{s.e.}$ single electron orbitals and the two electron states are constructed as symmetric

$$|\Psi_s^{(i,j)}\rangle = \frac{1}{\sqrt{2}}(|\psi_i\rangle|\psi_j\rangle + |\psi_j\rangle|\psi_i\rangle) \text{ for } i \neq j, \tag{5.43}$$

$$|\Psi_s^{(i,j)}\rangle = |\psi_i\rangle|\psi_j\rangle \text{ for } i = j, \tag{5.44}$$

and antisymmetric

$$|\Psi_t^{(i,j)}\rangle = \frac{1}{\sqrt{2}}(|\psi_i\rangle|\psi_j\rangle - |\psi_j\rangle|\psi_i\rangle), \tag{5.45}$$

with respect to the particle exchange. The typical value of $n_{s.e.}$ is 21. The total number of the two particle states is $n_{s.e.}^2$.

Since we do not consider the spin at this step, the spatial symmetry allows us to reduce the dimension of the two electron Hamiltonian matrix to diagonalize. Namely, the matrix is block diagonal, with the basis functions grouped according to the spatial symmetry (1, x,y, xy) and particle exchange symmetry (± 1). This results in 8 blocks and hold for zero perpendicular magnetic field. In finite field, we get 4 block, as there are only two spatial symmetry possible (1, or x). Each block is diagonalized separately.

The matrix element of the two electron Hamiltonian, Eq. (4.2), in our basis is

$$\begin{aligned}\langle\Psi_a^{(i,j)}|H_{orb}|\Psi_b^{(n,m)}\rangle &= (\epsilon_i + \epsilon_j)\delta_{i,m}\delta_{j,n}\delta_{a,b} + \\ &+ \delta_{a,b}\int d\mathbf{r}_1 \int d\mathbf{r}_2 \Psi_a^{(i,j)} \frac{e^2}{4\pi\varepsilon_0\varepsilon_r}\frac{1}{|\mathbf{r}_1 - \mathbf{r}_2|}\Psi_b^{(n,m)}.\end{aligned} \tag{5.46}$$

The last term in Eq. (5.46) is due to the Coulomb interaction and it leads to off-diagonal terms in the Hamiltonian. We diagonalize the matrix defined in Eq. (5.46) to get the eigenspectrum $\{(\Psi_i, E_i)\}$.

5.8. Matrix elements of single particle operators

After the diagonalization of the Coulomb interaction, we obtain intermediate eigenstates, denoted as a-states,

$$(H_{0,1} + H_{0,2} + H_C)|a\rangle = E_a|a\rangle, \tag{5.47}$$

where

$$|a\rangle = \sum_{i,j} c^a_{ijp}|ij\rangle_p, \tag{5.48}$$

Note that since H_C, Eq (5.33), commutes with the exchange of the orbital coordinates, each $|a\rangle$ contains either only symmetric states $|ij\rangle_+$ or antisymmetric states $|ij\rangle_-$. To proceed further, we sort the states $|a\rangle$ according the energies and choose certain number of the lowest ones (even all of them), as the basis for the diagonalization of the spin dependent part of the two particle Hamiltonian – at this stage we add the spin into consideration – we denote these states by

$$|b\rangle = |a\rangle|\Sigma\rangle. \tag{5.49}$$

To obtain the Hamiltonian matrix, we need to evaluate the matrix elements of the spin orbit interaction. The spin-orbit interaction is a sum of terms which are products of single particle spin and orbital operators, such as $\sigma_{y,1}K_{y,1}$. Such a term sandwiched between two two electron states $|b\rangle$, is

$$\langle b_1|\sigma_{y,1}K_{y,1}|b_2\rangle. \tag{5.50}$$

The details are given in the Appendix.

From the Eq. (5.50) follows: (i) The spin matrix elements can be worked out analytically. (ii) Since it is a single particle operator, for each given orbital operator appearing in the spin-orbit interactions there are only $N(N+1)/2 \sim N^2$ different matrix elements, compared to $\sim N^4$ for the two particle Coulomb operator. This means the time of evaluation of these matrix elements is negligible. (iii) There are strong coupling rules for a single particle operator – both two particle states have to contain at least one common single particle state, otherwise the matrix element is zero. (iv) Since each $|a\rangle$ is a linear combinations of many $|ij\rangle_p$, there will be no coupling rules in the basis of $|a\rangle$, and the Hamiltonian matrix for the last (third) diagonalization will not be sparse. This means the number of chosen states should not exceed several tens.

5.9. Coulomb integration

Computationally most demanding is the numerical calculation of the Coulomb integrals. Indeed, the typical size of Hamiltonian matrix, in the second step, is 441×441, requiring at least 10^6 Coulomb integrals. Writing functions involved in the Eq. (5.46) as Slater determinants, we can express the integral as a sum of terms like

$$\begin{aligned}
\langle \Psi^{(i,j)} | H_C | \Psi^{(m,n)} \rangle &= \int d\mathbf{r}_1 \int d\mathbf{r}_2 \Psi^{(i,j)*} \frac{U}{|\mathbf{r}_1 - \mathbf{r}_2|} \Psi^{(m,n)} = \\
&= \frac{U}{2} \left[\int \int d\mathbf{r}_1 d\mathbf{r}_2 \frac{\psi_i^*(\mathbf{r}_1)\psi_j^*(\mathbf{r}_2)\psi_m(\mathbf{r}_1)\psi_n(\mathbf{r}_2)}{|\mathbf{r}_1 - \mathbf{r}_2|} + \right. \\
&- \left. \int \int d\mathbf{r}_1 d\mathbf{r}_2 \frac{\psi_i^*(\mathbf{r}_1)\psi_j^*(\mathbf{r}_2)\psi_n(\mathbf{r}_1)\psi_m(\mathbf{r}_2)(\mathbf{r}_2)}{|\mathbf{r}_1 - \mathbf{r}_2|} \right] + \\
&- \frac{U}{2} \left[\int \int d\mathbf{r}_1 d\mathbf{r}_2 \frac{\psi_j^*(\mathbf{r}_1)\psi_i^*(\mathbf{r}_2)\psi_m(\mathbf{r}_1)\psi_n(\mathbf{r}_2)}{|\mathbf{r}_1 - \mathbf{r}_2|} + \right. \\
&+ \left. \int \int d\mathbf{r}_1 d\mathbf{r}_1 \frac{\psi_j^*(\mathbf{r}_1)\psi_i^*(\mathbf{r}_2)\psi_n(\mathbf{r}_1)\psi_m(\mathbf{r}_2)}{|\mathbf{r}_1 - \mathbf{r}_2|} \right], \qquad (5.51)
\end{aligned}$$

where $U = e^2/4\pi\varepsilon_0\varepsilon_r$. The same can be derived for the other combination between the symmetric and antisymmetric functions. This matrix element Eq. (5.51) is decomposed into 4 terms. Now our goal is to find a right numerical procedure to have a single term; the others can be obtained by a simple permutation of the functions.

5.9.1. Discrete Fourier Transform (DFT)

We want to compute numerically the integral Eq. (5.51); let us look at only the term:

$$C_{ijmn} = \int \int d\mathbf{r}_1 d\mathbf{r}_2 \frac{\psi_i^*(\mathbf{r}_1)\psi_j^*(\mathbf{r}_2)\psi_m(\mathbf{r}_1)\psi_n(\mathbf{r}_2)}{|\mathbf{r}_1 - \mathbf{r}_2|} = \int \int d\mathbf{r}_1 d\mathbf{r}_2 \frac{\mathcal{F}_{im}(\mathbf{r}_1)\mathcal{G}_{jn}(\mathbf{r}_2)}{|\mathbf{r}_1 - \mathbf{r}_2|}. \qquad (5.52)$$

We reduce the integration from four dimension to two dimension by introducing the Fourier transform. For a general complex function of two real variables, $f(\mathbf{r})$, we use the following definition:

$$\tilde{f}(\mathbf{q}) = \frac{1}{2\pi} \int d\mathbf{r} f(\mathbf{r}) e^{i\mathbf{q}\cdot\mathbf{r}}, \quad f(\mathbf{r}) = \frac{1}{2\pi} \int d\mathbf{q} \tilde{f}(\mathbf{q}) e^{-i\mathbf{q}\cdot\mathbf{r}}. \qquad (5.53)$$

Using the Fourier transformation, the Coulomb integral Eq. (5.52) simplifies into:

$$\begin{aligned} C_{ijmn} &= \int d\mathbf{r}_1 \int d\mathbf{r}_2 \frac{1}{2\pi} \int d\mathbf{q}_1 e^{-i\mathbf{q}_1\cdot\mathbf{r}_1} \tilde{\mathcal{F}}(\mathbf{q}_1) \cdot \frac{1}{2\pi} \int d\mathbf{q}_2 e^{-i\mathbf{q}_2\cdot\mathbf{r}_2} \tilde{\mathcal{G}}(\mathbf{q}_2) \cdot \\ &\cdot \frac{1}{2\pi} \int d\mathbf{q}_3 e^{-i\mathbf{q}_3\cdot(\mathbf{r}_1-\mathbf{r}_2)} \frac{1}{|\mathbf{q}_3|} = \\ &= \int d\mathbf{q}_1 d\mathbf{q}_2 d\mathbf{q}_3 \frac{1}{(2\pi)^3} \frac{1}{|\mathbf{q}_3|} \tilde{\mathcal{F}}(\mathbf{q}_1)\tilde{\mathcal{G}}(\mathbf{q}_2) \int d\mathbf{r}_1 \int d\mathbf{r}_2 e^{-i\mathbf{q}_1\cdot\mathbf{r}_1} e^{-i\mathbf{q}_2\cdot\mathbf{r}_2} e^{-i\mathbf{q}_3\cdot(\mathbf{r}_1-\mathbf{r}_2)} = \\ &= \int \frac{d\mathbf{q}_1 d\mathbf{q}_2 d\mathbf{q}_3}{(2\pi)^3} \frac{1}{|\mathbf{q}_3|} \tilde{\mathcal{F}}(\mathbf{q}_1)\tilde{\mathcal{G}}(\mathbf{q}_2)(2\pi)^4 \delta(\mathbf{q}_1+\mathbf{q}_3)\delta(\mathbf{q}_1-\mathbf{q}_3) = \\ &= \int \frac{2\pi}{|\mathbf{q}_3|} \tilde{\mathcal{F}}(-\mathbf{q}_3)\tilde{\mathcal{G}}(\mathbf{q}_3) d\mathbf{q}_3, \end{aligned} \tag{5.54}$$

where we have used the result $\int d\mathbf{r} e^{-i\mathbf{q}\cdot\mathbf{r}} = (2\pi)^2\delta(\mathbf{q})$. Finally, we have to compute only an integral of the following form:

$$C_{ijmn} = 2\pi \int \frac{1}{|\mathbf{q}|} F_{ijmn}(\mathbf{q}) d\mathbf{q}. \tag{5.55}$$

We now estimate the one dimensional Fourier transform of a function from a finite number of its sampled points. Let us suppose that we have N consecutive sampled values

$$f_k \equiv f(x_k), \qquad x_k \equiv k\Delta, \qquad k = 0, 1, 2, ..., N-1 \tag{5.56}$$

where Δ is the distance between two sampled points. Instead of trying to estimate the Fourier transform $\tilde{f(q)}$ at all values of p, we look for an estimation only at discrete values

$$q_n \equiv \frac{2\pi n}{N\Delta} = n\delta, \qquad n = -\frac{N}{2}, ..., \frac{N}{2}. \tag{5.57}$$

To calculate the Fourier transform, we approximate the integral by a discrete sum:

$$\tilde{f}(q_n) = \frac{1}{\sqrt{2\pi}} \int_{-\infty}^{+\infty} dr f(x) e^{2\pi i q x} \approx \frac{1}{\sqrt{2\pi}} \sum_{k=0}^{N-1} f(x_k) e^{2iq_n r_k} \Delta = \frac{\Delta}{\sqrt{2\pi}} \sum_{k=0}^{N-1} f_k e^{2\pi i k n/N}. \tag{5.58}$$

The final summation in Eq. (5.58) is called Discrete Fourier Transform of N points f_k. In the two dimensional case, we have

$$\tilde{f}(q_n, q_m) = \frac{\Delta_x \Delta_y}{2\pi} \sum_{k=1}^{N_x} \sum_{l=1}^{N_y} f(x_k, x_l) e^{2\pi i(nk/N_x + ml/N_y)}. \tag{5.59}$$

To compute the previous summation, we use the FFTW routine that computes in more efficient way the Discrete Fourier Transform (DFT) [85]. The output of a two-dimensional FFTW routine gives a unnormalized value. In our case, because the spatial grid is defined like in Eq (5.5), the normalization is $d_x d_y/2\pi$.

5.9.2. Correction factor for the DFT

Generally the DFT is a good approximation for the integral

$$\tilde{f}(q_n) = \frac{1}{\sqrt{2\pi}} \int_{-\infty}^{+\infty} dr f(x) e^{2\pi i q x}. \tag{5.60}$$

In particular in the cases when $f(x)$ is nonzero only in a finite interval of x and if the function is supposed to be at least similar in all kind of the finite interval. The problem of the approximation is the oscillatory nature of the integral. If q is large enough to imply several cycles in a given interval, then the value of the integral can be very small and it does not give any contribution. Furthermore, the parameter that characterizes the error term is not Δ/L (L is the length of the interval and Δ is the point spacing), but $q\Delta$. It can be large at large q.

As we can find in Ref. [86], we can rewrite the Eq. (5.58) adding an attenuation factor, which taks into account the possible oscillations of the function . The final form, that we use to correct the DFT, is:

$$\tilde{f}(q_n) = \Delta W(\theta)[DFT(q_1 ... q_N)]_n, \qquad W(\theta) = \left(\frac{6+\theta^2}{3\theta^4}\right)(3 - 4\cos\theta + \cos 2\theta), \tag{5.61}$$

where $\theta = 2\pi n/N$. The same formula can be written in a simple way for the two dimensional case:

$$\begin{aligned} \tilde{f}(q_n, q_m) &= \Delta_x \Delta_y W(\theta_1) W(\theta_2) [DFT(q_{11} ... q_{N_x \times N_y})]_{nm}, \\ W(\theta_1, \theta_2) &= \left(\frac{6+\theta_1^2}{3\theta_1^4}\right)(3 - 4\cos\theta_1 + \cos 2\theta_1) \times \\ &\times \left(\frac{6+\theta_2^2}{3\theta_2^4}\right)(3 - 4\cos\theta_2 + \cos 2\theta_2), \end{aligned} \tag{5.62}$$

where $\theta_1 = 2\pi n/N_x$ and $\theta_2 = 2\pi m/N_y$.

5.9.3. Numerical precision in the DFT method

Let us suppose to have a function, for example, the ground state in the harmonic potential

$$f_0(\mathbf{r}) = \frac{1}{l_0\sqrt{\pi}} \exp\left(-\frac{x^2+y^2}{2l_0^2}\right), \tag{5.63}$$

where $l_0 = \sqrt{\hbar/m^*\omega_0}$ is the effective length of the dot, typically $20 \div 30$ nm. It can be magnetic field dependent. In our numerical simulations, the function Eq. (5.63) is approximated by a finite set of equidistant points (N_x along x axis times N_y along the

y axis). The distance between the neighboring points is d_x and d_y, respectively. This approximation means that the function is effectively defined only on a finite interval $(-ld_x, ld_x) \times (-ld_y, ld_y)$. To have a correct approximation, the length $ld_x(ld_y)$ has to be large enough such that the exact function is small at boundary, and, on the other hand, small enough such that $d_x(d_y)$ is much smaller than the characteristic length of the exact function (l_0). The experience with harmonic single and double dot potentials showed it is enough for all purposes to take $ld_x(ld_y) = 5l_0$ and $N_x(N_y) = 40$. This means the neighbor distance on the grid is $d_x(d_y) = l_0/4$.

For the Coulomb matrix element, we need to compute

$$F_{00}(\mathbf{r}) = f_0^\dagger(\mathbf{r}_1) f_0(\mathbf{r}_1) = \frac{1}{l_0^2 \pi} \exp\left(-\frac{x^2+y^2}{l_0^2}\right). \tag{5.64}$$

To get a comparison to the spatial grid in the Fourier space, here we have the relative values for the nearest and the farther points for a grid dimension $d_x(d_y) = l_0/4$:

$$F_{00}(d_x, 0)/F_{00}(0,0) = \exp(-1/16) = 0.94, \tag{5.65}$$

$$F_{00}(ld_x, 0)/F_{00}(0,0) = \exp[-(10/2)^2] = 10^{-11}. \tag{5.66}$$

The real space grid defines the Fourier space with resolution

$$\delta_x = \frac{2\pi}{2ld_x} = \frac{2\pi}{10l_0} \approx 0.63/l_0, \qquad \delta_y = \frac{2\pi}{2ld_y} = \frac{2\pi}{10l_0} \approx 0.63/l_0, \tag{5.67}$$

which is independent of the resolution of the real space grid. In the real space, in order to have more resolution, we can simply enlarge the grid dimension $N_x(N_y)$ to get $d_x(d_y)$ smaller. In the Fourier space this effect does not give us a good degree of precision, because $\delta_x(\delta_y)$ does not depend on $N_x(N_y)$. The only effect is to get larger the maximal vector in the Fourier space, $q_{max} = N_x/2\delta = N_x \frac{\pi}{ld_x}$. Continuing with our example of the two electron ground state, we obtain

$$\tilde{F}_{00}(\mathbf{q}) = \frac{1}{l_0^2 \pi} \exp\left(-\frac{(q_x^2+q_y^2)l_0^2}{4}\right). \tag{5.68}$$

The resolution is illustrated by the value of the Fourier transform at the nearest and farther points

$$\tilde{F}_{00}(\delta_x, 0)/\tilde{F}_{00}(0,0) = \exp(-\pi^2/100) \approx 0.91, \tag{5.69}$$

$$\tilde{F}_{00}(q_{max}, 0)/\tilde{F}_{00}(0,0) = \exp[-4(\pi)^2] \approx 7 \cdot 10^{-18}. \tag{5.70}$$

This shows that the grid density in the Fourier space is slightly lower than in the real space, with a crucial difference that enlarging $N_x(N_y)$ does not make the Fourier grid denser.

To have more precision in the Fourier space, we use this strategy. The main points are:

- we set the spatial resolution of the grid (such as 50×50 points), where we diagonalize the single particle Hamiltonian;

- once we have the single electron wave-functions, we expand the spatial grid by a certain factor (such as 5, obtaining the grid 250×250), filling the wavefunctions by zeros;

- we do the FFT here, taking into account the attenuation factors helping in the DFT precision for high frequencies;

- at this point we use the numerical formula (explained in the next section) to obtain the Coulomb integral.

With this way, we increase the resolution in the Fourier space as we like.

5.9.4. Numerical formula

There are several possibilities how to solve the integral in Eq. (5.55) with desirable precision: Poisson equation, sampling theorem and others. At the end, we choose to use the Taylor expansion for the functions. This is not only the easiest approach, but it allows us to have a desirable precision by changing the order of the expansion.

Next we denote $F_{ijmn}(\mathbf{q}) = f(\mathbf{q})$ for brevity and continue with the integral; also we indicate $\mathbf{q}_{nm} = (q_n, q_m)$ and $\delta = (\delta_x, \delta_y)$ as the vector and the spatial grid in the Fourier space, N_x and N_y the number of the points in the two dimensional mesh. We compute the two dimensional integral in the Fourier space as follows:

$$\begin{aligned} C &= \int d\mathbf{q} f(\mathbf{q}) \frac{1}{q} = \sum_{n=1}^{N_x} \int_{(n-1/2)\delta_x}^{(n+1/2)\delta_x} dq_x \sum_{m=1}^{N_y} \int_{(m-1/2)\delta_y}^{(m+1/2)\delta_y} dq_y \frac{1}{q} f(\mathbf{q}) = \\ &= \sum_{n,m} \int_{\mathbf{q}_{nm} \pm \delta} d\mathbf{q} \frac{1}{q} f(\mathbf{q} - \mathbf{q}_{nm} + \mathbf{q}_{nm}) = \sum_{n,m} \int_{\mathbf{q}_{nm} \pm \delta} d\mathbf{q} \frac{1}{q} \left[e^{(\mathbf{q} - \mathbf{q}_{nm}) \cdot \nabla f(\mathbf{q})|_{\mathbf{q}_{nm}}} \right]. \end{aligned}$$

Considering the terms of the Taylor expansion up to the second order, we obtain

$$\begin{aligned} C &\approx \sum_{n,m} \int_{\mathbf{q}_{nm} \pm \delta} \frac{1}{q} [1 + (q_x - q_n)\partial_x + (q_y - q_m)\partial_y + \\ &+ \frac{1}{2}(q_x - q_n)^2 \partial_{xx} + (q_x - q_n)(q_y - q_m)\partial_{xy} + \frac{1}{2}(q_y - q_m)^2 \partial_{yy}] f(\mathbf{q})|_{\mathbf{q}_{nm}} . \end{aligned}$$

Then we rearrange the terms to have some analytical integral to compute:

$$\begin{aligned} C &\approx \sum_{n,m} I^{(0,0)}(n,m)\left(1 - q_n\partial_x - q_m\partial_y + \frac{1}{2}q_n^2\partial_{xx} + q_nq_m\partial_{xy} + \frac{1}{2}q_m^2\partial_{yy}\right) f(\mathbf{q})|_{\mathbf{q}_{nm}} + \\ &+ I^{(1,0)}(n,m)\left(\partial_x - q_n\partial_{xx} - q_m\partial_{xy}\right) f(\mathbf{q})|_{\mathbf{q}_{nm}} + \\ &+ I^{(0,1)}(n,m)\left(\partial_y - q_m\partial_{yy} - q_n\partial_{xy}\right) f(\mathbf{q})|_{\mathbf{q}_{nm}} + \\ &+ I^{(1,1)}(n,m)\partial_{xy}f(\mathbf{q})|_{\mathbf{q}_{nm}} + I^{(2,0)}(n,m)\frac{1}{2}\partial_{xx}f(\mathbf{q})|_{\mathbf{q}_{nm}} + \\ &+ I^{(0,2)}(n,m)\frac{1}{2}\partial_{yy}f(\mathbf{q})|_{\mathbf{q}_{nm}} . \end{aligned} \tag{5.71}$$

Here we have defined these integrals:

$$\begin{aligned} I^{(0,0)}(n,m) &= \int_{(n-1/2)\delta_x}^{(n+1/2)\delta_x} dx \int_{(m-1/2)\delta_y}^{(m+1/2)\delta_y} dy \frac{1}{\sqrt{x^2+y^2}} = \\ &= \left\{ \left[y\log(x+\sqrt{x^2+y^2}) + x\log(y+\sqrt{x^2+y^2}) \right]_{x=(n-1/2)\delta_x}^{x=(n+1/2)\delta_x} \right\}_{y=(m-1/2)\delta_y}^{y=(m+1/2)\delta_y} \\ I^{(1,0)}(n,m) &= \int dxdy \frac{x}{\sqrt{x^2+y^2}} = \frac{y}{2}\sqrt{x^2+y^2} + \frac{x^2}{2}\log(y+\sqrt{x^2+y^2}), \\ I^{(0,1)}(n,m) &= \int dxdy \frac{y}{\sqrt{x^2+y^2}} = \frac{x}{2}\sqrt{x^2+y^2} + \frac{y^2}{2}\log(y+\sqrt{x^2+y^2}), \\ I^{(1,1)}(n,m) &= \int dxdy \frac{xy}{\sqrt{x^2+y^2}} = \frac{1}{3}\left(\sqrt{x^2+y^2}\right)^3, \\ I^{(2,0)}(n,m) &= \int dxdy \frac{x^2}{\sqrt{x^2+y^2}} = \frac{xy}{6}\sqrt{x^2+y^2} + \frac{x^3}{3}\log(y+\sqrt{x^2+y^2}) + \\ &- \frac{y^3}{\sqrt{x^2+y^2}}\log(x+\sqrt{x^2+y^2}), \\ I^{(0,2)}(n,m) &= \int dxdy \frac{y^2}{\sqrt{x^2+y^2}} = \frac{xy}{6}\sqrt{x^2+y^2} + \frac{y^3}{3}\log(x+\sqrt{x^2+y^2}) + \\ &- \frac{x^3}{\sqrt{x^2+y^2}}\log(y+\sqrt{x^2+y^2}). \end{aligned}$$

To evaluate all the derivatives in Eq. (5.71) we use the 5 points formula, although it is enough using the lowest order formula.

The formula for the differential operator is:

$$\left.\frac{d^k f(x)}{dx^k}\right|_{x=x_j} \approx \frac{k!}{m!h^k}\sum_{i=0}^{m} A_i f(x_i), \tag{5.72}$$

where the coefficients for the five points formula ($m = 4$) are:

First derivative ($k = 1$)

j	A_0	A_1	A_2	A_3	A_4	$\frac{h^k}{k!}Error$
0	-50	96	-72	32	-6	$1/5h^5f^{(5)}$
1	-6	-20	36	-12	2	$-1/20h^5f^{(5)}$
2	2	-16	0	16	-2	$1/30h^5f^{(5)}$
3	-2	12	-36	20	6	$-1/20h^5f^{(5)}$
4	6	-32	72	-96	50	$1/5h^5f^{(5)}$

(5.73)

Second derivative ($k = 2$)

j	A_0	A_1	A_2	A_3	A_4	$\frac{h^k}{k!}Error$
0	35	-104	114	-56	11	$-5/12h^5f^{(5)}$
1	11	-20	6	4	-1	$1/24h^5f^{(5)}$
2	-1	16	-30	16	-1	$1/180h^6f^{(6)}$
3	-1	4	6	-20	11	$-1/24h^5f^{(5)}$
4	11	-56	114	-104	35	$5/12h^5f^{(5)}$

(5.74)

For more details about these formulas, see Ref. [51].

The most general formula, in which we use the Taylor expansion up to N-th order, is the following:

$$
\begin{aligned}
C_{ijkl} &= \sum_{n,m}\int_{\mathbf{q}_{nm}\pm\delta} d\mathbf{q}\frac{1}{q}\sum_{k=0}^{\infty}\frac{1}{k!}[(\mathbf{q}-\mathbf{q}_{nm})\cdot\nabla]^k f(\mathbf{q})|_{\mathbf{q}_{nm}} = [\text{up to N-th order}] \\
&= \sum_{n,m}\int_{\mathbf{q}_{nm}\pm\delta} d\mathbf{q}\frac{1}{q}\sum_{k_1,k_2=0}^{k_1+k_2\le N}\frac{1}{k_1!k_2!}[(q_x-q_n)\partial_x]^{k_1}[(q_y-q_m)\partial_y]^{k_2} f(\mathbf{q})|_{\mathbf{q}_{nm}} = \\
&= \sum_{n,m}\int_{\mathbf{q}_{nm}\pm\delta} d\mathbf{q}\frac{1}{q}\sum_{k_1,k_2=0}^{k_1+k_2\le N}\frac{1}{k_1!k_2!}\times \\
&\times \sum_{l_1,l_2=0}^{k_1,k_2}\begin{pmatrix} k_1 \\ l_1 \end{pmatrix} q_x^{l_1}(-q_n)^{k_1-l_1}\partial_x^{k_1}\begin{pmatrix} k_2 \\ l_2 \end{pmatrix} q_y^{l_2}(-q_m)^{k_2-l_2}\partial_y^{k_2} f(\mathbf{q})|_{\mathbf{q}_{nm}} = \\
&= \sum_{n,m}\sum_{k_1,k_2=0}^{k_1+k_2\le N}\sum_{l_1,l_2=0}^{k_1,k_2} I(l_1,l_2,n,m)\frac{(-q_n)^{(k_1-l_1)}}{(k_1-l_1)!l_1!}\frac{(-q_m)^{(k_2-l_2)}}{(k_2-l_2)!l_2!}\partial_x^{k_1}\partial_y^{k_2} f(\mathbf{q})|_{\mathbf{q}_{nm}}.
\end{aligned}
$$

Taking in account all pieces, Eqs. (5.71-5.72), the Coulomb matrix element can be written as a sum

$$C_{ijkl} = U\sum_{n,m} c_{n,m}\tilde{\mathcal{F}}_{ik}(\mathbf{q}_{nm})\tilde{\mathcal{G}}_{jl}(-\mathbf{q}_{nm}), \tag{5.75}$$

where $\tilde{\mathcal{F}}$ and $\tilde{\mathcal{G}}$ are the Fourier transform of the functions in Eq. (5.52), the coefficients $c_{n,m}(L_x, L_y, N_x, N_y)$ depend only on the geometry and they need to be computed only once for each program run. The U coefficient depends on the material that we want to use.

5.10. Precision of the numerical Coulomb integral

In the previous section, we have defined the details of the algorithm we have implemented to compute the Coulomb integral. To test the goodness of our method, we have performed a numerical benchmark with a simple function where we can compute the Coulomb integral analytically. We choose

$$f(\mathbf{r}) = \frac{1}{l_0\sqrt{\pi}} \exp\left(-\frac{x^2+y^2}{2l_0^2}\right), \tag{5.76}$$

which represents the lowest eigenfunction of the single dot problem. We discretize it on a grid ($N_x \times N_y$) and insert it in our code. The main steps of the procedure are:

- set the starting grid dimension and calculate the parameter d_x and d_y, using the value of l_0 arbitrary (in this example is $l_0 = 15$ nm and $ld_x(ld_y) = 5l_0$);
- evaluation of the four functions and the related products involved in the Eq. (5.52) on the mesh points;
- expand the grid dimension with the chosen expanding factor;
- use the external FFTW routine to compute the discrete Fourier transform;
- add the attenuation factors Eq. (5.62);
- use the formula Eq. (5.71) to have the Coulomb integral.

We have reproduced the first plots in the zero order approximation. This means, if we look the formulas Eq. (5.71), we approximate the function as a constant.

In Fig. 5.6 we plot the relative error versus the grid dimension for different expanding factors. The labels x1-x6 mean, for example, if the starting grid dimension is 50×50 and x3, we have the final grid dimension $(50 \times 3) \times (50 \times 3) = 150 \times 150$.

The relative error for a matrix element is defined as (numerical value - analytical value)/analytical value. The computed matrix element C_{0000} involves only the ground state Eq (5.76). Let us analyze the black line in the Fig 5.6. As we can see, the error does not decrease increasing the grid dimension. It stays near $\approx 0.1\%$. The reason is that the integration is done in the Fourier space and the precision does not change

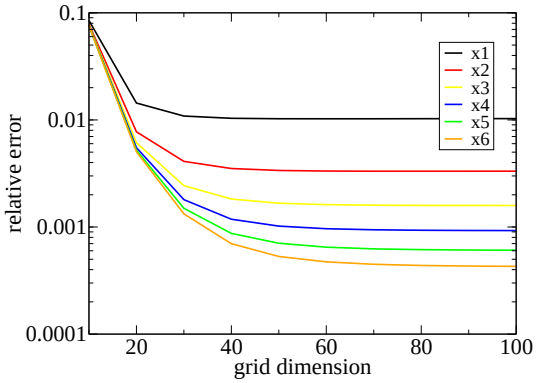

Figure 5.6.: Relative error as a function of the grid dimension up to 100 with different expanding factors from x1 to x6.

if we have a different grid dimension (as we have pointed in the previous section). The error decreases if we choose different expanding factors. To underline the role of the expanding factor, in Fig. 5.7 we plot the relative error as a function of the expansion factor. Here we see that independently of the spatial resolution, with or without expansion by same factor, the result changes by one order of magnitude. This improves our numerical precision.

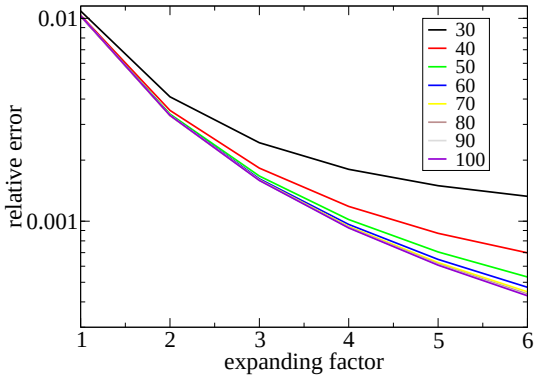

Figure 5.7.: Relative error as a function of the expanding factors up to 6 with different grid dimensions up to 100.

In order to have a quite high precision, we would need a better precision in the Coulomb elements. The precision in single particle energy after the first diagonalization, is of order of 10^{-7}. Because we need to diagonalize the whole matrix, it is better to have the Coulomb element at least with a precision 10^{-5}. Therefore we should improve our numerical results by adding the other terms in the Taylor expansion Eq. (5.71), up to the second order. If we would add only the first derivative, the precision will not change. We can understand that by the following example. Let us suppose to have one dimensional function $f(x)$ on a discrete equidistant line. We expand the function in the Taylor series in the middle point $x_m = x_i + x_{i+1}/2$:

$$f(x) = f(x_m) + f'(x_m)(x - x_m) + \frac{1}{2} f''(x_m)(x - x_m)^2 + \frac{1}{3!} f'''(x_m)(x - x_m)^3 + \dots . \quad (5.77)$$

Now we integrate the function in the interval (x_i, x_{i+1}):

$$\int_{x_i}^{x_{i+1}} dx(x-x_m)^p = \frac{1}{p+1}(x-x_m)|_{x_i}^{x_{i+1}} = ... = \begin{cases} 0 & \text{, if p is odd} \\ \frac{1}{2^p}\frac{1}{p+1}h_i^{p+1} & \text{, if p is even} \end{cases} \quad (5.78)$$

where h_i is the distance between the points. We integrate the function in that interval:

$$\int_{x_i}^{x_{i+1}} f(x)dx = h_i f(x_m) + \frac{1}{2!2^2 3}h_i^3 f''(x_m) + \frac{1}{4!2^4 5}h_i^5 f''''(x_m) + ... \,. \quad (5.79)$$

If we approximate the function as a costant, the error in the integration is of the order of h^3, the same if we add the first derivative approximation. For this reason we need to add, in our calculation, the derivative up to the second order.

We use the second order approximation in the Eq. (5.71) and reproduce the same kind of plots of the previous case. To compute the derivative, we wrote a routine to have the formula in the Eq. (5.72).

Let us a look, also in this case, the black line in the Fig. 5.8. In this case, the second derivative approximation decreases the error, but not too much. To have the error one order of magnitude less, we have to look at the other lines, for example the red line, where we use the expanding factor 2. In this case the relative error is $\approx 0.1\%$, while in the zero order approximation was $\approx 1\%$. The improvement is quite good.

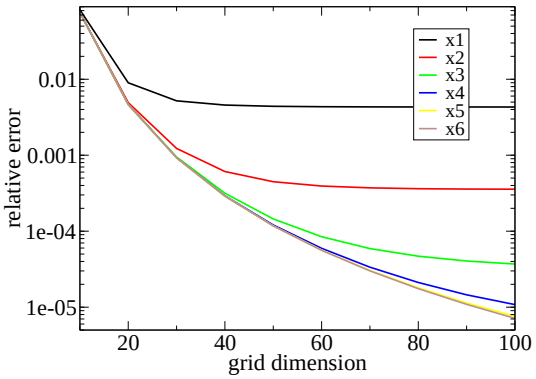

Figure 5.8.: Second order approximation. Relative error as a function of the grid dimension up to 100 with different expanding factors from x1 to x6.

Now let us look the plots in the Fig 5.10.

As we can see, the expanding factor 4 is enough for our goals. Indeed fixing the starting grid dimension and increasing the expanding factor, the error changes slightly. We do not need to go beyond 4. According to these results, a good choice is to have these parameters:

- starting grid dimension: 70×70;
- expanding factor: 4.

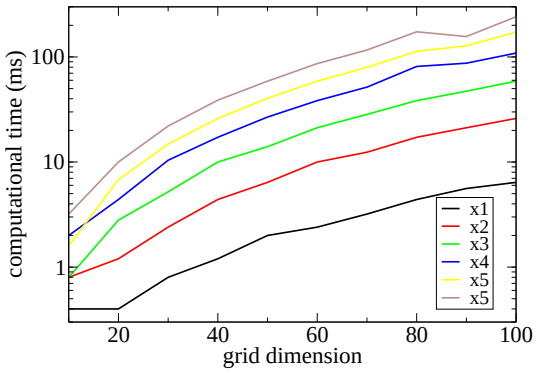

Figure 5.9.: Second order approximation. Computational calculation as a function of the grid dimension up to 100 with different expanding factors from x1 to x6.

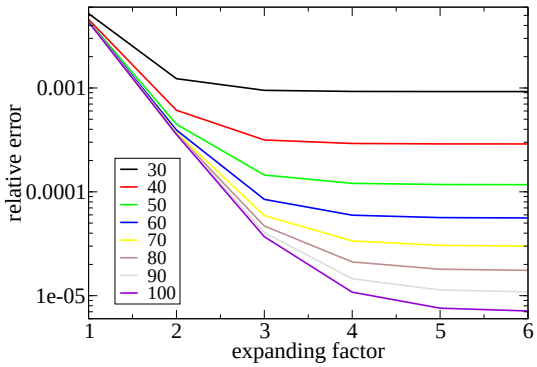

Figure 5.10.: Second order approximation. Left: Relative error as a function of the grid dimension up to 100 with different expanding factors from x1 to x6.

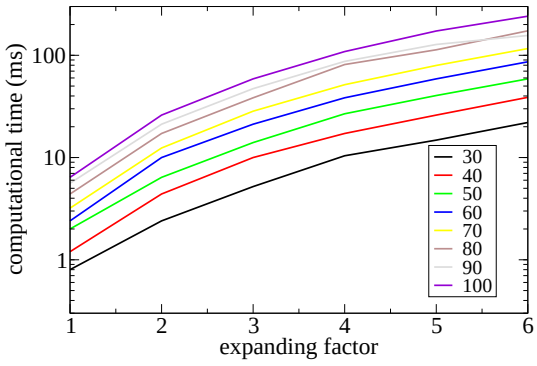

Figure 5.11.: Second order approximation. Time calculation as a function of the grid dimension up to 100 with different expanding factors from x1 to x6.

Now we have the relative error less than 0.01% and the computational time less than 100 ms. The computational time is of the order of $10 \div 100$ ms. This is a good result. Indeed, once we construct the Slater determinants, we need to compute the Coulomb matrix elements. They are at least ≈ 10000. The computational cost to have all the elements is of the order of 10 minutes, on the present workstation.

5.11. Spin-orbit matrix elements

The last step of our procedure is to add the spin dependent parts to the Hamiltonian. Also, we construct a new basis by expanding the wavefunctions obtained in the previous step by the spin. The orbital wavefunction Ψ_i acts the spinor according to its particle exchange symmetry. The symmetric function gets the singlet S while the antisymmetric appears in three copies, each with one of the three triplets T_0, T_+ and T_-. We denote the new states by

$$|\Phi_{i\Sigma}\rangle = |\Psi_i\rangle|\Sigma\rangle, \tag{5.80}$$

where $|\Sigma\rangle$ corresponds to one of the 4 spin states. The matrix elements of the total Hamiltonian Eq. (4.1) are

$$\begin{aligned}\langle\Phi_{i\Sigma}|H_{tot}|\Phi_{i'\Sigma'}\rangle &= E_i\delta_{i,i}\delta_{\Sigma,\Sigma'}+ \\ &+ g/2\mu_B B_z(\delta_{\Sigma,T_+} - \delta_{\Sigma,T_-}))\delta_{i,i}\delta\Sigma,\Sigma'+ \\ &+ \langle\Psi_i|\mathbf{w}|\Psi_{i'}\rangle\cdot\langle\Sigma|\boldsymbol{\sigma}|\Sigma'\rangle,\end{aligned} \tag{5.81}$$

where the last term is the matrix element of the spin-orbit interactions. The resulting matrix is diagonalized to get the final eigenstates. We choose a certain number n_s of lowest Ψ_i states. The number n_s to use depends on the precision that we wish to have on the spectrum. In our simulations $n_s = 250$, resulting to the accuracy of the order of 10^{-5} meV for the energy.

5.12. Spin-relaxation rate

In the last part of our numerical method, we focus on the spin-relaxation rate. We have derived a numerical formula, which still needs to be tested for the convergence and the precision.

Given an initial state α with energy E_α and a final state β with energy E_β, the spin-relaxation rate between these two states is defined by the formula

$$\begin{aligned}\Gamma^{2e}(\alpha\to\beta) &= \frac{2\pi}{\hbar}\sum_{ph,\mathbf{k}} C_{\mathbf{k}}\Big|\int d\mathbf{r}_1\int d\mathbf{r}_2\Psi^*_\alpha(\mathbf{r}_1,\mathbf{r}_2)[e^{i\mathbf{k}.\mathbf{r}_1}+e^{i\mathbf{k}.\mathbf{r}_2}]\Psi_\beta(\mathbf{r}_1,\mathbf{r}_2)\Big|^2\times \\ &\times\ \delta(E_\alpha - E_\beta - \hbar kc),\end{aligned} \tag{5.82}$$

where $C_{\mathbf{k}}$ is a coefficient which depends on phonon dispersion and bulk material and $\hbar kc$ is the phonon energy. The rate can be rewritten as:

$$\begin{aligned}\Gamma^{2e}(\alpha\to\beta) &= \frac{2\pi}{\hbar}\sum_{ph,\mathbf{k}} C_{\mathbf{k}}\Big|\int d\mathbf{r}_1\int d\mathbf{r}_2[\Psi^*_\alpha(\mathbf{r}_1,\mathbf{r}_2)\Psi_\beta(\mathbf{r}_1,\mathbf{r}_2)]e^{i\mathbf{k}.\mathbf{r}_1}+\\ &+ \int d\mathbf{r}_1\int d\mathbf{r}_2[\Psi^*_\alpha(\mathbf{r}_1,\mathbf{r}_2)\Psi_\beta(\mathbf{r}_1,\mathbf{r}_2)]e^{i\mathbf{k}.\mathbf{r}_2}\Big|^2\delta(E_\alpha-E_\beta-\hbar kc)=\\ &= \frac{2\pi}{\hbar}\sum_{ph,\mathbf{k}} C_{\mathbf{k}}\Big|M^{(1)}_{\alpha\beta}+M^{(2)}_{\alpha\beta}\Big|^2\delta(E_\alpha-E_\beta-\hbar kc), \qquad (5.83)\end{aligned}$$

where we have defined

$$\begin{aligned}M^{(1)}_{\alpha\beta} &= \int d\mathbf{r}_1 e^{i\mathbf{k}.\mathbf{r}_1}\Big(\int d\mathbf{r}_2\Psi^*_\alpha(\mathbf{r}_1,\mathbf{r}_2)\Psi_\beta(\mathbf{r}_1,\mathbf{r}_2)\Big)(\mathbf{r}_1)=\\ &= \int d\mathbf{r}_1 e^{i\mathbf{k}.\mathbf{r}_1}g_{\alpha\beta}(\mathbf{r}_1), \qquad (5.84)\\ M^{(2)}_{\alpha\beta} &= \int d\mathbf{r}_2 e^{i\mathbf{k}.\mathbf{r}_2}\Big(\int d\mathbf{r}_1\Psi^*_\alpha(\mathbf{r}_1,\mathbf{r}_2)\Psi_\beta(\mathbf{r}_1,\mathbf{r}_2)\Big)(\mathbf{r}_2)=\\ &= \int d\mathbf{r}_2 e^{i\mathbf{k}.\mathbf{r}_2}h_{\alpha\beta}(\mathbf{r}_2). \qquad (5.85)\end{aligned}$$

The first step of the algorithm is to provide the two coefficients $g_{\alpha\beta}(\mathbf{r}_1)$ and $h_{\alpha\beta}(\mathbf{r}_2)$ and then perform the two dimensional Fourier transformation on these functions. After that, using the formula Eq. (5.82) we get the relaxation rate by a summation over all the phonon momentum.

According to our notation (see Appendix), we can write

$$\begin{aligned}g_{\alpha\beta}(\mathbf{r}_1) &= \int d\mathbf{r}_2\Psi^*_\alpha(\mathbf{r}_1,\mathbf{r}_2)\Psi_\beta(\mathbf{r}_1,\mathbf{r}_2)=\sum_{a\Sigma}\sum_k\sum_{a'\Sigma'}\sum_{k'}(d^\alpha_{a\Sigma}c^a_k)^*(d^\beta_{a'\Sigma'}c^{a'}_{k'})\frac{1}{\sqrt{N_kN_{k'}}}\times\\ &\times \Big\langle(\langle i|\langle j|+(-i)^p\langle j|\langle i|)\Big|(|i'\rangle|j'\rangle+(-i)^{p'}|j'\rangle|i'\rangle)\Big\rangle_2\langle\Sigma|\Sigma'\rangle=\\ &= \sum_\Sigma\sum_k\sum_{k'}(e^\alpha_{k\Sigma})^*(e^\beta_{k'\Sigma})\frac{1}{\sqrt{N_kN_{k'}}}\times\\ &\times \Big\langle(\langle i|\langle j|+(-i)^p\langle j|\langle i|)\Big|(|i'\rangle|j'\rangle+(-i)^{p'}|j'\rangle|i'\rangle)\Big\rangle_2. \qquad (5.86)\end{aligned}$$

The last part of the summation is an integral over $\mathbf{r}_2$ which is

$$\Big\langle ...\Big\rangle_2=|i'\rangle\langle i|\delta_{jj'}+(-1)^p|i'\rangle\langle j|\delta_{ij'}+(-1)^{p'}|j'\rangle\langle i|\delta_{ji'}+(-1)^p(-1)^{p'}|j'\rangle\langle j|\delta_{ii'}.$$

The integration over $\mathbf{r}_1$ gives

$$\begin{aligned} h_{\alpha\beta}(\mathbf{r}_2) &= \int d\mathbf{r}_1 \Psi^*_\alpha(\mathbf{r}_1,\mathbf{r}_2)\Psi_\beta(\mathbf{r}_1,\mathbf{r}_2) = \sum_{a\Sigma}\sum_{k}\sum_{a'\Sigma'}\sum_{k'}(d^\alpha_{a\Sigma}c^a_k)^*(d^\beta_{a'\Sigma'}c^{a'}_{k'})\frac{1}{\sqrt{N_k N_{k'}}}\times \\ &\times \left\langle(\langle i|\langle j| + (-i)^p\langle j|\langle i|)\right|(|i'\rangle|j'\rangle + (-i)^{p'}|j'\rangle|i'\rangle)\Big\rangle_1\langle\Sigma|\Sigma'\rangle = \\ &= \sum_{\Sigma}\sum_{k}\sum_{k'}(e^\alpha_{k\Sigma})^*(e^\beta_{k'\Sigma})\frac{1}{\sqrt{N_k N_{k'}}}\times \\ &\times \left\langle(\langle i|\langle j| + (-i)^p\langle j|\langle i|)\right|(|i'\rangle|j'\rangle + (-i)^{p'}|j'\rangle|i'\rangle)\Big\rangle_1, \end{aligned} \tag{5.87}$$

where

$$\Big\langle ... \Big\rangle_1 = |j'\rangle\langle j|\delta_{ii'} + (-1)^p|j'\rangle\langle i|\delta_{ji'} + (-1)^{p'}|i'\rangle\langle j|\delta_{ij'} + (-1)^p(-1)^{p'}|i'\rangle\langle i|\delta_{jj'}.$$

Conclusions

In this thesis we have performed numerical and analytical study of the two-electron laterally coupled GaAs quantum dots. We have developed a very efficient numerical procedure, based on the Configuration Interaction, to calculate the two-electron spectrum. Most demanding part is to calculate the Coulomb integral numerically. Therefore, after a detailed numerical analysis, we have decided to use an algorithm based on the Discrete Fourier Transform, with also some modification to have a good numerical precision. We concentrated on the role of the spin-orbit interaction on the energy spectrum and how the isotropic and the anisotropic exchange couplings are modified.

On the other hand, since the quantum dot is one of the most important system for quantum computation applications, we have focused on the lowest part of the spectrum and derived an accurate analytical model, which provide us a good description of the role of the spin-orbit interaction. Our derived model is supported by precise numerics, which helped us to discriminate the existing models [26],[27]. The effective anisotropic exchange model is useful in precise analysis of the physical realizations of quantum computing schemes based on quantum dot spin qubits, as well as in the physics of electron spins in quantum dots in general. Our analysis should also improve the current understanding of the singlet-triplet spin relaxation [87],[64],[78].

In this work, we have derived the leading order anisotropic exchange terms which appear in a finite magnetic field. We have derived all anisotropic exchange parameters in a form valid for arbitrary interdot coupling. We also compared the results obtained using the first order versus the second order treatment of the spin-orbit interactions. The main goal of the presented work was a detailed assessment of the quantitative reliability of the presented anisotropic exchange model comparing with exact numerical results. Specifically, we examine the model in the strong and weak coupling regimes [corresponding to single and double dots, respectively] and in zero and finite perpendicular magnetic field. We also study the role of the cubic Dresselhaus term, whose action does not correspond to a spatial texture (in the leading order; that is, the unitary transformation does not remove it) and could potentially become dominant over the linear terms, changing the picture considerably.

The analytical pitfalls in evaluating the isotropic exchange are well known [65],[88]. On the top of that, the anisotropic exchange is a (very) small correction to the

exponentially sensitive isotropic exchange, and therefore it is involved to extract it even numerically. Our main result is that the presented analytical model is valid in all studied regimes. Quantitatively, the effective parameters are usually within a factor of 2 from their counterparts derived from the numerically exact spectra. The main source of the discrepancy is the cubic Dresselhaus term. Surprisingly, in the most important regime for quantum dot spin qubits, namely the weak coupling, the Heitler-London approximation works great for the anisotropic exchange, even though it fails badly for the isotropic one. This finding justifies using simple analytical formulas for the anisotropic exchange parameters.

We identify some important extensions to this work, taking into account the results presented in this thesis and the numerical approach developed.

The numerical diagonalization is based on the discretization scheme to solve the Schrödinger equation. This method is independent of the confinement potential we used. Therefore it is straightforward to investigate different kinds of geometries such quantum rings or biased dots. Latter it is very interesting, since we can simulate a more realistic gate operation, according to present experiments. This is currently under our investigation.

Another crucial issue is spin-relaxation, as this hinders the prospects of spin-based quantum computing. We have set up the code to perform realistic calculations of this phenomenon; the work is still under way.

The investigation of many electrons system is very interesting, since one can exploit and study different regimes, such as Kondo effect, quantum chaos, and transport.

A. Coulomb integrals

Here we list the integrals needed to compute the exchange coupling in the Heitler-London approximation.

$$
\begin{aligned}
E_{RI} &= \int d\mathbf{r}_1 d\mathbf{r}_2 |\psi_L(\mathbf{r}_1)|^2 |\psi_R(\mathbf{r}_2)|^2 \frac{e^2}{4\pi\varepsilon_0\varepsilon_r} \frac{1}{|\mathbf{r}_1 - \mathbf{r}_2|} = \\
&= \frac{e^2}{4\pi\varepsilon_0\varepsilon_r} \frac{1}{\pi^2 l_B^4} \int d\mathbf{r}_1 d\mathbf{r}_2 \exp\left[-\frac{(x_1 + l_0 d)^2 + y_1^2}{l_B^2}\right] \times \\
&\times \exp\left[-\frac{(x_2 - l_0 d)^2 + y_2^2}{l_B^2}\right] \frac{1}{|\mathbf{r}_1 - \mathbf{r}_2|} = \\
&= \frac{e^2}{4\pi\varepsilon_0\varepsilon_r} \frac{1}{\pi^2 l_B^4} \exp\left[-2\zeta d^2\right] \int d\mathbf{r}_1 d\mathbf{r}_2 \exp\left[-\frac{x_1^2 + y_1^2}{l_B^2}\right] \exp\left[-\frac{x_2^2 + y_2^2}{l_B^2}\right] \times \\
&\times \frac{\exp\left[2\zeta d / l_0 (x_2 - x_1)\right]}{|\mathbf{r}_1 - \mathbf{r}_2|} = \\
&= \frac{e^2}{4\pi\varepsilon_0\varepsilon_r} \frac{1}{\pi^2 l_B^4} \exp\left[-2\zeta d^2\right] \int d\mathbf{r}_1 d\mathbf{r}_2 \frac{F(\mathbf{r}_1) G(\mathbf{r}_2)}{|\mathbf{r}_1 - \mathbf{r}_2|}.
\end{aligned}
\tag{A.1}
$$

The Fourier Transform is useful to reduce the four dimensional integration in two dimension, namely

$$
\int d\mathbf{r}_1 d\mathbf{r}_2 \frac{F(\mathbf{r}_1) G(\mathbf{r}_2)}{|\mathbf{r}_1 - \mathbf{r}_2|} = \int \frac{2\pi}{|\mathbf{q}|} \tilde{F}(-\mathbf{q}) \tilde{G}(\mathbf{q}),
\tag{A.2}
$$

where $\tilde{F}(\mathbf{q})$ and $\tilde{G}(\mathbf{q})$ are the Fourier transform of the functions $F(\mathbf{r})$ and $G(\mathbf{r})$ respectively. Hence

$$\begin{aligned}
E_{RI} &= \frac{e^2}{4\pi\varepsilon_0\varepsilon_r}\frac{2\pi}{\pi^2 l_B^4}\times \\
&\times \exp\left[-2\zeta d^2\right]\int d\mathbf{q}\frac{l_B^4}{4}\exp\left[-1/2l_B^2(q_x^2+q_y^2-4i(\zeta d/l_0)q_x-4(\zeta d/l_0)^2)\right]\frac{1}{|\mathbf{q}|}= \\
&= \frac{e^2}{4\pi\varepsilon_0\varepsilon_r}\frac{1}{2\pi}\int d\mathbf{q}\exp\left[-\frac{l_B^2|\mathbf{q}|^2}{2}\right]\exp\left[2idl_0q_x\right]\frac{1}{|\mathbf{q}|}= \\
&= \frac{e^2}{4\pi\varepsilon_0\varepsilon_r}\frac{1}{2\pi}\int_0^\infty dR\exp\left[-\frac{l_B^2R^2}{2}\right]\int_0^{2\pi}d\phi\exp\left[2idl_0R\cos(\phi)\right]= \\
&= \frac{e^2}{4\pi\varepsilon_0\varepsilon_r}\int_0^\infty dR\exp\left[-\frac{l_B^2R^2}{2}\right]J_0(2dl_0R)= \\
&= \frac{e^2}{4\pi\varepsilon_0\varepsilon_r}\sqrt{\frac{\pi}{2}}\frac{\sqrt{\zeta}}{l_0}\exp\left[-\zeta d^2\right]I_0(\zeta d^2). \qquad \text{(A.3)}
\end{aligned}$$

$$\begin{aligned}
E_{W_{RI}} &= -m\omega_0^2 l_0 d\left\{\int d\mathbf{r}_1 d\mathbf{r}_2|\psi_L(\mathbf{r}_1)|^2|\psi_R(\mathbf{r}_2)|^2(|x_1|+x_1+|x_2|-x_2)\right\}= \\
&= -m\omega_0^2 l_0 d\frac{1}{\pi^2 l_B^4}\Big\{\int d\mathbf{r}_1(|x_1|+x_1)\exp\left[-\frac{(x_1+l_0d)^2+y_1^2}{l_B^2}\right]\times \\
&\times \int d\mathbf{r}_2\exp\left[-\frac{(x_2-l_0d)^2+y_2^2}{l_B^2}\right]+\int d\mathbf{r}_1\exp\left[-\frac{(x_1+l_0d)^2+y_1^2}{l_B^2}\right]\times \\
&\times \int d\mathbf{r}_2(|x_2|-x_2)\exp\left[-\frac{(x_2-l_0d)^2+y_2^2}{l_B^2}\right]\Big\}= \\
&= -m\omega_0^2 l_0 d\frac{\pi l_B^2}{\pi^2 l_B^4}\left\{\int d\mathbf{r}_1|x_1|\exp\left[-\frac{(x_1+l_0d)^2+y_1^2}{l_B^2}\right]+\right. \\
&+ \left.\int d\mathbf{r}_2\,|x_2|\exp\left[-\frac{(x_2-l_0d)^2+y_2^2}{l_B^2}\right]\right\}+ \\
&- m\omega_0^2 l_0 d\frac{\pi l_B^2}{\pi^2 l_B^4}\left\{\int d\mathbf{r}_1 x_1\exp\left[-\frac{(x_1+l_0d)^2+y_1^2}{l_B^2}\right]+\right. \\
&- \left.\int d\mathbf{r}_2 x_2\exp\left[-\frac{(x_2-l_0d)^2+y_2^2}{l_B^2}\right]\right\}= \\
&= -m\omega_0^2 l_0 d\frac{\sqrt{\pi}l_B}{\pi l_B^2}\left\{2l_B^2\exp\left[-\zeta d^2\right]+2l_Bl_0d\sqrt{\pi}\mathrm{Erf}(d\sqrt{\zeta})-2\sqrt{\pi}l_Bl_0d\right\}= \\
&= m\omega_0^2 l_0^2\left[2d^2(1-\mathrm{Erf}(d\sqrt{\zeta}))-\frac{2d}{\sqrt{\zeta\pi}}\exp\left[-\zeta d^2\right]\right]= \\
&= \hbar\omega_0\left[2d^2(1-\mathrm{Erf}(d\sqrt{\zeta}))-\frac{2d}{\sqrt{b\pi}}\exp\left[-\zeta d^2\right]\right]. \qquad \text{(A.4)}
\end{aligned}$$

$$
\begin{aligned}
E_{CE} &= \frac{e^2}{4\pi\varepsilon_0\varepsilon_r}\int \psi_R(\mathbf{r}_1)^*\psi_L(\mathbf{r}_2)^*\frac{1}{|\mathbf{r}_1-\mathbf{r}_2|}\psi_L(\mathbf{r}_1)\psi_R(\mathbf{r}_2)d\mathbf{r}_1 d\mathbf{r}_2 = \\
&= \frac{e^2}{4\pi\varepsilon_0\varepsilon_r}\frac{1}{\pi^2 l_B^4}\int d\mathbf{r}_1 d\mathbf{r}_2 \exp\left[-\frac{(x_1-l_0 d)^2+y_1^2}{2l_B^2}\right]\exp\left[-\frac{(x_2+l_0 d)^2+y_2^2}{2l_B^2}\right]\times \\
&\times \frac{1}{|\mathbf{r}_1-\mathbf{r}_2|}\exp\left[-2i\frac{\zeta d\vartheta}{l_0}y_1\right]\exp\left[2i\frac{\zeta d\vartheta}{l_0}y_2\right]\times \\
&\times \exp\left[-\frac{(x_1+l_0 d)^2+y_1^2}{2l_B^2}\right]\exp\left[-\frac{(x_2-l_0 d)^2+y_2^2}{2l_B^2}\right] = \\
&= \frac{e^2}{4\pi\varepsilon_0\varepsilon_r}\frac{\exp\left[-2\zeta d^2\right]}{\pi^2 l_B^4}\int d\mathbf{r}_1 d\mathbf{r}_2 \exp\left[-\frac{x_1^2+y_1^2}{l_B^2}\right]\exp\left[-2i\frac{\zeta d\vartheta}{l_0}y_1\right]\times \\
&\times \exp\left[-\frac{x_2^2+y_2^2}{l_B^2}\right]\exp\left[2i\frac{\zeta d\vartheta}{l_0}y_2\right]\frac{1}{|\mathbf{r}_1-\mathbf{r}_2|} = \\
&= \frac{e^2}{4\pi\varepsilon_0\varepsilon_r}\frac{\exp\left[-2\zeta d^2\right]}{\pi^2 l_B^4}\int d\mathbf{r}_1 d\mathbf{r}_2 \frac{F(\mathbf{r}_1)G(\mathbf{r}_2)}{|\mathbf{r}_1-\mathbf{r}_2|}.
\end{aligned}
\tag{A.5}
$$

$$
\begin{aligned}
E_{CE} &= \frac{e^2}{4\pi\varepsilon_0\varepsilon_r}\frac{2\pi}{\pi^2 l_B^4}\exp\left[-2\zeta d^2\right]\frac{l_B^4}{4}\times \\
&\times \int d\mathbf{q}\exp\left[-1/2l_B^2(q_x^2+q_y^2+4(\zeta d\vartheta/l_0)q_y+4(\zeta d\vartheta/l_0)^2)\right]\frac{1}{|\mathbf{q}|} = \\
&= \frac{e^2}{4\pi\varepsilon_0\varepsilon_r}\frac{1}{2\pi}\exp\left[-2\zeta d^2\right]\exp\left[-2\zeta d^2\vartheta^2\right]\times \\
&\times \int d\mathbf{q}\exp\left[-\frac{l_B^2|\mathbf{q}|^2}{2}\right]\exp\left[-2dl_0\vartheta q_y\right]\frac{1}{|\mathbf{q}|} = \\
&= \frac{e^2}{4\pi\varepsilon_0\varepsilon_r}\frac{1}{2\pi}\exp\left[-2\zeta d^2\right]\exp\left[-2\zeta d^2\vartheta^2\right]\times \\
&\times \int_0^\infty dR\exp\left[-\frac{l_B^2R^2}{2}\right]\int_0^{2\pi}d\phi\exp\left[-2dl_0\vartheta R\sin(\phi)\right] = \\
&= \frac{e^2}{4\pi\varepsilon_0\varepsilon_r}\exp\left[-2\zeta d^2\right]\exp\left[-2\zeta d^2\vartheta^2\right]\int_0^\infty dR\exp\left[-\frac{l_B^2R^2}{2}\right]I_0(2dl_0\vartheta R) = \\
&= \frac{e^2}{4\pi\varepsilon_0\varepsilon_r}\sqrt{\frac{\pi}{2}}\frac{\sqrt{\zeta}}{l_0}\exp\left[-\zeta d^2(\vartheta^2+2)\right]I_0(\zeta d^2\vartheta^2).
\end{aligned}
\tag{A.6}
$$

$$
\begin{aligned}
E_{W_{CE}} &= \int d\mathbf{r}_1 \int d\mathbf{r}_2 \psi_R(\mathbf{r}_1)^* \psi_L(\mathbf{r}_2)^* W \psi_L(\mathbf{r}_1)\psi_R(\mathbf{r}_2) = \\
&= -m\omega_0^2 l_0 d \times \\
&\times \int d\mathbf{r}_1 \int d\mathbf{r}_2 \psi_R(\mathbf{r}_1)^* \psi_L(\mathbf{r}_2)^* (|x_1| + x_1 + |x_2| - x_2)\psi_L(\mathbf{r}_1)\psi_R(\mathbf{r}_2) = \\
&= -m\omega_0^2 l_0 d \frac{1}{\pi^2 l_B^4} \exp\left[-2\zeta d^2\right] \times \\
&\times \Big\{ \int d\mathbf{r}_1 \int d\mathbf{r}_2 \exp\left[-\frac{x_1^2+y_1^2}{l_B^2}\right] \exp\left[-2i\zeta d\vartheta \frac{y_1}{l_0}\right] \left(|x_1| + x_1 + |x_2| - x_2\right) \times \\
&\times \exp\left[-\frac{x_2^2+y_2^2}{l_B^2}\right] \exp\left[2i\zeta d\vartheta \frac{y_2}{l_0}\right] \Big\} = \\
&= -m\omega_0^2 l_0 d \frac{1}{\pi^2 l_B^4} \exp\left[-2\zeta d^2\right] \times \\
&\times \Big\{ \pi l_B^2 \exp\left[-\zeta d^2\vartheta^2\right] \int d\mathbf{r}_1 \exp\left[-\frac{x_1^2+y_1^2}{l_B^2}\right] \exp\left[-2i\zeta d\vartheta \frac{y_1}{l_0}\right] (|x_1| + x_1) \\
&+ \pi l_B^2 \exp\left[-\zeta d^2\vartheta^2\right] \int d\mathbf{r}_2 \exp\left[-\frac{x_2^2+y_2^2}{l_B^2}\right] \exp\left[2i\zeta d\vartheta \frac{y_2}{l_0}\right] (|x_2| - x_2) \Big\} = \\
&= -m\omega_0^2 l_0 d \frac{1}{\pi^2 l_B^4} \exp\left[-2\zeta d^2\right] \Big\{ \pi l_B^2 \exp\left[-\zeta d^2\vartheta^2\right] \left(2\sqrt{\pi} l_B^3 \exp\left[-\zeta d^2\vartheta^2\right]\right) \Big\} = \\
&= -m\omega_0^2 l_0^2 \frac{2d}{\sqrt{\pi\zeta}} \exp\left[-2\zeta d^2(\vartheta^2+1)\right] = -\hbar\omega_0 \frac{2d}{\sqrt{\pi\zeta}} \exp\left[-2\zeta d^2(\vartheta^2+1)\right]. \qquad \text{(A.7)}
\end{aligned}
$$

The components of the vectors $\mathbf{a}'$ and $\mathbf{b}'$ are

$$
\begin{aligned}
a'_x &= 0, \qquad a'_y = 0, && \text{(A.8)} \\
b'_x &= -\frac{\hbar^2}{2ml_d} \frac{\Omega^2}{\sqrt{1-\Omega^4}} \frac{\zeta d}{l_0}(1-\vartheta^2), && \text{(A.9)} \\
b'_y &= -\frac{\hbar^2}{2ml_{br}} \frac{\Omega^2}{\sqrt{1-\Omega^4}} \frac{\zeta d}{l_0}(1-\vartheta^2). && \text{(A.10)}
\end{aligned}
$$

where l_{br} and l_d are the spin-orbit lengths for the Rashba and Dresselhaus respectively.

The matrix elements of the vector $\mathbf{n}$ are

$$
\begin{aligned}
\langle \Psi_+ | n_x | \Psi_- \rangle &= -\frac{dl_0}{\sqrt{1-\Omega^4}} \left(\frac{1}{l_d} + i\Omega^2 \frac{\vartheta}{l_{br}} \right), && \text{(A.11)} \\
\langle \Psi_+ | n_y | \Psi_- \rangle &= -\frac{dl_0}{\sqrt{1-\Omega^4}} \left(\frac{1}{l_{br}} + i\Omega^2 \frac{\vartheta}{l_d} \right), && \text{(A.12)}
\end{aligned}
$$

and

$$
\mu B_{so} = \frac{K_-}{1-\Omega^2} \vartheta \left[1 - \Omega^2(1 - \zeta d - \zeta d^2\vartheta^2)\right]. \qquad \text{(A.13)}
$$

B. Spin matrices

In the singlet and triplet basis, one can evaluate the sixteen matrices which can be formed as the direct product of two Pauli matrices and the identity. Here we list only the matrices needed for our purposes, and we regroup them to combinations in which they appear in the text.

$$\boldsymbol{\sigma}_1 \cdot \boldsymbol{\sigma}_2 = \begin{pmatrix} -3 & 0 & 0 & 0 \\ 0 & 1 & 0 & 0 \\ 0 & 0 & 1 & 0 \\ 0 & 0 & 0 & 1 \end{pmatrix}, \tag{B.1}$$

$$\frac{1}{\sqrt{2}}(\boldsymbol{\sigma}_1 - \boldsymbol{\sigma}_2) = \left\{ \begin{pmatrix} 0 & 0 & -1 & 1 \\ 0 & 0 & 0 & 0 \\ -1 & 0 & 0 & 0 \\ 1 & 0 & 0 & 0 \end{pmatrix}, \begin{pmatrix} 0 & 0 & -i & -i \\ 0 & 0 & 0 & 0 \\ i & 0 & 0 & 0 \\ i & 0 & 0 & 0 \end{pmatrix}, \begin{pmatrix} 0 & 1 & 0 & 0 \\ 1 & 0 & 0 & 0 \\ 0 & 0 & 0 & 0 \\ 0 & 0 & 0 & 0 \end{pmatrix} \right\}, \tag{B.2}$$

$$\frac{1}{\sqrt{2}}(\boldsymbol{\sigma}_1 \times \boldsymbol{\sigma}_2) = \left\{ \begin{pmatrix} 0 & 0 & -i & i \\ 0 & 0 & 0 & 0 \\ i & 0 & 0 & 0 \\ -i & 0 & 0 & 0 \end{pmatrix}, \begin{pmatrix} 0 & 0 & 1 & 1 \\ 0 & 0 & 0 & 0 \\ 1 & 0 & 0 & 0 \\ 1 & 0 & 0 & 0 \end{pmatrix}, \begin{pmatrix} 0 & i & 0 & 0 \\ -i & 0 & 0 & 0 \\ 0 & 0 & 0 & 0 \\ 0 & 0 & 0 & 0 \end{pmatrix} \right\}, \tag{B.3}$$

$$\frac{1}{\sqrt{2}}(\boldsymbol{\sigma}_1 + \boldsymbol{\sigma}_2) = \left\{ \begin{pmatrix} 0 & 0 & 0 & 0 \\ 0 & 0 & 1 & 1 \\ 0 & 1 & 0 & 0 \\ 0 & 1 & 0 & 0 \end{pmatrix}, \begin{pmatrix} 0 & 0 & 0 & 0 \\ 0 & 0 & i & -i \\ 0 & -i & 0 & 0 \\ 0 & i & 0 & 0 \end{pmatrix}, \begin{pmatrix} 0 & 0 & 0 & 0 \\ 0 & 0 & 0 & 0 \\ 0 & 0 & 1 & 0 \\ 0 & 0 & 0 & -1 \end{pmatrix} \right\}. \tag{B.4}$$

C. Detailed algorithm

C.1. Spin basis

For the spin, it is useful to choose the quantization axis to lie in the direction of the magnetic field, since then the Zeeman term is diagonal. If the magnetic field orientation is given by the polar and azimuthal angles (ϕ, θ), then the explicit form of spin 1/2 up and down spinors is

$$|\uparrow\rangle = \begin{pmatrix} e^{\mathrm{i}\phi}\cos(\theta/2) \\ \sin(\theta/2) \end{pmatrix}, \quad |\downarrow\rangle = \begin{pmatrix} e^{\mathrm{i}\phi}\sin(\theta/2) \\ -\cos(\theta/2) \end{pmatrix}. \tag{C.1}$$

Two spins can form four different states labeled by the projection of the total spin (being one or zero) along a chosen axis,

$$S = \frac{1}{\sqrt{2}}(|\uparrow\downarrow\rangle - |\downarrow\uparrow\rangle), \quad T_0 = \frac{1}{\sqrt{2}}(|\uparrow\downarrow\rangle + |\downarrow\uparrow\rangle), \quad T_+ = |\uparrow\uparrow\rangle, \quad T_- = |\downarrow\downarrow\rangle, \tag{C.2}$$

from which the singlet S is antisymmetric, while the three triplets T are symmetric with respect to the particle exchange.

The small letter σ usually denotes the spin 1/2 (spin of a single electron), while Σ is used to denote the composite two spin state.

C.2. States

Eigenstates of H_0 together with the spin part (can have definite orbital symmetries, Pauli spin like, but can be also without any symmetry)

$$|i\sigma\rangle = \psi_i(\mathbf{r}, \sigma) = \begin{pmatrix} \psi_i^{\uparrow}(\mathbf{r}) \\ \psi_i^{\downarrow}(\mathbf{r}) \end{pmatrix}, \tag{C.3}$$

eigenstates of H_0 without the spin part (usually with definite orbital symmetries)

$$|i\rangle = \psi_i(\mathbf{r}), \tag{C.4}$$

two particle state (not physical, just a term in a basis) with the spin

$$|i\sigma\rangle \otimes |j\sigma\rangle = \psi_i(\mathbf{r_1}, \sigma_1)\psi_j(\mathbf{r_2}, \sigma_2), \tag{C.5}$$

and without the spin

$$|i\rangle \otimes |j\rangle = \psi_i(\mathbf{r_1})\psi_j(\mathbf{r_2}). \tag{C.6}$$

The Slater determinant (a physical two electron state) build from states with spin

$$|ij\Sigma\rangle = \frac{1}{\sqrt{2}} \left(|i\sigma\rangle \otimes |j\sigma\rangle - |j\sigma\rangle \otimes |i\sigma\rangle \right), \tag{C.7}$$

orbital part of a physical two electron state build from states without spin (can be symmetric or antisymmetric)

$$|ij\rangle_p = \frac{1}{\sqrt{2}} \left(|i\rangle \otimes |j\rangle + \mathrm{sign}(p)|j\rangle \otimes |i\rangle \right). \tag{C.8}$$

The $|a\rangle$-states are two particle eigenstates of $H_{0,1} + H_{0,2} + H_C$ without spin (some $|a\rangle$-states are symmetric, then in the sum all p=+1, some antisymmetric, then all p=-1)

$$|a\rangle = \sum_{ij} c_{ij}^a |ij\rangle_p, \tag{C.9}$$

The $|b\rangle$-states are two particle eigenstates of $H_{0,1} + H_{0,2} + H_C$ with spin (all $|b\rangle$-states are antisymmetric – therefore if p=+1, $|\Sigma\rangle = |S\rangle$, if p=-1, then $|\Sigma\rangle = |T_x\rangle$, where x=0,+, or -)

$$|b\rangle = |a\rangle|\Sigma\rangle. \tag{C.10}$$

The $|f\rangle$-states are two particle eigenstates of the total Hamiltonian H_{tot} – are antisymmetric with respect to particle exchange, no other symmetry in general

$$|f\rangle = \sum_b d_b^f |b\rangle. \tag{C.11}$$

C.3. Algorithm

Here we list detailed steps of the algorithm implementing the second approach.

1 Set the desired perpendicular magnetic field, a very large inplane magnetic field (say 10^8 T), zero for all spin-orbit couplings and diagonalize the single particle Hamiltonian– obtain certain number of lowest single particle orbital states $|i\sigma\rangle$; $i\sigma = 1, \ldots N$, and their energies $E_{i\sigma}$. Since there is no spin orbit in the Hamiltonian, these states are spin pure states – throw away the spin (=do not do anything, just remember we will not use the spin down part of the wavefunctions, which is zero anyway) and you get states $|i\rangle$, and energies $E_i = E_{i\sigma}$.

2 "Build" symmetric and antisymmetric states $|ij\rangle_p$ using states $|i\rangle$. That is fill in arrays in the following way: StateIJ[k,1]=i, StateIJ[k,2]=j, StateIJ[k,3]=+1 represents the symmetric state $|ij\rangle_+$. For an antisymmetric state, there would be StateIJ[k,3]=-1. Remember, there is no antisymmetric combination if $i = j$.

3 Identify which spatial symmetries are present out of the four possible 1, I_x, I_{xy}, I_y (lets say these four are labeled as 1,2,3, and 4). The results are: number of symmetries present, NS, and an array enumerating the present symmetries, Symmetries[i], i=1,..., NS. For example, if there is only the total inversion, then NS=2, and Symmetries={1,3}. Which symmetries are present can be found by checking the parameters – if perpendicular magnetic field is present, 2 and 4 are not present. If the dot is biased 2 and 3 are not present (for now, there is no bias implemented in the single particle potential, but it is trivial to add, so we can keep this possibility in mind here). We could also think about the case of $d = 0$, where the states have definite angular momenta, but that would require a modification of the symmetries labeling, so I propose to put this aside for now. Another way (more robust) how to check whether we have certain symmetry (e.g. I_x) is to go through all the single particle states and check what is the "eigenvalue" of that symmetry (for this example vectors stats at position 6). If the eigenvalue is close enough to a natural number (say it is not farther away from plus minus 1 that 10^{-2}) for each single particle state, then the symmetry is present.

4 Identify the spatial symmetry of each of the $|ij\rangle_p$ states. That is, StateIJ[k,4]=s (being a number from 1 to NS) according to the state spatial symmetry. For this, use the mean values of single particle states returned by the diagonalization routine in step 1 in the array "stats". Mean value number 6 and 7 contains the "eigenvalue" of the I_x and I_y operators, respectively.

5 For each x from 1 to 2 NS represeting a pair (p, s) construct the block of the Hamiltonian matrix:
Put l=0. Check each state k – if StateIJ[k,3]=p and StateIJ[k,4]=s, add label l into vector

StateAux[x,l]=k
l=l+1

After going through all k, there will be N_x states in StateAux[x], save also this

number, StateAuxDim[x]=N_x. After that build one block of the Hamiltonian matrix (it has dimension $N_x \times N_x$)

MatrixAux[x,l1,l2]=$\langle$ StateIJ[StateAux[x,l1]]|C|StateIJ[StateAux[x,l2]]$\rangle$ +
+ $\delta_{l1,l2}(E_{l1})$,

If k1=StateAux[x,l1] and StateIJ[k1]=$\{i_{k1}, j_{k1}, p_{k1}, .\}$, and analogously for StateAux[x,l2], then the first term in the previous equation is

$$\begin{aligned}
&\frac{1}{2}(\langle i_{k1}| \otimes \langle j_{k1}| + \mathrm{sign}(p_{k1})\langle j_{k1}| \otimes \langle i_{k1}|C|i_{k2}\rangle \otimes |j_{k2}\rangle + \mathrm{sign}(p_{k2})|j_{k2}\rangle \otimes |i_{k2}\rangle) = \\
&= \frac{1}{2}(C_{i_{k1}j_{k1}i_{k2}j_{k2}} + \mathrm{sign}(p_{k1})C_{j_{k1}i_{k1}i_{k2}j_{k2}} + \mathrm{sign}(p_{k2})C_{i_{k1}j_{k1}j_{k2}i_{k2}} + \\
&+ \mathrm{sign}(p_{k1}p_{k2})C_{j_{k1}i_{k1}j_{k2}i_{k2}}) \\
&= \frac{1}{2}\left(C_{i_{k1}j_{k1}i_{k2}j_{k2}}(1 + \mathrm{sign}(p_{k1}p_{k2})) + C_{j_{k1}i_{k1}i_{k2}j_{k2}}(\mathrm{sign}(p_{k1}) + \mathrm{sign}(p_{k2}))\right) = \\
&= \frac{1}{2}\left(1 + \mathrm{sign}(p_{k1}p_{k2})\right)\left(C_{i_{k1}j_{k1}i_{k2}j_{k2}} + \mathrm{sign}(p_{k1})C_{j_{k1}i_{k1}i_{k2}j_{k2}}\right).
\end{aligned} \tag{C.12}$$

We need two evaluations of C_{ijkl} for each matrix element in MatrixAux. On the other hand, use Hermitivity of this matrix, $M(k1, k2) = M^*(k2, k1)$, to get, say, the entries below the diagonal from the ones above the diagonal. The energy is $E_{k1} = E_{i_{k1}} + E_{j_{k1}}$.

6 Diagonalize each MatrixAux using ARPACK (we may consider also other means of diagonalization, since this matrix is not sparse) – you obtain coefficients defining the states $|a\rangle$, Eq. (C.9), say you save them into StateA[a,x]=c^a_x, and the energies into EnergyA[a]=E_a. Fill the StateA consecutively, if the last state from the group $s = 1$ is at position a, the first state from $s = 2$ will be at a+1 position.

7 Sort the states StateA according their energies.

8 Choose certain number of the lowest in energy states and add the spin part – create an array StateB[b,1]=a, StateB[b,2]=Σ where b is the label of a new state with spin, a points into StateA, and Σ=1,2,3, or 4 for singlet and the three triplets. Remember, that if StateA[a] is symmetric with respect to the particle exchange (check it by looking at the symmetry of any of the StateIJ which StateA contains), the spin part has to be antisymmetric - singlet. If

StateA is antisymmetric, there will be three states in StateB, with the three possible triplet spin states and the same orbital part (that is the same label a).

9 Set the appropriate values for the inplane magnetic field and spin-orbit interaction strengths.

10 Compute all possible single particle matrix elements of all orbital operators appearing in the spin-orbit interactions. (I will provide a interface for that, you just call it.) Save the results into an array SingleOrbital[i,j,operator], where $|i\rangle$ and $|j\rangle$ are single particle wavefunctions and operator=1,2,3, or 4 for P_x, P_y, $(P_xP_y^2 + P_y^2P_x)/2$, and $(P_yP_x^2 + P_x^2P_y)/2$.
For example, SingleOrbital[i,j,1]=$\langle i|P_x|j\rangle$.

11 Compute all possible matrix elements of all spin operators of the spin-orbit interaction. Remember, that the spin is chosen to lie along the magnetic field. Similarly as in the previous point, fill the results into array
SingleSpin[σ,π,operator], where now operator=1,2,3, or 4 for $\sigma_{x,1}$,$\sigma_{x,2}$, $\sigma_{y,1}$ and $\sigma_{y,2}$, and σ, π=1,2,3, or 4 for $|\Sigma_1\rangle$,..., $|\Sigma_4\rangle$.

12 Construct the final Hamiltonian matrix FinalMatrix for the basis consisting of StateB states – by computing the spin-orbit matrix elements and adding the energy from EnergyA and Zeeman energy on the diagonal.

FinalMatrix[b1,b2]=$\delta_{b1,b2}$(Zeeman(b1)+EnergyA[StateB[b1,1]])+
+SpinOrbit[b1,b2]

The detailed formula for the three terms using the arrays defined above, similarly as in Eq. (C.12) is in the next section. The matrix elements of the previous equation are SingleOrbital[j_{a1},j_{a2},1], and SingleSpin[Σ_{b1},Σ_{b2},1].

13 Diagonalize FinalMatrix and obtain the coefficients expressing a final state $|f\rangle$ as a sum of states StateB[b], FinalState[f,b]=d_b^f. The energies are stored in FinalEnergy[f].

14 Produce output using FinalState and Final Energy – first we look just at the spectrum, later we extract the regular part of the exchange interaction, anisotropic exchange, and so on.

C.4. Formula for spin-orbit matrix elements

We want to derive a numerical formula to compute the spin-orbit matrix elements. Because we found some problem with the normalization, to be more clear, we report the detail of the formulas.

After the two electron diagonalization, the numerical eigenfunctions are normalized. This means:

$$\langle a'|a\rangle = \sum_{a}\sum_{a'} c^{a'*}c^{a}\langle a'|a\rangle = \delta_{a,a'}. \tag{C.13}$$

In the next step, we construct the state $|b\rangle = |a\rangle|\Sigma\rangle$ and we want to work with the spin-orbit interaction. Because the $|a\rangle$ states are the combination of $|i,j\rangle$ states, we have 4 different formulas.

Let us consider the case of an operator acting on the particle 1. The matrix elements that we need to compute are:

$$\begin{aligned}\langle b1|P_{x,1}\sigma_{x,1}|b2\rangle &= \sum_{a1,a2} c^{a1}_{b1}c^{a2}_{b2}\langle i_{a1}j_{a1}|P_{x,1}\sigma_{x,1}|i_{a2}j_{a2}\rangle\langle\Sigma_{b1}|\sigma^{(1)}|\Sigma_{b2}\rangle = \\ &= \sum_{a1,a2} c^{a1}_{b1}c^{a2}_{b2}\left(\langle i_{a1}|\langle j_{a1}| + \mathrm{sign}(p_{a1})\langle j_{a1}|\langle i_{a1}|\right)P_{x,1} \\ &\quad \left(|i_{a2}\rangle|j_{a2}\rangle + \mathrm{sign}(p_{a2})|j_{a2}\rangle|i_{a2}\rangle\right)\langle\Sigma_{b1}|\sigma_{x,1}|\Sigma_{b2}\rangle. \end{aligned}\tag{C.14}$$

The previous formula is valid in any case. In the next calculation, we assume that the $|\Sigma\rangle$ states are normalized and we want to know what is the normalization for the spatial part.

From the previous formula, we can have 4 different cases:

1. Case : $i_{a1} \neq j_{a1}$ and $i_{a2} \neq j_{a2}$

   $$\begin{aligned}\langle b1|P_{x,1}\sigma_{x,1}|b2\rangle = N_1\sum_{a1,a2} c^{a1}_{b1}c^{a2}_{b2}\Big(&\langle i_{a1}|P_x|i_{a2}\rangle\delta_{j_{a1},j_{a2}} + \mathrm{sign}(p_{a1})\langle j_{a1}|P_x|i_{a2}\rangle\delta_{i_{a1},j_{a2}} + \\ &+\mathrm{sign}(p_{a2})\langle i_{a1}|P_x|j_{a2}\rangle\delta_{j_{a1},i_{a2}} + \mathrm{sign}(p_{a1}p_{a2})\langle j_{a1}|P_x|j_{a2}\rangle\delta_{i_{a1},i_{a2}}\Big)\langle\Sigma_{b1}|\sigma_{x,1}|\Sigma_{b2}\rangle,\end{aligned}$$

   where N_1 is some number that depend of the normalization of the states.

2. Case : $i_{a1} \neq j_{a1}$ and $i_{a2} = j_{a2}$

   $$\begin{aligned}\langle b1|P_{x,1}\sigma_{x,1}|b2\rangle = N_2\sum_{a1,a2} c^{a1}_{b1}c^{a2}_{b2}(1+\mathrm{sign}(p_{a2})) \\ \Big(\langle i_{a1}|P_x|i_{a2}\rangle\delta_{j_{a1},j_{a2}} + \mathrm{sign}(p_{a1})\langle j_{a1}|P_x|i_{a2}\rangle\delta_{i_{a1},j_{a2}}\Big)\langle\Sigma_{b1}|\sigma_{x,1}|\Sigma_{b2}\rangle,\end{aligned}$$

   where N_2 is some number that depend of the normalization of the states.

3. Case : $i_{a1} = j_{a1}$ and $i_{a2} \neq j_{a2}$

$$\langle b1|P_{x,1}\sigma_{x,1}|b2\rangle = N_3 \sum_{a1,a2} c_{b1}^{a1} c_{b2}^{a2} (1 + \text{sign}(p_{a1}))$$
$$\Big(\langle i_{a1}|P_x|i_{a2}\rangle \delta_{j_{a1},j_{a2}} + \text{sign}(p_{a2}) \langle i_{a1}|P_x|j_{a2}\rangle \delta_{j_{a1},i_{a2}}\Big) \langle \Sigma_{b1}|\sigma_{x,1}|\Sigma_{b2}\rangle,$$

   where N_3 is some number that depend of the normalization of the states.

4. Case : $i_{a1} = j_{a1}$ and $i_{a2} = j_{a2}$

$$\langle b1|P_{x,1}\sigma_{x,1}|b2\rangle = N_4 \sum_{a1,a2} c_{b1}^{a1} c_{b2}^{a2} (1 + \text{sign}(p_{a1}))$$
$$(1 + \text{sign}(p_{a2}))\Big(\langle i_{a1}|P_x|i_{a2}\rangle \delta_{j_{a1},j_{a2}}\Big) \langle \Sigma_{b1}|\sigma_{x,1}|\Sigma_{b2}\rangle,$$

   where N_4 is some number that depend of the normalization of the states.

In the case of the operator acting on the particle 2, the formulas are the same if you exchange the indices like $i_{a1} \to j_{a1}$ and $i_{a2} \to j_{a2}$. The normalization constants are:

1. $N_1 = \frac{1}{2}$,
2. $N_2 = \frac{1}{2\sqrt{2}}$,
3. $N_3 = \frac{1}{2\sqrt{2}}$,
4. $N_4 = \frac{1}{4}$.

Bibliography

[1] G. E. Moore. Cramming more components onto integrated circuits. *Electronics*, 38, 1965.

[2] A. M. Turing. On computable numbers, with an application to the entscheidungsproblem. *Proc. Lond. Math. Soc.*, 42, 1936.

[3] R. P. Feynman. There's a plenty of room at the bottom. *Eng. and Sci.*, 23, 1960.

[4] R. P. Feynman. Quantum mechanical computers. *Optics News*, 11, 1985.

[5] P. W. Shor. Algorithms for quantum computation: Discrete logarithms and factoring. *Proc. 35nd Annual Symposium on Fundation of Computer Science*, 1994.

[6] J. Preskill. *Lecture notes for physics: quantum information and computation.*

[7] D.P. DiVincenzo. Quantum computation. *Science*, 270, 1995.

[8] Daniel Loss and David P. DiVincenzo. Quantum computation with quantum dots. *Phys. Rev. A*, 57(1):120–126, Jan 1998.

[9] R. Hanson, L. P. Kouwenhoven, J. R. Petta, S. Tarucha, and L. M. K. Vandersypen. Spins in few-electron quantum dots. *Rev. Mod. Phys.*, 79(4):1217–1265, Oct 2007.

[10] J. M. Taylor, J. R. Petta, A. C. Johnson, A. Yacoby, C. M. Marcus, and M. D. Lukin. Relaxation, dephasing, and quantum control of electron spins in double quantum dots. *Phys. Rev. B*, 76(3):035315, Jul 2007.

[11] J. M. Elzerman, R. Hanson, L. H. Willems van Beveren, B Witkamp, L. M. K. Vandersypen, and L. P. Kouwenhoven. Single-shot read-out of an individual electron spin in a quantum dot. *Nature*, 430:431–435, 2004.

[12] F. H. L. Koppens, K. C. Nowack, and L. M. K. Vandersypen. Spin echo of a single electron spin in a quantum dot. *Phys. Rev. Lett.*, 100(23):236802, Jun 2008.

[13] J. R. Petta, A. C. Johnson, J. M. Taylor, E. A. Laird, A. Yacoby, M. D. Lukin, C. M. Marcus, M. P. Hanson, and A. C. Gossard. Coherent Manipulation of Coupled Electron Spins in Semiconductor Quantum Dots. *Science*, 309(5744):2180–2184, 2005.

[14] K. C. Nowack, F. H. L. Koppens, Yu. V. Nazarov, and L. M. K. Vandersypen. Coherent Control of a Single Electron Spin with Electric Fields. *Science*, 318(5855):1430–1433, 2007.

[15] Xuedong Hu and S. Das Sarma. Hilbert-space structure of a solid-state quantum computer: Two-electron states of a double-quantum-dot artificial molecule. *Phys. Rev. A*, 61(6):062301, May 2000.

[16] D. Stepanenko, N. E. Bonesteel, D. P. DiVincenzo, G. Burkard, and Daniel Loss. Spin-orbit coupling and time-reversal symmetry in quantum gates. *Phys. Rev. B*, 68(11):115306, Sep 2003.

[17] D. Stepanenko and N. E. Bonesteel. Universal quantum computation through control of spin-orbit coupling. *Phys. Rev. Lett.*, 93(14):140501, Sep 2004.

[18] Nan Zhao, L. Zhong, Jia-Lin Zhu, and C. P. Sun. Spin entanglement induced by spin-orbit interactions in coupled quantum dots. *Phys. Rev. B*, 74(7):075307, Aug 2006.

[19] Suhas Gangadharaiah, Jianmin Sun, and Oleg A. Starykh. Spin-orbit-mediated anisotropic spin interaction in interacting electron systems. *Phys. Rev. Lett.*, 100(15):156402, Apr 2008.

[20] L. Shekhtman, O. Entin-Wohlman, and Amnon Aharony. Moriya's anisotropic superexchange interaction, frustration, and dzyaloshinsky's weak ferromagnetism. *Phys. Rev. Lett.*, 69(5):836–839, Aug 1992.

[21] A. Zheludev, S. Maslov, G. Shirane, I. Tsukada, T. Masuda, K. Uchinokura, I. Zaliznyak, R. Erwin, and L. P. Regnault. Magnetic anisotropy and low-energy spin waves in the dzyaloshinskii-moriya spiral magnet $ba2cuge2o7$. *Phys. Rev. B*, 59(17):11432–11444, May 1999.

[22] Yaroslav Tserkovnyak and Markus Kindermann. Aharonov-casher effect in exchange interactions in a wigner crystal. *Phys. Rev. Lett.*, 102(12):126801, Mar 2009.

[23] Sucismita Chutia, Mark Friesen, and Robert Joynt. Detection and measurement of the dzyaloshinskii-moriya interaction in double quantum dot systems. *Phys. Rev. B*, 73(24):241304, Jun 2006.

[24] L. P. Gor'kov and P. L. Krotkov. Spin relaxation and antisymmetric exchange in n-doped iii-v semiconductors. *Phys. Rev. B*, 67(3):033203, Jan 2003.

[25] Sharif D. Kunikeev and Daniel A. Lidar. Spin density matrix of a two-electron system. ii. application to a system of two quantum dots. *Phys. Rev. B*, 77(4):045320, Jan 2008.

[26] K. V. Kavokin. Anisotropic exchange interaction of localized conduction-band electrons in semiconductors. *Phys. Rev. B*, 64(7):075305, Jul 2001.

[27] K. V. Kavokin. Symmetry of anisotropic exchange interactions in semiconductor nanostructures. *Phys. Rev. B*, 69(7):075302, Feb 2004.

[28] Fabio Baruffa, Peter Stano, and Jaroslav Fabian. Spin-orbit coupling and anisotropic exchange in two-electron double quantum dots. *arXiv:1004.2610 (unpublished)*, Apr 2010.

[29] Fabio Baruffa, Peter Stano, and Jaroslav Fabian. Theory of anisotropic exchange in laterally coupled quantum dots. *Phys. Rev. Lett.*, 104(12):126401, Mar 2010.

[30] G. P. Berman, G. D. Doolen, R. Mainieri, and V. I. Tsifrinovich. *Introduction to Quantum computers*. World Scientific, 2003.

[31] N. D. Mermin. *Quantum computer science*. Cambridge University Press, 2007.

[32] M. A. Nielsen and I. L. Chuang. *Quantum Computation and Quantum Computation*. Cambridge University Press, 2002.

[33] A. Einstein, B. Podolsky, and N. Rosen. Can quantum-mechanical description of physical reality be considered complete? *Phys. Rev.*, 47, 1935.

[34] Adriano Barenco, Charles H. Bennett, Richard Cleve, David P. DiVincenzo, Norman Margolus, Peter Shor, Tycho Sleator, John A. Smolin, and Harald Weinfurter. Elementary gates for quantum computation. *Phys. Rev. A*, 52(5):3457–3467, Nov 1995.

[35] B. H. Bransden and C. J. Joachain. *Physics of atoms and molecules*. Prentice Hall, 2003.

[36] Guido Burkard, Daniel Loss, and David P. DiVincenzo. Coupled quantum dots as quantum gates. *Phys. Rev. B*, 59(3):2070–2078, Jan 1999.

[37] V. Mitin, A. Kochelap, and A. Stroscio. *Quantum Heterostructures*. Cambridge University Press, 2001.

[38] P. Harrison. *Quantum Wells, Wires and Dots*. Wiley, 2005.

[39] L. P. Kouwenhoven, D. G. Austing, and S. Tarucha. Few electron quantum dots. *Rep. Prog. Phys.*, 64.

[40] Stephanie M. Reimann and Matti Manninen. Electronic structure of quantum dots. *Rev. Mod. Phys.*, 74(4):1283–1342, Nov 2002.

[41] Arvind Kumar, Steven E. Laux, and Frank Stern. Electron states in a gaas quantum dot in a magnetic field. *Phys. Rev. B*, 42(8):5166–5175, Sep 1990.

[42] L. P. Kouwenhoven, T. H. Oosterkamp, M. W. Danoesastro, M. Eto, D. G. Austing, T. Honda, and S. Tarucha. Excitation spectra of circular, few-electron quantum dots. *Science*, 278, 1997.

[43] Mark Friesen, Charles Tahan, Robert Joynt, and M. A. Eriksson. Spin readout and initialization in a semiconductor quantum dot. *Phys. Rev. Lett.*, 92(3):037901, Jan 2004.

[44] Hans-Andreas Engel, Vitaly N. Golovach, Daniel Loss, L. M. K. Vandersypen, J. M. Elzerman, R. Hanson, and L. P. Kouwenhoven. Measurement efficiency and n-shot readout of spin qubits. *Phys. Rev. Lett.*, 93(10):106804, Sep 2004.

[45] R. Hanson, L. H. Willems van Beveren, I. T. Vink, J. M. Elzerman, W. J. M. Naber, F. H. L. Koppens, L. P. Kouwenhoven, and L. M. K. Vandersypen. Single-shot readout of electron spin states in a quantum dot using spin-dependent tunnel rates. *Phys. Rev. Lett.*, 94(19):196802, May 2005.

[46] F. H. L. Koppens, C. Buizert, K. J. Tielrooij, I. T. Vink, K. C. Nowack, T. Meunier, L. P. Kouwenhoven, and L. M. K. Vandersypen. Driven coherent oscillations of a single electron spin in a quantum dot. *Nature*, 442(7104):766–771, 2006.

[47] N. W. Ashcroft and N. D. Mermin. *Solid State Physics*. Thomson Learning, 1976.

[48] Jaroslav Fabian, Alex Matos-Abiague, Christian Ertler, Peter Stano, and Igor Žutić. Semiconductor spintronics. *Acta Phys. Slov.*, 57:565, 2007.

[49] G. Dresselhaus. Spin-orbit coupling effects in zinc blende structures. *Phys. Rev.*, 100(2):580–586, Oct 1955.

[50] E. I. Rashba. Properties of semiconductors with an extremum loop. *Fiz Tverd. Tela (Leningrad)*, 2(1224), 1960.

[51] M. Abramowitz and I. A. Stegun. *Handbook of Mathematical Functions*. Dover Publications, 1965.

[52] Peter Stano and Jaroslav Fabian. Spin-orbit effects in single-electron states in coupled quantum dots. *Phys. Rev. B*, 72(15):155410, Oct 2005.

[53] V. Sih and D. Awschalom. Electrical manipulation of spin-orbit coupling in semiconductor heterostructures. *J. Appl. Phys.*, 101:081710, 2007.

[54] P. Lucignano, B. Jouault, and A. Tagliacozzo. Spin exciton in a quantum dot with spin-orbit coupling at high magnetic field. *Phys. Rev. B*, 69(4):045314, Jan 2004.

[55] Peter Stano and Jaroslav Fabian. Theory of phonon-induced spin relaxation in laterally coupled quantum dots. *Phys. Rev. Lett.*, 96(18):186602, May 2006.

[56] W. A. Coish and Daniel Loss. Exchange-controlled single-electron-spin rotations in quantum dots. *Phys. Rev. B*, 75(16):161302, Apr 2007.

[57] V. Popsueva, R. Nepstad, T. Birkeland, M. Førre, J. P. Hansen, E. Lindroth, and E. Waltersson. Structure of lateral two-electron quantum dot molecules in electromagnetic fields. *Phys. Rev. B*, 76(3):035303, Jul 2007.

[58] E. A. Laird, J. R. Petta, A. C. Johnson, C. M. Marcus, A. Yacoby, M. P. Hanson, and A. C. Gossard. Effect of exchange interaction on spin dephasing in a double quantum dot. *Phys. Rev. Lett.*, 97(5):056801, Jul 2006.

[59] Guido Burkard, Georg Seelig, and Daniel Loss. Spin interactions and switching in vertically tunnel-coupled quantum dots. *Phys. Rev. B*, 62(4):2581–2592, Jul 2000.

[60] U. Merkt, J. Huser, and M. Wagner. Energy spectra of two electrons in a harmonic quantum dot. *Phys. Rev. B*, 43(9):7320–7323, Mar 1991.

[61] Rogerio de Sousa, Xuedong Hu, and S. Das Sarma. Effect of an inhomogeneous external magnetic field on a quantum-dot quantum computer. *Phys. Rev. A*, 64(4):042307, Sep 2001.

[62] W. Dybalski and P. Hawrylak. Two electrons in a strongly coupled double quantum dot: From an artificial helium atom to a hydrogen molecule. *Phys. Rev. B*, 72(20):205432, Nov 2005.

[63] Jesper Pedersen, Christian Flindt, Niels Asger Mortensen, and Antti-Pekka Jauho. Failure of standard approximations of the exchange coupling in nanostructures. *Phys. Rev. B*, 76(12):125323, Sep 2007.

[64] Juan I. Climente, Andrea Bertoni, Guido Goldoni, Massimo Rontani, and Elisa Molinari. Magnetic field dependence of triplet-singlet relaxation in quantum dots with spin-orbit coupling. *Phys. Rev. B*, 75(8):081303, Feb 2007.

[65] L. P. Gor'kov and P. L. Krotkov. Exact asymptotic form of the exchange interactions between shallow centers in doped semiconductors. *Phys. Rev. B*, 68(15):155206, Oct 2003.

[66] Dmitriy V. Melnikov, Jean-Pierre Leburton, Ahmed Taha, and Nahil Sobh. Coulomb localization and exchange modulation in two-electron coupled quantum dots. *Phys. Rev. B*, 74(4):041309, Jul 2006.

[67] Tien Quang Nguyen, Mary Clare Sison Escaño, Nobuaki Shimoji, Hiroshi Nakanishi, and Hideaki Kasai. Adsorption of diatomic molecules on iron tape-porphyrin: A comparative study. *Phys. Rev. B*, 77(19):195307, May 2008.

[68] B. S. Kandemir. Variational study of two-electron quantum dots. *Phys. Rev. B*, 72(16):165350, Oct 2005.

[69] Daniela Pfannkuche, Vidar Gudmundsson, and Peter A. Maksym. Comparison of a hartree, a hartree-fock, and an exact treatment of quantum-dot helium. *Phys. Rev. B*, 47(4):2244–2250, Jan 1993.

[70] Constantine Yannouleas and Uzi Landman. Group theoretical analysis of symmetry breaking in two-dimensional quantum dots. *Phys. Rev. B*, 68(3):035325, Jul 2003.

[71] Yannouleas Constantine and Landman Uzi. Magnetic-field manipulation of chemical bonding in artificial molecules. *Int. J. Q. Chem.*, 90(2):699–708, Sep 2002.

[72] L. Serra, Rashid G. Nazmitdinov, and Antonio Puente. Symmetry breaking and the random-phase approximation in small quantum dots. *Phys. Rev. B*, 68(3):035341, Jul 2003.

[73] H. Saarikoski, E. Räsänen, S. Siljamäki, A. Harju, M.J. Puska, and R.M. Nieminen. Electronic properties of model quantum-dot structures in zero and finite magnetic fields. *Eur. Phys. J. B*, 26:241–252, 2002.

[74] Lixin He, Gabriel Bester, and Alex Zunger. Singlet-triplet splitting, correlation, and entanglement of two electrons in quantum dot molecules. *Phys. Rev. B*, 72(19):195307, Nov 2005.

[75] I. L. Aleiner and Vladimir I. Fal'ko. Spin-orbit coupling effects on quantum transport in lateral semiconductor dots. *Phys. Rev. Lett.*, 87(25):256801, Nov 2001.

[76] Elliott Lieb and Daniel Mattis. Theory of ferromagnetism and the ordering of electronic energy levels. *Phys. Rev.*, 125(1):164–172, Jan 1962.

[77] J. Fabian and S. Das Sarma. Spin relaxation of conduction electrons in polyvalent metals: Theory and a realistic calculation. *Phys. Rev. Lett.*, 81(25):5624–5627, Dec 1998.

[78] O. Olendski and T. V. Shahbazyan. Theory of anisotropic spin relaxation in quantum dots. *Phys. Rev. B*, 75(4):041306, Jan 2007.

[79] L.-A. Wu and D. A. Lidar. Dressed qubits. *Phys. Rev. Lett.*, 91(9):097904, Aug 2003.

[80] K V Kavokin. Spin relaxation of localized electrons in n-type semiconductors. *Semiconductor Science and Technology*, 23(11):114009 (13pp), 2008.

[81] http://www.netlib.org/lapack/.

[82] S. Sorella, G. Santoro, and F. Becca. *SISSA Lecture notes on Numerical methods for strongly correlated electrons.*

[83] http://www.caam.rice.edu/software/ARPACK/.

[84] H. Haken and H. C. Wolf. *Molecular Physics and Elements of Quantum Chemistry.* Springer, 2004.

[85] http://www.fftw.org/.

[86] W. H. Press, S. A. Teukolsky, W. T. Vetterling, and B. P. Flannery. *Numerical Recipes 3rd Edition: The Art of Scientific Computing.* Cambridge University Press, 2007.

[87] K. Shen and M. W. Wu. Triplet-singlet relaxation in semiconductor single and double quantum dots. *Phys. Rev. B*, 76(23):235313, Dec 2007.

[88] Conyers Herring. Critique of the heitler-london method of calculating spin couplings at large distances. *Rev. Mod. Phys.*, 34(4):631–645, Oct 1962.